The LINNEAN SOCIETY of London ZOOLOGICAL Journal of the Linnean Society

Zoological Journal of the Linnean Society, 2010, **159**, 435–502. With 10 figures

Global phylogeny of Hadrosauridae (Dinosauria: Ornithopoda) using parsimony and Bayesian methods

ALBERT PRIETO-MÁRQUEZ*

Division of Paleontology, American Museum of Natural History, Central Park West & 79th Street, New York, NY 10024-5192, USA

Received 11 March 2009; accepted for publication 2 April 2009

The late Cretaceous hadrosaurids were the most specialized and diverse clade of ornithopod dinosaurs. Parsimony and Bayesian methods were implemented to elucidate the phylogenetic relationships of all hadrosaurid species. Traditional and geometric morphometrics were applied to discover patterns of variation containing phylogenetic information. In total, 286 phylogenetically informative characters (196 cranial and 90 postcranial) were defined and documented: the most extensive character data set ever constructed for hadrosaurid dinosaurs. Of these, 136 characters were used for the first time in phylogenetic analysis of these ornithopods, and 93 were modified from those of other authors. Parsimony and the Bayesian analysis (using the Mk model without the gamma parameter) confirmed the split of hadrosaurids into Saurolophinae and Lambeosaurinae. Saurolophines included a major clade composed of the *Prosaurolophus–Saurolophus* and the *Kritosaurus–Gryposaurus–Secernosaurus* subclades. *Edmontosaurus* and *Shantungosaurus* were recovered outside the major clade of saurolophines. The *Brachylophosaurus* clade was recovered as the most basal clade of saurolophines in the parsimony analysis, whereas following the Bayesian analysis it was recovered as the sister clade to the *Kritosaurus–Gryposaurus–Secernosaurus* clade. These two analyses resulted in a Lambeosaurinae composed of a succession of Eurasian sister taxa to two major clades: the *Parasaurolophus* clade and the *Hypacrosaurs altispinus–Corythosaurus* clade. In contrast, the Bayesian analysis using the Mk model with the gamma parameter included, resulted in an unbalanced hadrosauroid tree, with a paraphyletic Saurolophinae, and with the *Prosaurolophus* clade, *Edmontosaurus*, and *Shantungosaurus* as successively closer sister taxa to Lambeosaurinae. Based on the strict reduced consensus tree derived from the parsimony analysis, Hadrosauridae was redefined as the clade stemming from the most recent common ancestor of *Hadrosaurus foulkii* and *Parasaurolophus walkeri*.

doi: 10.1111/j.1096-3642.2009.00617.x

ADDITIONAL KEYWORDS: dinosaur – hadrosaur – Hadrosaurinae – Lambeosaurinae – Saurolophidae – Saurolophinae.

INTRODUCTION

Hadrosauridae Cope, 1870 includes the most morphologically derived ornithopod dinosaurs (Horner, Weishampel & Forster, 2004). In the most recent revision of Hadrosauridae, Horner *et al.* (2004) defined Hadrosauridae as the clade consisting of the most recent common ancestor of *Telmatosaurus* Nopcsa, 1903 and *Parasaurolophus* Parks, 1922, and all its descendants. Hadrosaurids were very common during the Late Cretaceous of Europe, Asia, the Americas, and Antarctica (Forster, 1997a; Case *et al.*, 2000; Lund & Gates, 2006). Their fossil record is the richest among non-avian dinosaurs, including dozens of articulated skeletons (Lull & Wright, 1942), thousands of disarticulated bones from multi-individual assemblages (Dodson, 1971; Varricchio & Horner, 1993), growth series (Horner, 2000), soft tissue impressions (Osborn, 1912; Murphy, Trexler & Thompson, 2007), stomach contents, coprolites, trackways (Currie, Nadon & Lockley, 1991), and eggs, nests, and neonates (Horner & Makela, 1979; Horner, 1982; Horner & Currie, 1994).

*E-mail: redshore@gmail.com

Hadrosaurids are remarkable for their mediolaterally-expanded rostra (Morris, 1970), hypertrophied nasal passages (Weishampel, 1981). and, in many species, the presence of conspicuous supracranial crests (Lull & Wright, 1942; Ostrom, 1962). The function of some of these crests might be related to species recognition and other display behaviours (Hopson, 1975; Evans, 2006). The earliest record of Hadrosauridae (considering the clade restricted to Hadrosaurinae and Lambeosaurinae, as in Godefroit *et al.*, 2008) is from the Santonian (Averianov & Nessov, 1995; Averianov, 2007), and the largest taxonomic diversity of the clade spans from the late Campanian to the early Maastrichtian (Gates, 2007).

Because of their abundance, widespread distribution, and excellent preservation (Horner *et al.*, 2004), hadrosaurids provide an excellent model for studying dinosaurian evolution and paleobiology. For example, they can be used to elucidate how geological events affected the evolution and distribution of terrestrial faunas, how their anatomy relates to biomechanical form, function, and ecology, and, owing to their large sample sizes, how anatomical variation relates to species recognition, reproductive behaviour, and population biology. These and many other questions can be best approached in a phylogenetic context to provide an all-encompassing evolutionary understanding for the group. However, a comprehensive and well-resolved phylogeny of hadrosaurids has yet to be inferred.

A global and well-resolved phylogenetic hypothesis of hadrosurid interrelationships is crucial if one is to understand their origin, how they became so widespread, and how they acquired their unique suite of skeletal attributes. However, a cladistic analysis with complete taxonomic sampling, and using modern methods of phylogenetic inference, has yet to be conducted. Previous cladistic studies have only included a limited number of taxa and/or a limited number of characters documenting selected regions of the hadrosaurid anatomy (Head, 1998; Casanovas *et al.*, 1999; Godefroit, Zan & Jin, 2000; You *et al.*, 2003). This has occurred in spite of theoretical studies that have shown that the addition of phylogenetically informative characters generally increses accuracy, even when there are numerous missing entries (Wiens, 1998, 2003). Other studies have demonstrated that including a large number of taxa typically leads to an increase in phylogenetic accuracy, even for incompletely scored taxa (Wiens & Reeder, 1995; Hillis, 1996). In this regard, the inclusion of the hadrosaurid and outgroup hadrosauroid species from Asia (Godefroit *et al.*, 1998; Norman, 2002; You *et al.*, 2003), South America (Brett-Surman, 1979; Bonaparte *et al.*, 1984; Powell, 1987), and Europe (Casanovas *et al.*, 1999; López-Martínez *et al.*, 2001; Prieto-Márquez *et al.*, 2006a) that have not been integrated in previous analyses may provide a more accurate hypothesis of the evolutionary history of these animals.

Additionally, many lower level relationships within Hadrosauridae are still contentious. For example, whereas in some studies *Gryposaurus* Lambe, 1914 has been positioned as the sister taxon to the *Prosaurolophus–Saurolophus* clade (Prieto-Márquez, 2005; Prieto-Márquez *et al.*, 2006a), in others it has been recovered as the sister taxon to the *Brachylophosaurus–Maiasaura* clade (Weishampel & Horner, 1990; Weishampel, Norman & Grigorescu, 1993; Gates & Sampson, 2007). Similar disagreements have appeared in phylogenetic studies of lambeosaurines. For example, *Hypacrosaurus altispinus* Brown, 1912 and *Hypacrosaurus stebingeri* Horner & Currie, 1994 have been inferred to form a monophyletic group in some studies (Evans & Reisz, 2007), but not in others (Suzuki, Weishampel & Minoura, 2004; Prieto-Márquez *et al.*, 2006a). Another subject of disagreement has concerned the inference of the most closely related outgroup taxa to Hadrosauridae, a debate that has obvious implications for the reconstruction of the ancestral area of the clade. Thus, for example, various taxa have been recovered as the sister taxa to Hadrosauridae, including *Telmatosaurus transsylvanicus* Nopcsa, 1900 (Godefroit *et al.*, 1998; You *et al.*, 2003), *Shantungosaurus giganteus* Hu, 1972 (Hu *et al.*, 2001), *Probactrosaurus gobiensis* Rozhdestvensky, 1966 (Norman, 2002), *Protohadros byrdi* Head, 1998, *Eolambia caroljonesa* Kirkland, 1998 (Horner *et al.*, 2004), *Pararhabdodon isonensis* Casanovas-Cladellas, Santafé-Llopis & Isidro-Llorens, 1993 (Prieto-Márquez *et al.*, 2006a), and *Bactrosaurus johnsoni* Gilmore, 1933 (Godefroit *et al.*, 2008).

Finally, in virtually all the previous studies the data and methods used to discover and define characters and character states were never explicit. Indeed, this is not exclusive to the research in hadrosaurid systematics, but is a common practice in vertebrate paleontology.

This study is concerned with resolving the lower level interrelationships of Hadrosauridae using, for the first time, a complete taxonomic sampling of species. Discussions on the historical biogeography and character evolution of hadrosaurids, which may be based on the phylogenetic results presented herein, are beyond the scope of this paper, and will be dealt with in separate studies. Resolving the phylogenetic relationships of hadrosaurids required an exhaustive revision of the patterns of variation in their crania and postcrania, which resulted in the most extensive character data set for a phylogenetic study of these animals. In doing so, I also provided a

complete illustrated documentation of the character data, so that it can serve as the framework for future studies seeking a better and more complete understanding of the evolutionary relationships of hadrosaurid dinosaurs.

Institutional abbreviations

AMNH, American Museum of Natural History, New York, NY, USA; NHM, Natural History Museum, London, UK; BYU, Brigham Young University, Provo, UT, USA; CMN, Canadian Museum of Nature, Ottawa, ON, Canada; FGUUB, Facultatea de Geologie si Geofizica, Universitatea Bucuresti, Bucharest, Romania; FMNH, The Field Museum, Chicago, IL, USA; MACN, Museo Argentino de Ciencias Naturales Bernardino Rivadavia, Buenos Aires, Argentina; MOR, Museum of the Rockies, Bozeman, MT, USA; MSNM, Museo Civico di Storia Naturale di Milano, Milano, Italy; NMMNH, New Mexico Museum of Natural History and Science, Albuquerque, NM, USA; PIN, Palaeontologiceski Institut, Akademii Nauk, Moscow, Russia; ROM, Royal Ontario Museum, Toronto, ON, Canada; SBDE, Sino-Belgian Dinosaur Experdition; TMP, Royal Tyrrell Museum of Paleontology, Drumheller, AB, Canada; UHR, University of Hokkaido Registration; UTEP, Centennial Museum at the Univesity of Texas at El Paso, El Paso, TX, USA.

REVIEW OF PREVIOUS STUDIES ON HADROSAURID SYSTEMATICS

Pre-cladistic studies

The first description of hadrosaurid remains consisted of tooth fragments collected in the Judith River Formation of Montana (‘T*rachodon mirabilis*’ Leidy, 1856a). The family Hadrosauridae was originally erected by Cope in 1870 to include *Hadrosaurus foulkii* Leidy, 1858 and ‘*Hadrosaurus mirabilis*’ (= ‘T*rachodon mirabilis*’). However, scientists would not gain a complete knowledge of the skeletal anatomy of hadrosaurids until the end of the 19th century, when the first complete articulated skeletons were found (Cope, 1883; Lund & Gates, 2006). These skeletons, corresponding to the genus *Edmontosaurus* Lambe, 1917b, came from late Maastrichtian formations of the Dakotas and Wyoming, northern USA. In the next few decades, numerous complete skulls and skeletons were collected in the western interior of the USA and southern Alberta, Canada, including genera such as *Kritosaurus* Brown, 1910, *Saurolophus* Brown, 1912, *Hypacrosaurus* Brown, 1913, *Corythosaurus* Brown, 1914, *Prosaurolophus* Brown, 1916, *Gryposaurus* Lambe, 1914, *Parasaurolophus* Parks, 1922, and *Lambeosaurus* Gilmore, 1924.

Brown (1914) was the first to propose the split of hadrosaurids into the flat-headed forms (Trachodontinae) and the crested forms (Saurolophinae). Lambe (1920) suggested that hadrosaurids diversified into three main lineages, based on the morphology and the absence or presence of cranial crests: Hadrosaurinae (= Trachodontinae or non-crested forms), Saurolophinae (solid-crested forms), and the Stephanosaurinae (hollow-crested forms) (Lambe, 1920). Parks (1923) renamed the Stephanosaurinae as Lambeosaurinae, after invalidating the name ‘S*tephanosaurus*’ Lambe, 1902, upon which the former subfamily had been based.

In their classic monograph on North American hadrosaurids, Lull & Wright (1942) included Saurolophinae within Hadrosaurinae, and supported the classification of hadrosaurids into Lambeosaurinae and Hadrosaurinae. These authors regarded ‘kritosaurs’ (*Gryposaurus* and *Kritosaurus*) and ‘saurolophines’ (*Saurolophus* and *Prosaurolophus*) as morphologically intermediate between non-crested and lambeosaurine hadrosaurids. This classification was also supported by Sternberg (1954), who, in addition, proposed the abandonment of Saurolophinae and the inclusion of *Prosaurolophus* and *Saurolophus* within Hadrosaurinae.

von Huene (1908; 1956) erected the name Hadrosauria to include hadrosaurids and all those forms that were morphologically more similar to them than to *Iguanodon*. Hadrosauria included the following families: Prohadrosauridae, Hadrosauridae, Saurolophidae, Cheneosauridae and Lambeosauridae. In the Prohadrosauridae, von Huene included relatively basal forms such as *Telmatosaurus* and *Tanius*. Within Hadrosauridae, he included ‘*Ornithotarsus*’ Cope, 1869, along with ‘flat-headed’ or ‘low-crested’ taxa such as ‘T*hespesius*’ Leidy, 1856b (= *Edmontosaurus annectens* Marsh, 1892), ‘*Anatosaurus*’ Lull & Wright, 1942 (= *E. annectens*), *Edmontosaurus*, ‘*Mandschurosaurus*’ Riabinin, 1930 (= *Gilmoreosaurus* Brett-Surman, 1979, in part), *Kritosaurus* (= *Kritosaurus navajovius* Brown 1910 and *Gryposaurus* spp.) and *Brachylophosaurus* Sternberg, 1953. The Saurolophidae was composed of *Saurolophus*, *Prosaurolophus*, and *Bactrosaurus*. As in Lull & Wright (1942), the Cheneosauridae included the small (juvenile lambeosaurine) forms ‘*Cheneosaurus*’ Lambe, 1917a and ‘*Procheneosaurus*’ Matthew, 1920. Finally, von Huene’s Lambeosaurinae was equivalent to the Lambeosaurinae of other authors, in that it included those hadrosaurs with large hollow crests, such as *Lambeosaurus*, *Corythosaurus*, *Hypacrosaurus*, and *Parasaurolophus*. However, von Huene also considered as ‘lambeosaurids’ ‘*Trachodon*’, *Jaxartosaurus* Riabinin, 1939, and *Nipponosaurus* Nagao, 1936.

Young (1958) concluded that Saurolophinae was a valid taxonomic grouping, one that included solid-crested forms that, along with Hadrosaurinae, Lambeosaurinae, and the primitive Prohadrosaurinae, formed Hadrosauridae. Ostrom (1961) supported the re-establishment of Saurolophinae as a subfamily of hadrosaurids possessing solid cranial crests that were excluded from the nasal passages, in contrast to those of lambeosaurines that were hollow and contained the nassal passages. Ostrom regarded Saurolophinae as intermediate between the non-crested Hadrosaurinae and the crested Lambeosaurinae. Furthermore, he suggested that *Claosaurus* Marsh, 1872 might have been the most primitive hadrosaurid because of the late Coniacian stratigraphic position (thought to be the oldest occurrence of a hadrosaurian taxon at the time) and the primitive morphology of the postcranial bones.

Hopson (1975) supported Sternberg's division of Hadrosauridae into the two subfamilies Hadrosaurinae and Lambeosaurinae. However, he divided Hadrosaurinae into three informally named groups on the basis of their facial anatomy: the 'kritosaurs', the 'edmontosaurs', and the 'saurolophines', composed of *Prosaurolophus*, *Saurolophus*, *Tsintaosaurus* Young, 1958, and *Lophorhothon* Langston, 1960. Hopson (1975) regarded the premaxillonasal structure of 'kritosaurs' as the ancestral condition from which the more excavated circumnarial fossae of other forms derived. He also considered the genus *Lophorhothon* as intermediate between 'kritosaurs' and 'saurolophines'.

The work of Brett-Surman (1975, 1979, 1989) represented one of the landmarks of hadrosaurid systematics because of the inclusion of taxa from Europe, Asia, and South America, and his extensive revision of the taxonomy and postcranial anatomy of these animals. That study also led to a greater appreciation of the postcrania as a source of diagnostic and phylogenetically informative characters. In 1979, he presented the first evolutionary hypothesis to encompass all genera known at the time. *Probactrosaurus* was placed at the base of the tree as the ancestor of all hadrosaurids. Among lambeosaurines, *Jaxartosaurus* was posited as the direct ancestor of a *Corythosaurus* lineage, and *Bactrosaurus* was forwarded as the ancestor of a *Parasaurolophus* lineage. Among hadrosaurines, *Gilmoreosaurus* was inferred to be the direct ancestor of this subfamily.

Cladistic studies of hadrosaurids

All the above classification schemes and phylogenetic hypotheses were characterized by subjective weighting of characters. Researchers used personal judgment to consider particular characters as those from which groups were established and evolutionary trends hypothesized. This approach changed with the implementation of cladistic methods of phylogenetic inference. For the first time researchers had a tool to minimize subjectivity and conduct more explicit and operative analyses of evolutionary relationships, where all observed characters could play a role in the formulation of phylogenetic hypotheses.

Norman (1984) and Sereno (1986) carried out the first cladistic (although not yet numerical) studies of iguanodontian ornithopods, supporting the monophyly of Hadrosauridae, and its divergence into Hadrosaurinae and Lambeosaurinae. This topology and the monophyly of these three clades figured prominently in subsequent phylogenetic analyses (Weishampel & Horner, 1990; Weishampel *et al.*, 1993; Forster & Sereno, 1994; Forster, 1997a; Head 1998, 2001; Godefroit *et al.*, 1998, 2008; Norman, 2002; You *et al.*, 2003; Horner *et al.*, 2004; Prieto-Márquez *et al.*, 2006a; Evans & Reisz, 2007; Gates *et al.*, 2007).

The cladistic analysis of Weishampel & Horner (1990) was the first to focus on the relationships within Hadrosauridae. Within hadrosaurines, two clades were identifed: one composed of *Gryposaurus*, *Aralosaurus* Rozhdestvensky, 1968, *Maiasaura* Horner & Makela, 1979, and *Brachylophosaurus* Sternberg, 1953; the other included *Saurolophus*, *Prosaurolophus*, *Lophorhothon*, *Edmontosaurus*, and *Shantungosaurus*. Lambeosaurinae included *Parasaurolophus* and a subclade composed of *Corythosaurus*, *Hypacrosaurus*, and *Lambeosaurus*. *Bactrosaurus* was tentatively placed within lambeosaurines. *Telmatosaurus* and *Gilmoreosaurus* appeared as sister taxa to hadrosaurids.

Horner (1985, 1990) proposed a diphyletic origin for hadrosaurids. He redefined Hadrosauridae to include only hadrosaurines. Lambeosaurinae was elevated to family rank and renamed as Lambeosauridae. He used the name Hadrosauria (von Huene, 1956) for the clade including Hadrosauridae and *Iguanodon* Boulenger, 1881, erecting Lambeosauria as the clade including Lambeosauridae and *Ouranosaurus* Taquet, 1976. Lambeosauria and Hadrosauria were then united as sister taxa within Iguanodontoidea. Horner's argument in support of his diphyletic hypothesis was that *Iguanodon* shared more characters with his definition of Hadrosauridae than with 'lambeosaurids', whereas *Ouranosaurus* shared more characters with the latter group than with remaining hadrosaurids. His subsequent phylogeny of Hadrosauridae (Horner, 1992) included an unbalanced tree composed of four clades, i.e. Maiasaurinae, Gryposaurinae, Saurolophinae, and Edmontosaurinae, respectively.

One of the most cited phylogenetic analyses is that of Weishampel *et al.* (1993), the first hadrosaurid

phylogeny that included a matrix along with the list of characters. These authors erected a new name, Euhadrosauria, for the clade composed of Hadrosaurinae and Lambeosaurinae. Their Hadrosauridae was a more inclusive clade composed of *Telmatosaurus* and Euhadrosauria. Euhadrosaur relationships were the same as those in the analysis of Weishampel & Horner (1990).

In a brief abstract, Forster & Sereno (1994) presented the results of a phylogeny where Hadrosaurinae contained two clades. The first clade was composed of broad-snouted forms such as *Maiasaura* and *Edmontosaurus*. The remaining hadrosaurines formed a clade characterized by narial fossae joined along the dorsal margin of the internarial bar. Later, Forster (1997b) restricted the name Hadrosauridae to include only Hadrosaurinae and Lambeosaurinae. All taxa lying outside this clade were referred to the more inclusive Iguanodontia.

Head (1998) redefined Hadrosauridae to include *Protohadros*. In his phylogeny, *Protohadros*, *Gilmoreosaurus*, *Telmatosaurus*, and *Bactrosaurus* figured as outgroup taxa to Hadrosauridae. *Bactrosaurus* was sister taxon to Lambeosaurinae. In the same year, Godefroit *et al.* (1998) agreed with Forster (1997a) in restricting Hadrosauridae to the more stable clade composed of Hadrosaurinae and Lambeosaurinae.

Subsequently, Hu *et al.* (2001) proposed a phylogenetic hypothesis that was very different from those published up until that time. In their phylogeny, non-lambeosaurine hadrosaurids formed an unnamed clade composed of Saurolophinae and Hadrosaurinae. Hadrosaurines included two main subclades. One of them included primitive genera such as *Telmatosaurus*, *Tanius* Wiman, 1929, *Claosaurus*, and *Edmontosaurus*. The other hadrosaurine clade was composed of forms such as *Maiasaura*, *Gryposaurus*, and *Aralosaurus*. Saurolophinae included *Kritosaurus*, *Lophorhothon*, *Saurolophus*, *Prosaurolophus*, and a clade composed of *Tsintaosaurus* and *Jaxartosaurus*. Lambeosaurinae included *Bactrosaurus* being sister taxon to *Nipponosaurus*, and *Parasaurolophus* as sister taxon to *Hypacrosaurus*.

In Norman's (2002) analysis, *Probactrosaurus* appeared as the sister taxon to Hadrosauridae, and *Protohadros*, *Eolambia*, and *Altirhinus* Norman, 1998 represented progressively less-derived outgroup taxa. *Telmatosaurus* and *Bactrosaurus* were hadrosaurids leading towards the Saurolophidae. Conversely, You *et al.* (2003) included several basal hadrosauroid genera from Asia, and proposed that hadrosaurid outgroups were, moving crownward toward Hadrosauridae, *Equijubus* You *et al.*, 2003, *Probactrosaurus*, *Bactrosaurus*, *Protohadros*, and *Telmatosaurus*.

In 2004, Horner and colleagues updated their previous phylogeny (Weishampel & Horner, 1990). Within Hadrosaurinae, *Lophorhothon* now appeared as the most basal form. Two hadrosaurine clades were recognized. One of the clades was composed of *Brachylophosaurus*, *Maiasaura*, *Gryposaurus*, *Edmontosaurus*, and *Prosaurolophus*. The other hadrosaurine clade consisted of a polytomy of '*Naashoibitosaurus*' Hunt & Lucas, 1993 (= *Kritosaurus navajovius*), *Saurolophus*, and *Kritosaurus australis* Bonaparte *et al.*, 1984. Lambeosaurines included an unbalanced tree composed of *Tsintaosaurus*, *Parasaurolophus*, and a polytomy formed by *Lambeosaurus*, *Hypacrosaurus*, and *Corythosaurus*.

The analysis of Suzuki *et al.* (2004) focused on Lambeosaurinae. In their analysis, *Parasaurolophus* appeared as a sister taxon to all other lambeosaurines. The systematic position of *Hypacrosaurus stebingeri* differed in the most parsimonious trees (MPTs), and, as a result, its position was uncertain, as represented by the polytomy in the strict consensus. *Nipponosaurus* and *Hypacrosaurus altispinus* were found to form a clade in all of the MPTs (as well as in the strict consensus), as were *Corythosaurus* and *Lambeosaurus*.

Prieto-Márquez *et al.* (2006a) restricted Hadrosauridae to include Hadrosaurinae and Lambeosaurinae. *Edmontosaurus* appeared as a sister taxon to the remaining hadrosaurines. Two other clades were recognized: one composed of *Brachylophosaurus* and *Maiasaura*, and another integrated by *Gryposaurus*, *Saurolophus*, and *Prosaurolophus*. Lambeosaurines were composed of three clades of unresolved relationships. The first clade included *Parasaurolophus* and *Olorotitan*. Another lineage consisted of *Hypacrosaurus altispinus*. Finally, a third clade included a succession of progressively more inclusive clades that culminated in the sister taxa *Lambeosaurus* and *Corythosaurus*. The genus *Hypacrosaurus* was found to be paraphyletic.

In recent years, the work of Godefroit and various colleagues (2000, 2008; Godefroit, Zan & Jin, 2001; Godefroit, Bolotsky & Alifanov, 2003; Godefroit, Bolotsky & Van Itterbeeck, 2004a; Godefroit, Alifanov & Bolotsky, 2004b) in the Upper Maastrichtian of the Amur region of far eastern Russia, and adjacent regions of China, has had considerable impact on our knowledge of hadrosaurid taxonomic diversity, phylogeny, and biogeography. Various new lambeosaurine (*Charonosaurus* Godefroit *et al.*, 2000, *Olorotitan* Godefroit *et al.*, 2003, and *Sahaliyania* Godefroit *et al.*, 2008) and hadrosaurine (*Kerberosaurus* Bolotsky & Godefroit, 2004 and *Wulagasaurus* Godefroit *et al.*, 2008) genera were described. The phylogeny of Godefroit *et al.* (2008) recovered the clades and topologies inferred in all previous collaborative works

by Godefroit and colleagues. Hadrosaurinae was composed of *Wulagasaurus* and a monophyletic group including the *Maiasaura–Brachylophosaurus* clade and another clade formed by *Gryposaurus*, *Kerberosaurus*, *Prosaurolophus*, and *Edmontosaurus*. On the other side of the cladogram, lambeosaurines were composed of an unbalanced topology that included *Aralosaurus*, *Tsintaosaurus*, *Jaxartosaurus*, *Amurosaurus* Bolotsky & Kurzanov, 1991, and a clade composed of two lineages. The first lineage included *Lambeosaurus* and a polytomy formed by *Corythosaurus*, *Hypacrosaurus*, and *Olorotitan*. The other derived lineage was composed of *Parasaurolophus*, *Charonosaurus*, and *Sahaliyania*.

Gates & Sampson (2007) inferred the position of *Lophorhothon* as the most basal hadrosaurine. Two subclades were inferred among hadrosaurines. One clade included *Edmontosaurus*, *Saurolophus*, and *Prosaurolophus*. The other clade consisted of *Naashoibitosaurus* (= *Kritosaurus navajovius*) and a polytomy formed by four species of *Gryposaurus* and the *Brachylophosaurus–Maiasaura* clade.

Finally, two similar phylogenies of lambeosaurine hadrosaurids were recently presented by Evans & Reisz (2007) and Gates *et al.* (2007). Evans & Reisz (2007) were the first to conduct a complete species-level phylogeny of Lambeosaurinae. They showed a succession of Asian species (from *Aralosaurus tuberiferus* Rozhdestvensky, 1968 to *Amurosaurus riabinini* Bolotsky & Kurzanov, 1991) as sister taxa to a rather specious clade. The first subclade of this clade was composed of *Charonosaurus* and three species of *Parasaurolophus*. The other clade was composed of *Lambeosaurus* and a trichotomy composed of *Olorotitan*, *Corythosaurus*, and a monophyletic *Hypacrosaurus*. Their phylogeny revealed that a greatly enlarged cranial crest evolved independently at least three times within Lambeosaurinae. On the other hand, Gates *et al.* (2007) used the matrix of Evans & Reisz (2007). Their analysis differed from that in Evans & Reisz (2007) in the inclusion of *Velafrons* Gates *et al.*, 2007, and in having a polytomy composed of *Olorotitan ararhensis* Godefroit *et al.*, 2003, *Lambeosaurus* spp., *Corythosaurus casuarius* Brown, 1914, *Hypacrosaurus* spp., and *Velafrons coahuilensis* Gates *et al.*, 2007.

MATERIAL AND METHODS

Selection of taxa and exemplars

The present study included 12 outgroup and 41 ingroup (hadrosaurid) taxa. Outgroup taxa consisted of two non-hadrosauroid iguanodontoideans and ten non-hadrosaurid hadrosaurs (Table 1). The ingroup taxa include all valid species of hadrosaurids, as well as a few unnamed operational taxonomic units (OTUs) from usually poorly sampled geographical areas (Table 2). *Iguanodon bernissartensis* Boulenger, 1881 and *Mantellisaurus atherfieldensis* Hooley, 1925, which are iguanodontoideans distantly related to hadrosaurids, were chosen to root the tree by outgroup comparison (Wiley, 1981; Maddison, Donoghue & Maddison, 1984). The majority of taxa included in this analysis were scored from direct examination of actual fossil material. The following species were not accessible to the author for logistic reasons, and had to be scored using anatomical descriptions from the literature: *Probactrosaurus gobiensis* Rozhdestvensky, 1966 (see also Norman, 2002), *Eolambia caroljonesa* Kirkland, 1998 (see also Head, 2001), *Wulagasaurus dongi* Godefroit *et al.*, 2008, *Sahaliyania elunchunorum* Godefroit *et al.*, 2008, *Kerberosaurus manakini* Bolotsky & Godefroit, 2004, *Aralosaurus tuberiferus* (Godefroit *et al.*, 2004b), and some skeletal elements of *Shantungosaurus giganteus* Hu, 1972 (see also Hu *et al.*, 2001). *Jaxartosaurus aralensis* and most of the adult material of *Saurolophus angustirostris* were exclusively scored from digital photographs and video footage provided by Gregory M. Erickson and David C. Evans.

The taxonomy of several hadrosauroid taxa has been contentious. Here I provide a brief dicussion of my position regarding the taxonomic status of these taxa. This is summarized in Tables 1 and 2.

I followed Godefroit *et al.* (1998) in the material referred to *Bactrosaurus johnsoni* and *Gilmoreosaurus mongoliensis*. In particular, the bones from the AMNH quarries (field numbers) 149 and 145, AMNH 6551, and the predentary AMNH 6369 were used to score *G. mongoliensis*. The material regarded here as belonging to *B. johnsoni* included all the original bones documented by Gilmore (1933) from AMNH quarry 141, as well as the cranial remains of PIN 2549-1 and the more recently discovered cranial and postcranial bones of the SBDE 95/E5 collection (Godefroit *et al.*, 1998).

Dalla Vecchia (2006, 2007) pointed out that material referred to *Telmatosaurus transsylvanicus* (Nopcsa, 1900, 1928; Weishampel *et al.*, 1993; Therrien, 2005) was collected from four different formations in the Hateg Basin, a combined sedimentary sequence of at least 800 m. No data was recorded on the specific stratigraphic provenance of the fossils. Thus, material referable to this species was here restricted to the type skull NHM R3386 and other material that was regarded by Nopcsa (1900) as belonging to that same specimen: NHM R3387, R3388, and R3841. In addition, two maxillae, FGUUB 1010 and NHM R4911, were tentatively referred here to *T. transsylvanicus* for being morphologically indistinct from that in NHM 3386.

Table 1. List of the outgroup taxa used in the phylogenetic analyses, showing the genera and species considered in the present study

Outgroup taxa (original name)	Outgroup taxa (this study)	Occurrence	Age
Bactrosaurus johnsoni Gilmore, 1933	*Bactrosaurus johnsoni*	Iren Dabasu Fm., Inner Mongolia, China	Late Campanian–?Early Maastrichtian (Van Itterbeek *et al.*, 2005)
Claosaurus agilis Marsh, 1872; 1890	*Claosaurus agilis*	Niobrara Chalk Fm. (Smoky Hill Chalk Member), Kansas, USA	Late Coniacian (Everhart & Ewell, 2006)
Eolambia caroljonesa Kirkland, 1998	*Eolambia caroljonesa*	Cedar Mountain Fm., Utah, USA	Late Albian–Early Cenomanian (Lund & Gates, 2006)
Equijubus normani You *et al.*, 2003	*Equijubus normani*	Xinnminbao Group (middle Grey Unit), Gongpoquan Basin, Mazongshan region, Gansu Province, China	Late Barremian–Aptian (Tang *et al.*, 2001)
Gilmoreosaurus mongoliensis Gilmore, 1933; Brett-Surman, 1979	*Gilmoreosaurus mongoliensis*	Iren Dabasu Fm., Inner Mongolia, China	Late Campanian–?Early Maastrichtian (Van Itterbeek *et al.*, 2005)
Iguanodon bernissartensis Boulenger in Beneden, 1881	*Iguanodon bernissartensis*	Upper Hainaut Group, south-western Belgium	Mid–Late Barremian to earliest Aptian (Paul, 2008)
Lophorothon atopus Langston, 1960	*Lophorothon atopus*	Mooresville Chalk Fm. (lower unnamed member), Alabama, USA	Santonian–Campanian boundary (Lamb, pers. comm.)
Mantellisaurus atherfieldensis Hooley, 1925	*Mantellisaurus atherfieldensis*	Upper Vectis and lower Greensand Fm., England	Early Aptian (Paul, 2008)
Probactrosaurus gobiensis Rozhdestvensky, 1966	*Probactrosaurus gobiensis*	Dashiguo Fm., Mongolia	Barremian–Albian (Norman, 2002)
Protohadros byrdi Head, 1998	*Protohadros byrdi*	Woodbine Fm., Texas, USA	Middle Cenomanian (Head, 1998)
Tanius sinensis Wiman, 1929	*Tanius sinensis*	Jiangjun Fm. (Hu *et al.*, 2001), Wangshi Group, Shandong Province, China	Early Campanian (Hong & Miyata, 1999)
Telmatosaurus transsylvanicus Nopcsa, 1900; 1903	*Telmatosaurus transsylvanicus*	?Sampetru Fm., near Sampetru (= Szentpeterfalva), Sibisel River valley, Romania	Early Maastrichtian (Dalla Vecchia, pers. comm.)

In the column of the original names, when two citations are present, the first one refers to the specific name, and the second refers to the generic name.

Table 2. List of the ingroup hadrosaurid taxa used in the phylogenetic analyses, showing the genera and species considered in the present study

Ingroup taxa (original name)	Ingroup taxa (this study)	Occurrence	Age
Amurosaurus riabinini Bolotsky & Kurzanov, 1991	*Amurosaurus riabinini*	Udurchukan Fm., Amur Region, Russia	Middle–Late Maastrichtian (Godefroit *et al.*, 2004a)
Anasazisaurus horneri Hunt & Lucas, 1993	*Kritosaurus navajovius*	Lower Kirtland Fm. (Farmington Member), Kimbeto Arroyo, New Mexico, USA	Late Campanian (Lund & Gates, 2006)
Anatotitan copei Chapman & Brett-Surman, 1990	*Edmontosaurus annectens*	Hell Creek Fm., Montana and South Dakota, USA; Lance Fm., Wyoming, USA	Late Maastrichtian (Horner *et al.*, 2004)
Aralosaurus tuberiferus Rozhdestvensky, 1968	*Aralosaurus tuberiferus*	Bostobe (Bostobynskaya) Fm., Shak Shak locality, north-eastern Aral Sea region, southwestern Kazakhstan	Late Santonian–Early Campanian (Kordikova *et al.*, 2001; Averianov, 2007)
Barsboldia sicinskii Maryanska & Osmolska, 1981	*Barsboldia sicinskii*	Nemegt Fm., northern Sayr, Nemegt, Mongolia	Middle Maastrichtian (Wilson, 2005)
Brachylophosaurus canadensis Sternberg, 1953	*Brachylophosaurus canadensis*	Judith River Fm., Montana, USA; Oldman Fm., Alberta, Canada	Late Campanian (LaRock, 2000)
Brachylophosaurus goodwini Horner, 1988	*Brachylophosaurus canadensis*	Judith River Fm., Hill County, Montana, USA	Late Campanian (LaRock, 2000)
Charonosaurus jiayinensis Godefroit *et al.*, 2000	*Charonosaurus jiayinensis*	Yuliangze Fm., near Jiayin, Heilongjang Province, north-eastern China	Late Maastrichtian (Godefroit *et al.*, 2000)
Corythosaurus casuarius Brown, 1914	*Corythosaurus casuarius*	Dinosaur Park Fm. (lower third), Alberta, Canada	Late Campanian (Evans, 2007b)
Corythosaurus intermedius Parks, 1923	*Corythosaurus intermedius*	Dinosaur Park Fm. (middle third), Alberta, Canada	Late Campanian (Evans, 2007b)
Edmontosaurus annectens Marsh, 1892	*Edmontosaurus annectens*	Hell Creek Fm., Montana and South Dakota, USA; Lance Fm., South Dakota and Wyoming, USA; Laramie Fm., Colorado, USA; Scollard Fm., Alberta, Canada	Late Maastrichtian (Horner *et al.*, 2004)
Edmontosaurus saskatchewanensis Sternberg, 1926	*Edmontosaurus annectens*	Frenchman Fm., Saskatchewan, Canada	Late Maastrichtian (Horner *et al.*, 2004)
Edmontosaurus regalis Lambe, 1917b	*Edmontosaurus regalis*	Hell Creek Fm., Montana, North and South Dakota, USA; Lance Fm., Wyoming, USA; Laramie Fm., Colorado, USA; Scollard Fm., St. Mary River Fm. and Horeshoe Canyon Fm., Canada	Early–Late Maastrichtian (Horner *et al.*, 2004)
Gryposaurus notabilis Lambe, 1914	*Gryposaurus notabilis*	Dinosaur Park Fm. (lower third), Alberta, Canada	Late Campanian (Evans, 2007b)
Gryposaurus incurvimanus Parks, 1920	*Gryposaurus notabilis*	Dinosaur Park Fm. (lower third), Alberta, Canada	Late Campanian (Gates, 2007)
Gryposaurus latidens Horner, 1992	*Gryposaurus latidens*	Two Medicine Fm. (lower section), near Two Medicine River, Pondera County, Montana, USA	Late Santonian–Early Campanian (Horner, 1992)
Gryposaurus monumentensis Gates & Sampson, 2007	*Gryposaurus monumentensis*	Kaiparowits Fm., southern Utah, USA	Late Campanian (Gates & Sampson, 2007)
Hadrosaurus foulkii Leidy, 1858	*Hadrosaurus foulkii*	Woodbury Fm., Haddonfield, New Jersey, USA	Campanian (Prieto-Márquez *et al.*, 2006b)
Hypacrosaurus altispinus Brown, 1912	*Hypacrosaurus altispinus*	Horseshoe Canyon Fm., Alberta, Canada	Early Maastrichtian (Evans, 2007b)
Hypacrosaurus stebingeri Horner & Currie, 1994	*Hypacrosaurus stebingeri*	Two Medicine Fm. (upper section), Montana, USA; Oldman Fm., Alberta, Canada	Middle–Late Campanian (Horner *et al.*, 2004)
Jaxartosaurus aralensis Riabinin, 1939	*Jaxartosaurus aralensis*	Syuksyuk Fm., Kazakhstan	Santonian (Averianov & Nessov, 1995)
Kerberosaurus manakini Bolotsky & Godefroit, 2004	*Kerberosaurus manakini*	Tsagayan Fm. (upper section), Nagornaia street in Blagoveschensk city, Amur Region, Russia	?Late Maastrichtian (Bolotsky & Godefroit, 2004)
Koutalisaurus kohlerorum Prieto-Márquez *et al.*, 2006a	*Pararhabdodon isonensis*	Tremp Fm., Catalunya, north-eastern Spain	Late Maastrichtian (Prieto-Márquez *et al.*, 2006a)
Kritosaurus navajovius Brown, 1910	*Kritosaurus navajovius*	Kirtland Fm. (De-Na-Zin Member), San Juan Basin, New Mexico, USA	Late Campanian (Sullivan, 1999)
Kritosaurus australis Bonaparte *et al.*, 1984	*Secernosaurus koerneri*	Los Alamitos Fm., Rio Negro Province, north-eastern Patagonia, Argentina	Late Campanian–Early Maastrichtian (Apesteguia, 2005)
Kritosaurus sp. (referral by Kirkland *et al.*, 2006)	Sabinas OTU	Olmos Fm. (lower section), near Sabinas, Coahuila, Mexico	Latest Campanian (Kirkland *et al.*, 2006)

Lambeosaurus lambei Parks, 1923	*Lambeosaurus lambei*	Dinosaur Park Fm. (middle-upper sections), Alberta, Canada	Late Campanian (Evans, 2007b)
Lambeosaurus magnicristatus Sternberg, 1935	*Lambeosaurus magnicristatus*	Dinosaur Park Fm. (upper section), Alberta, Canada	Late Campanian (Evans, 2007b)
Lambeosaurus laticaudus Morris, 1981	*Lambeosaurus laticaudus*	El Gallo Fm., north of Arroyo del Rosario, El Rosario, northern Baja California, Mexico	Campanian (Horner *et al.*, 2004)
Maiasaura peeblesorum Horner & Makela, 1979	*Maiasaura peeblesorum*	Two Medicine Fm., Montana, USA	Middle–Late Campanian (Horner *et al.*, 2004)
Naashoibitosaurus normani Hunt & Lucas, 1993	*Kritosaurus navajovius*	Kirtland Fm. (Naashoibito Member), New Mexico, USA	Late Campanian (Lund & Gates, 2006)
Nipponosaurus sachalinensis Nagao, 1936	*Nipponosaurus sachalinensis*	Upper Yezo Group, Sinegorsk, southern Sakhaklin, Russia	Late Santonian–Early Campanian (Suzuki *et al.*, 2004)
Olorotitan ararhensis Godefroit *et al.*, 2003	*Olorotitan ararhensis*	Kundur, Amur Region, Far Eastern Russia	Middle–Late Maastrichtian (Godefroit *et al.*, 2003)
Pararhabdodon isonensis Casanovas-Cladellas *et al.*, 1993	*Pararhabdodon isonensis*	Tremp Fm., Catalunya, north-eastern Spain	Late Maastrichtian (Prieto-Márquez *et al.*, 2006a)
Parasaurolophus walkeri Parks, 1922	*Parasaurolophus walkeri*	Dinosaur Park Fm. (lower third), Alberta, Canada	Late Campanian (Evans, 2007b)
Parasaurolophus tubicen Wiman, 1931	*Parasaurolophus tubicen*	Kirtland Fm. (lower section), New Mexico, USA	Late Campanian (Horner *et al.*, 2004)
Parasaurolophus cyrtocristatus Ostrom, 1961	*Parasaurolophus cyrtocristatus*	Kaiparowits Fm., Utah, USA; Fruitland Fm., New Mexico, USA	Late Campanian (Horner *et al.*, 2004)
Prosaurolophus maximus Brown, 1916	*Prosaurolophus maximus*	Dinosaur Park Fm. (upper half), Alberta, Canada	Late Campanian (Evans, 2007b)
Prosaurolophus blackfeetensis Horner, 1992	*Prosaurolophus maximus*	Two Medicine Fm. (upper section), Landslide Butte, Glacier County, Montana, USA	Late Campanian (Horner, 1992)
Sahaliyania elunchunorum Godefroit *et al.*, 2008	*Sahaliyania elunchunorum*	Yuliangze Fm., near Wulaga, Heilongjang Province, north-eastern China	?Late Maastrichtian (Godefroit *et al.*, 2008)
Saurolophus osborni Brown, 1913	*Saurolophus osborni*	Horseshoe Canyon Fm., Alberta, Canada	Early Maastrichtian (Horner *et al.*, 2004)
Saurolophus angustirostris Rozhdestvensky, 1952	*Saurolophus angustirostris*	Nemegt Fm. (white beds of Hermiin Tsav), N. Sayr, Nemegt, Mongolia	Middle Maastrichtian (Wilson, 2005)
Secernosaurus koerneri Brett-Surman, 1979	*Secernosaurus koerneri*	Upper Bajo Barreal Fm., Lago Colhue Huapi, Rio Negro Province, Argentina	Late Campanian–Early Maastrichtian (Salinas, pers. comm.)
Shantungosaurus giganteus Hu, 1972	*Shantungosaurus giganteus*	Xingezhuang Fm. (Hu *et al.*, 2001), Wangshi Group, Shandong Province, China	Early Campanian (Hong & Miyata, 1999)
Tsintaosaurus spinorhinus Young, 1958	*Tsintaosaurus spinorhinus*	Jingangkou Fm. (Hu *et al.*, 2001), Wangshi Group, Shandong Province, China	Early Campanian (Hong & Miyata, 1999)
Velafrons coahuilensis Gates *et al.*, 2007	*Velafrons coahuilensis*	Cerro del Pueblo Fm., Coahuila, Mexico	Late Campanian (Gates *et al.*, 2007)
Wulagasaurus dongi Godefroit *et al.*, 2008	*Wulagasaurus dongi*	Yuliangze Fm., near Wulaga, Heilongjang Province, north-eastern China	?Late Maastrichtian (Godefroit *et al.*, 2008)
Unnamed hadrosaurid from Big Bend National Park (Davies, 1983)	Big Bend UTEP OTU	Aguja Fm. (upper shale member), Texas, USA	Campanian–?Early Maastrichtian (Wagner, 2001)
Unnamed hadrosaurid from the Wahweap Fm. (Gates, pers. comm.)	Wahweap OTU	Wahweap Fm (upper section)	Late Campanian (Gates, 2007)
Unnamed hadrosaurid from Salitral Moreno (Powell, 1987)	Salitral Moreno OTU	Allen Fm., Rio Negro Province, Argentina	Late Campanian–Early Maastrichtian (Salgado *et al.*, 2007)

In the column of the original names, when two citations are present, the first one refers to the specific name, and the second refers to the generic name.

Horner (1992) and Williamson (2000) summarized the evidence supporting the synonymy of *Anasazisaurus horneri* Hunt & Lucas, 1993 (Lucas *et al.*, 2006) and *Naashoibitosaurus ostromi* Hunt & Lucas, 1993 with *Kritosaurus navajovius*. In agreement with Williamson (2000), the specimens BYU 12950 and NMMNH P-16106 were referred to *K. navajovius*.

I also agree with Wagner (2001) in that *Gryposaurus incurvimanus* Parks, 1919 is a junior synonym of *Gryposaurus notabilis* Lambe, 1914. Parks (1920) originally distinguished *G. incurvimanus* on the basis of its deep and narrow skull, the presence of a 'probable' median protuberance, the 'peculiarities' of the integument in ROM 764 with dermal callosities along the median line of the vertebral column, two wedge-shaped manual phalanges, four phalanges in the fifth digit, and 'peculiarities' of mandibular teeth. None of these characters allows distinction of *G. incurvimanus* (ROM 764 and TMP 80.22.1) from other hadrosaurid taxa. Additional characters provided by Parks (1920) to distinguish *G. incurvimanus* from *G. notabilis* are not useful in this regard either. Thus, the shape of the orbit is variable within *G. notabilis*, and is not diagnostic to generic or specific level. The more rostral position of the nasal protuberance in ROM 764 and TMP 80.22.1 is probably a subadult condition, as is the lack of emargination on the rostral margin of the orbit (probably related to the immature development of the nasal arch). That the *G. incurvimanus* specimens represent subadult individuals of *G. notabilis* is supported by the smaller size of the skulls of *G. incurvimanus* (58–60 cm in length, compared with approximately 80 cm in length in *G. notabilis* skulls). The greater separation between the jugal and the quadrate varies among hadrosaurid specimens depending on the circumstances of preservation and articulation. Finally, the U- or V-shape of the caudodorsal margin of the external naris is too variable among specimens of *G. notabilis* to have diagnostic value: it is U-shaped in ROM 873, but more V-shaped in CMN 2278 and MSNM V345.

More recently, Gates & Sampson (2007) regarded *G. incurvimanus* as a distinct species and provided a revised diagnosis. The new characters provided by these authors as diagnostic for this species were: dorsal premaxillary process that is more concave caudally than in other species of the genus; jugal with a small spur on the caudal margin of the caudoventral flange; and slightly excavated ventral surface of the nasal hump. The degree of excavation of the caudal region of the dorsal process of the premaxilla could only be observed in TMP 80.22.1 for *G. incurvimanus*, as it was not preserved (and, unfortunately, entirely reconstructed) in ROM 764. Comparison of TMP 80.22.1 with *G. notabilis* skulls (e.g. ROM 873 and CMN 2278) showed no differences in the relief of the caudal region of the premaxillary dorsal process among these specimens. The slight excavation of the ventral surface of the nasal hump or arch was present in all *G. notabilis* specimens, as well as in TMP 80.22.1, and corresponded to the lightly incised caudodorsal region of the circumnarial fossa. Examination of TMP 80.22.1 and ROM 764 revealed no spur on the caudal margin of the caudoventral flange that might allow distinction between the jugals of these skulls and those of the *G. notabilis* specimens. Immature characters of *G. notabilis* that Gates & Sampson (2007) considered as a unique combination to diagnose *G. incurvimanus* included: gracility, smaller premaxillary lip, premaxillae angled more steeply, and rostrocaudally shortened and deeper skull. Finally, the infratemporal fenestra being larger than the orbit was a character also present in *G. notabilis*, and the straight ventral margin of the maxilla was too variable intraspecifically to be of diagnostic value.

None of the characters used by Chapman & Brett-Surman (1990) to diagnose *Anatotitan copei* were unique or allowed distinction of this taxon from other hadrosauids. Likewise, examination of the skull of AMNH 5730 revealed several areas with signs of postdepositional dorsoventral compression. For example, each dentary had a longitudinal ridge protruding laterally, probably produced by bending of the lateral surface of the bone (the same deformation ridge was present in the right, but not the left, dentary of the paratype specimen of *Edmontosaurus regalis* Lambe, 1917b, CMN 2289) (Fig. 1); the dorsal region of the left quadrate had a transverse fissure (Fig. 2A); and the left postorbital 'inflation' of its central body appeared crushed inwards (medioventrally) (Fig. 2B), with a nearly vertical indented line on the lateral bone surface. Aside from the very shallow skull, AMNH 5730 and 5886 were indistinguishable from any specimen of *Edmontosaurus annectens*. Therefore, *A. copei* was regarded as a junior synonym of *E. annectens* in the present study, in agreement with Horner *et al.* (2004).

I also concluded that *Edmontosaurus saskatchewanensis* Sternberg, 1926 (CMN 8509) was founded on subadult material of *E. annectens*. Differences in skull morphology between CMN 8509 and other specimens of *E. annectens* and *E. regalis*, such as the poorly developed lateral inflation of the central body of the postorbital and the relatively gracile jugal, could be attributed to the immature development of the specimen. Likewise, even at its relatively smaller size, CMN 8509 already had a preorbital region that was nearly 1.6 times the length of the quadrate, indicating that later in ontogeny the skull of this animal would probably reach the more elongated proportions of *E. annectens*. Therefore, *E. saskatchewanensis* was regarded as a junior synonym of *E. annectens*.

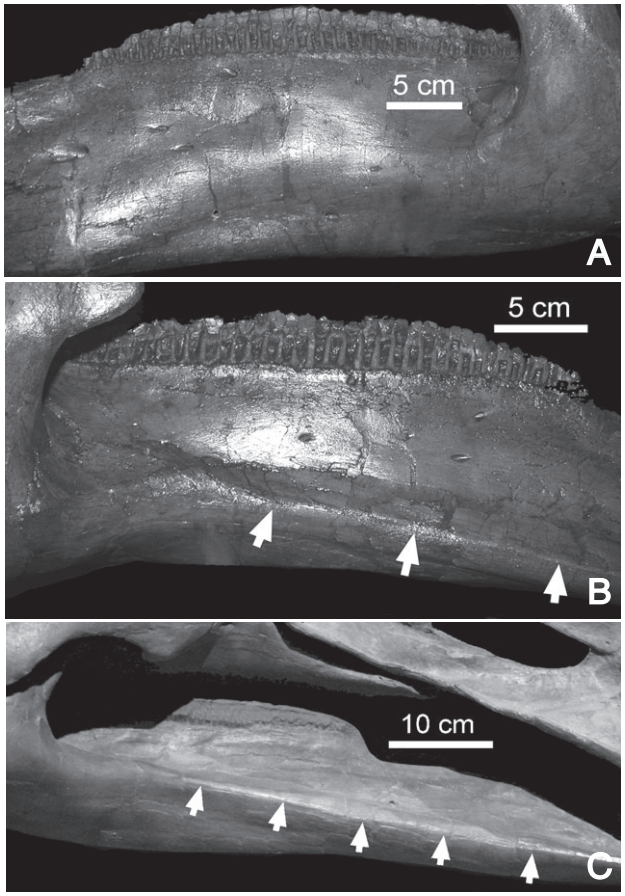

Figure 1. Dentaries of two specimens of *Edmontosaurus* in lateral view, showing evidence of postdepositional dorsoventral compression in the form of bending lines (arrows). A, left dentary of *Edmontosaurus regalis*, CMN 2289. B, right dentary of CMN 2289. C, right dentary of *Edmontosaurus annectens*, cast of AMNH 5730 (= '*Anatotitan copei*').

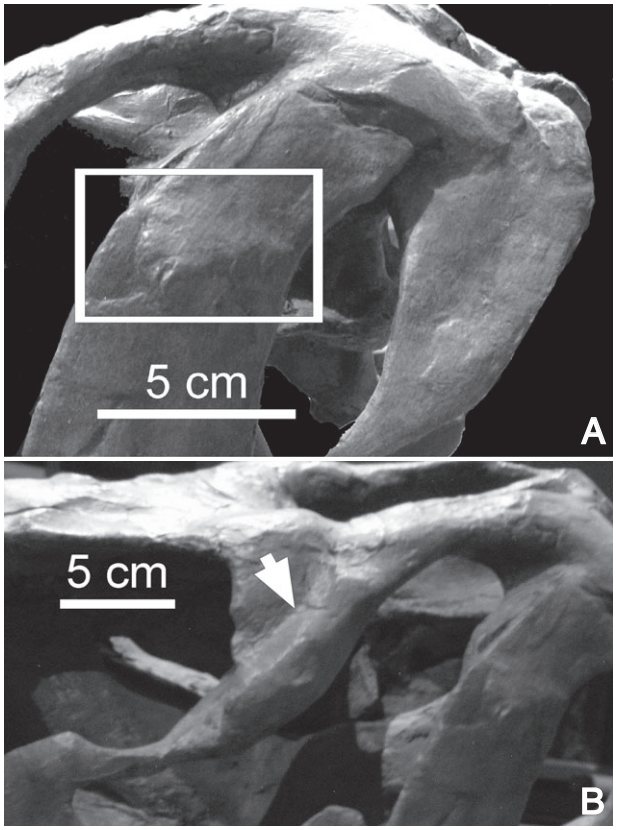

Figure 2. Signs of postdepositional dorsoventral compression (rectangle and arrow) in a specimen of *Edmontosaurus annectens*, cast of AMNH 5730 (type of '*Anatotitan copei*'), lateral view. A, dorsal region of the left quadrate. B, left postorbital.

Horner (1992) described *Prosaurolophus blackfeetensis* from the Upper Two Medicine Formation of Montana. This species was diagnosed by the exclusion of the prefrontal and premaxilla from the lateral concavity of the nasal, as well as by the greater caudal extension of the crest relative to that of *Prosaurolophus maximus* Brown, 1916. However, the dorsal surface of the prefrontal in *P. blackfeetensis* (e.g. MOR 454-6-24-6-2) was actually concave medial to the orbital rim (Fig. 3), as in *P. maximus*. As for the length of the crest, this was variable within the genus (e.g. longer in ROM 787 than in the larger TMP 84.1.1) and actually not longer in MOR 454 relative to that of other specimens within the genus. Thus, I agree with Wagner (2001) in regarding *P. blackfeetensis* as a junior synonym of *P. maximus*.

I regard *Secernosaurus koerneri* Brett-Surman, 1979 as a senior synonym of *Kritosaurus australis* (Bonaparte *et al.*, 1984). The type material of *S. koerneri* (FMNH P13423) was found to be indistinct from the type and other referred material of *K. australis* (Bonaparte *et al.*, 1984). The morphology of the pubis of FMNH P13423 was nearly identical to that of *K. australis* (MACN-RN 2), particularly the geometry of the prebupic process, the length and width of the proximal constriction, and the length of the ischial peduncle. Likewise, the right ilium of FMNH P13423 (the left one is distorted) shared with those of the MACN specimens a shallow proximal margin of the preacetabular process, craniocaudally extensive supra-acetabular process that did not project ventrally more than half the depth of the iliac central plate, and a morphologically unique brevis shelf.

The hadrosaurid material from the Salitral Moreno bone bed (Powell, 1987), Rio Negro, Argentina, was also included as a single OTU to further document the diversity of these animals in South America. This material is currently under study by a team of

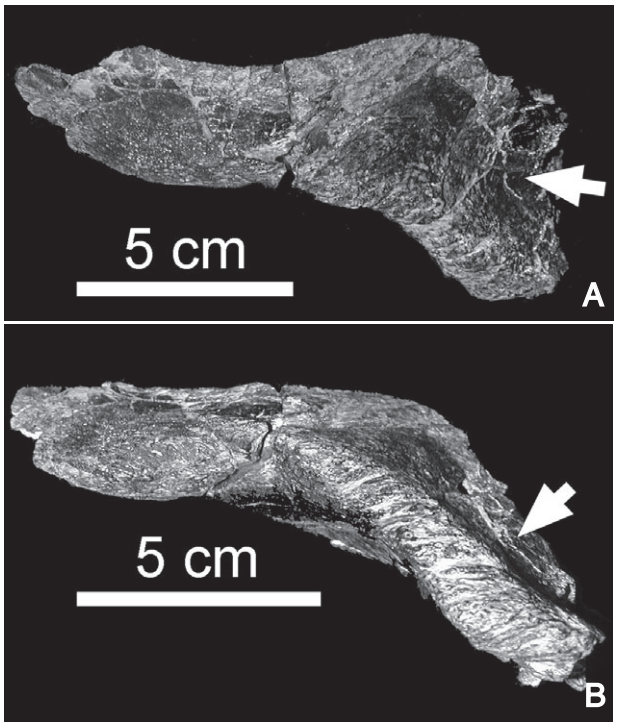

Figure 3. Right prefrontal of *Prosaurolophus maximus* (MOR 454-6-24-6-2), part of the holotype of *Prosaurolophus blackfeetensis*, showing a concave surface (arrows) dorsomedial to the orbital margin, in (A) dorsal and (B) lateral views.

paleontologists from the Centro Paleontólogico Lago Los Barreales, led by Jorge Calvo.

Two other unnamed hadrosaurids were also included as OTUs to further represent the diversity of hadrosaurids in southern North America. The first OTU was a set of skeletal elements from the UTEP collection at the University of Texas in Austin, documented by Davies (1983) and regarded by Wagner (2001) as a lambeosaurine hadrosaurid. The ilium (UTEP P37.7.222) was particularly interesting because it was the only hadrosaurid specimen that I observed that shared a unique morphological type of brevis shelf with the ilia of *Secernosaurus koerneri* and those collected from Salitral Moreno. The second OTU was a recently described large skeleton collected near the Mexican town of Sabinas, Coahuila, referred to *Kritosaurus* sp. by Kirkland *et al.* (2006).

Finally, I followed Evans (2007b) in recognizing *Corythosaurus intermedius* Parks, 1923 as a valid species distinct from *Corythosaurus casuarius*, whereas *Koutalisaurus kohlerorum* Prieto-Márquez *et al.*, 2006a was regarded as a junior synonym of *Pararhabdodon isonensis* (A. Prieto-Márquez, unpubl. data; see also Prieto-Marquez, 2008).

Character definition and character state delimitation

The definition of morphological characters required the reassessment of characters used in previous analyses by other authors (some of which needed to be redefined in face of the new data), as well as the discovery of new ones based on analysis of variation in the crania and postcrania of hadrosaurids. I followed three approaches for discovering and evaluating characters from skeletal morphological variation: qualitative comparative anatomy of specimens, analysis of linear and angular measurements, and geometric morphometrics.

Qualitative osteological comparisons and linear and angular data

Direct visual comparisons among hadrosaurid cranial and postcranial structures allowed identification of discrete primary homologies. In addition, linear and angular measurements were taken from the actual specimens and from high-resolution digital images of the bones taken myself (for detailed information of the landmarks used to conduct the measurements, see the documentation of characters provided in Morphbank; see the Appendix). In the latter case, measurements were obtained using the Image J program (Abramoff, Magelhaes & Ram, 2004). Linear measurements were used to calculate ratios that served to describe quantitatively a particular anatomical character.

Geometric morphometrics: analysis of planar shapes using geodesic paths

The analysis of planar shapes using geodesic paths is a relatively new morphometric method developed by Klassen *et al.* (2004): in its first implementation for research within the biological sciences, Prieto-Márquez *et al.* (2007) referred to this as geodesic Distance Analysis (GDA). Prieto-Márquez *et al.* (2007) used GDA to quantify differences in the geometry of the pelvic canal of iguanids and crocodilian reptiles.

In GDA, dissimilarities between shapes are quantified using geodesic distances within a Riemannian (i.e. non-Euclidean) shape space. The term 'geodesic' refers to the shortest path between two points in a curved space. GDA considers the shapes of planar continuous curves in R^2. Shapes are invariant to rigid motions (translation and rotation), uniform scaling, and to the placement of origin (or starting point) of the parameterization. The objects of study are represented by the continuous curves of their boundaries. The arc length of these contours is used as a parameter to model the shapes. The angle between the tangent vector to the curve and the positive x-axis is defined as a function of the arc length (Srivastava

et al., 2005). In this way, shapes are compared and represented using their angle functions. Then, geodesic paths (or geodesics) are constructed between them. A geodesic between two shapes is the path that minimizes the difference between their angle functions. I implemented an updated version of the method, called 'elastic' GDA (Mio, Srivastava & Joshi, 2007). Although the original approach described in Klassen *et al.* (2004) modelled shapes by 'bending only', in the approach of Mio *et al.* (2007) curves along the geodesic paths are transformed by bending, stretching, or compressing segments non-uniformly along their lengths. Thus, elastic GDA is a more appropiate method to study local changes among shapes, quantifying only those differences that are found in smaller, more concrete regions of the curves. Likewise, elastic GDA allows the modelling of open curves as well as closed ones.

The benefit of GDA is that it allows for the quantification of continuous curves that are very difficult or impossible to discretize using landmarks. Thus, the method was applied in searching for and defining patterns of variation on skeletal elements where the identification of homologous points is ambiguous. An example is the lateral profile of the prepubic process of the pubis, where it cannot be assumed that a given point along its margin is homologous with that of another exemplar. Landmark-based methods (Bookstein *et al.*, 1985; Dryden & Mardia, 1998; Zelditch, Swiderski & Fink, 2000) are limited in scope because they depend heavily on the chosen homologous points. Several other methods of shape analysis represent geometries by parametric splines using Fourier descriptors (Persoon & Fu, 1986). However, a drawback of using splines is that Fourier descriptors ignore the nonlinear geometry of the shape space of closed curves. Although such representations can be used to classify shapes, it is not possible to perform statistical analyses that are intrinsic to the shape space. This is because spline control points only represent a finite number of coefficients, and the continuity of the boundaries that connect those coefficients are ignored: the space of all spline functions becomes a finite dimensional shape space, unlike the infinite space of shapes of continuous curves. Another statistical approach, called active shape models (Cootes *et al.*, 1995), uses principal component analysis of landmarks to model shape variability. Despite its simplicity and efficacy, this approach is rather limited because it ignores the nonlinear geometry of shape space where the geometries of study are contained.

In practice, the continuous curves for input into the GDA analysis were obtained by tracing the contour of fossil bones with a Wacom Graphire graphic tablet (Wacom Co., Ltd, Saltama, Japan) in Illustrator CS2 (Adobe Systems Inc., San Jose, CA, USA). Each drawing of a curve was saved as a vector file and imported into Matlab 6.5 (The MathWorks, Natick, MA, USA), the software used to run the GDA algorithms. The GDA output consisted of a matrix of pairwise geodesic distances among all the curves of a collection of bone shapes. Because the application of the method of cluster analysis implemented in this study required that the data had a finite number of dimensions, the next step consisted on reducing the number of dimensions of the GDA dissimilarity matrix. This was accomplished via non-metric multidimensional scaling (or NMMDS; Young, 1985), implemented in the R statistical package (Ihaka & Gentleman, 1996). NMMDS transforms an infinite, non-euclidean space into a coordinate Euclidean space with a limited number of dimensions. The method uses Euclidean distance to model dissimilarity by means of a monotonic transformation (Young, 1985).

Discretization of continuous data derived from morphometric analyses

Whereas morphometric approaches were used to discover and evaluate patterns of variation containing phylogenetic information, other methods were required to transform those patterns into discrete character states. A model-based clustering method (Mclust in the R statistical package; Fraley & Raftery, 2002, 2003, 2006) was applied to these quantitative data in order to minimize the subjectivity in distinguishing clusters and deciding the number of character states to be considered. Model-based clustering attempts to describe the data as a mixture model with a density distribution among a fixed number of components (clusters). For simplicity, the technique used here assumes a multivariate normal distribution for each component with unknown parameters (mean and variance) for each measured variable. The parameters are then estimated by maximum likelihood using an expectation-maximization (EM) algorithm. Each EM iteration involves an E-step, which computes the conditional probability that an object belongs to a particular cluster given an estimate of the cluster means, covariances, and mixing proportions, and an M-step, which computes the cluster parameters given the conditional probabilities. The steps are iterated until convergence is achieved. One potential drawback of this method is that the number of components (clusters) and the nature of constraints on parameterization (e.g. equality of variance among clusters, covariance of variables) need to be specified. The procedure used here increments the EM algorithm over solutions incorporating between one and ten clusters and a number of different parameter constraints. For each solution, it calculates a Bayesian information criterion (BIC). The BIC is the value

of the maximized log-likelihood with an additional penalty based on the number of parameters in each solution, thus allowing comparison of solutions with different numbers of clusters and varying constraints on the parameters. The solution with the highest BIC is used to subdivide the continuous variable(s) into discrete states.

The result of this type of analysis is summarized in a bivariate plot (Fig. 4). For example, Figure 4A shows a graphical output from Mclust, resulting from cluster analysis of the angle between the acetabular and articular margins of the iliac peduncle of the ischium (character 276). The *x*-axis represents the number of clusters into which the data may be classified, and the *y*-axis shows the values of the BIC. The BIC is the value of the maximized log-likelihood with a cost on the number of parameters of each model (Fraley & Raftery, 2003). Each one of the two lines in the plot represents a clustering model. Because the data used in the analysis contains only one dimension, there are only two possible models (hence, only two lines are shown in the plot). These models contain ellipsoidal clusters that vary according to the value of the BIC. Likewise, the BIC varies for each one of the number of clusters considered for each model. These two models differ depending on whether the variance is equal or variable (abbreviated as 'E' and 'V', respectively, as shown in the lower right corner of the graph). The method favours selecting the number of clusters that correspond to the greater (i.e. less negative) BIC values. In the case of Figure 4A, the method favoured grouping the data into two clusters of equal variance because that model showed the greatest (less negative) BIC value. Three clusters of equal variance would be the next optimal grouping of the data, and so forth.

In multidimensional data sets such as those derived from the analysis of planar shapes using geodesic paths, the method also considers the geometric characteristics of various clustering models, like orientation, volume, or shape of the clusters. An example is shown in Figure 4B, consisting of a model clustering analysis of the shape of the postacetabular process of the ilium (character 259). A total of eight coloured lines are present in that bivariate plot, each one representing a clustering model characterized by a specific shape, volume and distribution of the clusters. In the case of Figure 4B for character 259, the method favoured clustering the data into two groups of equal shape and equal volume, with data points distributed diagonally (abbreviated EEI).

Boxplot distributions of the raw data were also considered in deciding the number of clusters in which each quantitative character was divided. These graphs provided a visual representation of the variation of a ratio or an angle among the sampled taxa,

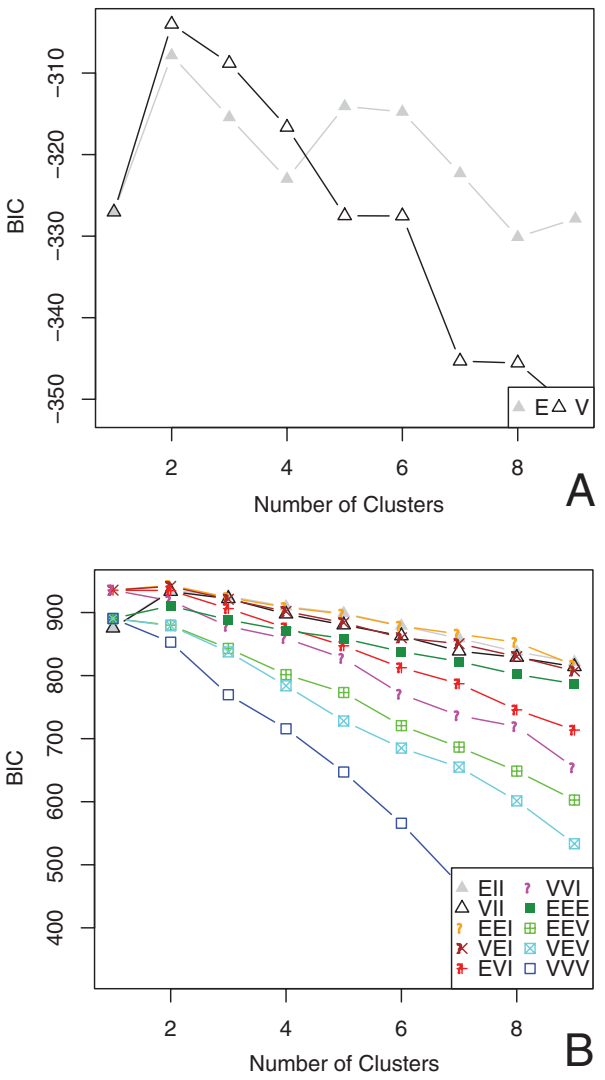

Figure 4. Bayesian information criterion (BIC) plots resulting from the clustering model analysis implemented in Mclust (within the R statistical package). A, BIC plot of two clustering models for a one-dimensional data set (i.e. a character quantified with a linear measurement). B, BIC plot for various clustering models of NMMDS derived from a geodesic distance analysis (GDA) dissimilarity matrix. Indentifiers of clustering models indicate the type of distribution (spherical, diagonal, or ellipsoidal), volume (equal or variable), shape (equal or variable), and orientation (not applicable, coordinate axes, equal, or variable) of the clusters: EEE = ellipsoidal, equal volume, shape and orientation; EEI = diagonal, equal volume, variable shape; EEV = ellipsoidal, equal volume and shape, variable orientation; EII, spherical, equal volume and shape; EVI = diagonal, equal volume, variable shape; VEI = diagonal, variable volume, equal shape; VEV = ellipsoidal, variable volume, equal shape; VII, spherical, variable volume, equal shape; VVI = diagonal, variable volume and shape; VVV = ellipsoidal, variable volume and shape (Fraley & Raftery, 2003).

as well as an insight into the variance within each species. The information provided by the BIC and boxplots was combined to help decide how many character states would be considered for a given character. In a few cases, the data would be clearly separated in the boxplot in a determinate number of clusters that was not supported by the BIC plot. In such cases, I favoured the pattern displayed in the boxplot in my decision of establishing the number of states for the characters.

Finally, K-means (R statistical package) clustering analysis was used to assign each specimen of the data to one of more of the character states (clusters) resulting from the analyses described above. K-means clustering (similar to the EM procedure above) starts by partitioning the objects randomly into k initial sets, and then calculates the mean point, or centroid, of each set. It then constructs a new partition by associating each point with the closest centroid, and recalculates centroids for the new clusters, repeating until convergence.

The value of the boundry delimiting two given character states was calculated using the following expression:

$$(m_2 - m_1)[s_1/(s_1 + s_2)] + 1,$$

where m_1 and m_2 are the means, and s_1 and s_2 are the standard deviations, of clusters (states) 1 and 2, respectively. m_1 and s_1 represent the mean and standard deviations of the cluster containing values closer to 0.

Character state coding

A total of 286 characters (196 cranial and 90 postcranial) were derived from the qualitative and quantitative (morphometric) studies, and are included in this analysis. Of these, 136 characters were used for the first time in a phylogenetic analysis, and 93 were modified from those of other authors. The characters of the present analysis are listed in the Appendix, and are illustrated and documented online in Morphbank (http://www.morphbank.net, 28 October 2008; Florida State University, School of Computational Science, Tallahassee, FL, USA). Specific web links to collections of characters (organized by anatomical region) and also for each particular character are included in the Appendix.

Polymorphic characters were coded by scoring all states found in a given taxon in the same cell of the character matrix (i.e. using the notation '0 & 1 & 2' when states 0–2 are present in the same taxon). Because fossil remains are often incompletely preserved, it is not uncommon to encounter uncertainty in scoring characters. The shape of the quadratojugal notch of the quadrate (character 127) will illustrate this case. This character includes three states. In *Kerberosaurus manakini*, the notch is partially preserved so that, although it is possible to rule out the presence of state '0', it is uncertain which of the other two states was present in this species. In those instances I scored in the same cell of the data matrix the state codes that were possible for the taxon (in the example of *K. manakini*, using the notation '1/2'). Inapplicable characters were coded as '–'. This coding was chosen because various studies have concluded that this is the less problematic way of dealing with inapplicable characters (Strong & Lipscomb, 1999; Seitz, Garcia & Liston, 2000).

All characters were equally weighted. The only ordered characters were the number of dentary and maxillary alveoli (characters 1 and 16, respectively), and the maximum number of teeth exposed on the dentary and maxillary occlusal planes (characters 4 and 19, respectively). Justification for ordering these four characters came from observing sequences of changes among characters that were consistent throughout ontogeny, and throughout the stratigraphic succession of the fossil record of iguanodontoideans. For example, in the case of character 1, there is a positve correlation between the number of tooth families and specimen size (Prieto-Marquez, 2008: 265–267). At the same time, the oldest and more basal taxa tend to show fewer teeth in their dentaries than stratigraphically younger and relatively more derived taxa. This same pattern was observed for characters 4 (number of functional teeth in the dentary occlusal plane), 16 (number of maxillary tooth families), and 19 (number of functional teeth in the maxillary occlusal plane). Although many other cranial and postcranial elements are known in subadult and adult specimens, in most cases these were recorded only in a few taxa or in a few exemplars within a species. For example, although numerous complete skulls document a growth series in the lambeosaurine genera *Corythosaurus* and *Lambeosaurus*, similar cranial ontogentic series for other taxa are wanting. Likewise, in spite of the completely known cranial anatomy of *Corythosaurus* and *Lambeosaurus* throughout development, ontogenetic data for the postcrania are lacking.

Methods of phylogenetic inference

A total of three analyses were conducted. The analyses included maximum parsimony and Bayesian inference with equal and variable rates of character change. Given the substantial quantity of missing data (36%) present in the character matrix, this was subjected, prior to the phylogenetic analyses, to safe taxonomic reduction (Wilkinson, 2003). In doing so, I sought to identify taxa that could be pruned from the

matrix to reduce the number of most parsimonious trees (MPTs), improving the resolution of the resulting consensus topology. Safe taxonomic reduction was implemented using the program TAXEQ3 (Wilkinson, 2001a). No taxon was found to be 'safely' removable without leading to changes in the resulting topology and, thus, no taxon was pruned from the matrix prior to the analyses.

Parsimony analysis

The search for the optimal tree(s) using parsimony was carried out in TNT 1.0 (Goloboff, Farris & Nixon, 2002). I conducted a heuristic search of 10 000 replicates using random addition sequences, followed by branch swapping by tree–bisection–reconnection (TBR; holding ten trees per replicate) to minimize algorithm 'greediness' and maximize the thoroughness of the search (Swofford *et al.*, 1996). Posterior to the analysis, the reduced consensus method of Wilkinson (1995, 2003) was applied in order to identify unstable (i.e. 'wild-card') taxa, the deletion of which produced a more resolved strict (reduced) consensus tree. This technique was implemented using the 'strict' program of the REDCON 3.0 package (Wilkinson, 2001b). Bremer support (Bremer, 1988) was assessed by computing decay indices (Donoghue *et al.*, 1992) with MacClade 4.0 (Maddison & Maddison, 2003) and PAUP 4.0b10 (Swofford, 2002). Bootstrap proportions (Felsenstein, 1985) were also computed in PAUP. The bootstrap analysis was set to 5000 replicates using heuristic searches, where each search was conducted using random additional sequences with branch-swapping by subtree pruning and regrafting (SPR) and 25 replicates. Reconstruction of ancestral states was conducted using Fitch (1971) parsimony in MacClade 4.0.

In order to assess the strength of the phylogenetic signal of the data this was subjected to a permutation tail probability test (PTP). The PTP test was run on PAUP, using a heuristic search with random addition sequences, branch-swapping by TBR, and 100 replicates. This test was followed by topology-dependant (T-PTP) tests on selected clades recovered in the strict and strict reduced consensus trees of the MPTs derived from the parsimony analysis. The T-PTP tests were also set to run using random addition sequences, branch-swapping by TBR, and 100 replicates.

Bayesian analyses

There have been relatively few Bayesian analyses of morphological data (Lewis, 2001; Nylander *et al.*, 2004; Lee, 2005; Wiens, Bonett & Chippindale, 2005). Furthermore, in only a few cases have Bayesian methods been used to reconstruct the phylogeny of fossil groups (Snively, Russell & Powell, 2004; Müller & Reisz, 2006). Notably, these included one on hadrosaurids (Evans, 2007a). Here, I used the maximum-likelihood model of Lewis (2001) (Markov k or Mk) for discrete morphological data, implemented in MrBayes 3.1.2 (Huelsenbeck & Ronquist, 2001). Müller & Reisz (2006) showed that the implementation of the Mk model appears to be appropriate only if autapomorphies are included. Thus, a total of 84 autapomorphic characters (nearly all of them culled from the literature) were added to the data set (see the Appendix). Two different variations of the Mk model were applied. In a first model, I assumed equal rates of character change. In the second model, I incorporated the gamma shape parameter to allow for variable rates of character change, as in Nylander *et al.* (2004). Priors other than the default for the models were not specified for all the analyses. The analysis without gamma used four chains and ran for 14 000 000 generations, sampled every 100 generations. Stationarity was achieved with a standard deviation of split frequencies of 0.004. Trees generated during the first 140 000 generations were discarded as 'burn in'. This was further assessed by visual examination of plots generated with the 'sump' command of MrBayes. The analysis with gamma used four chains and 10 000 000 generations sampled every 100 generations, reaching stationarity with a 0.005 standard deviation of split frequencies. Trees generated during the first 100 000 generations were also discarded as 'burn in'.

Criteria for comparing phylogenies

The preferred Bayesian topology was selected by comparing the harmonic mean of the log-likelihood of each of the two analyses. The analysis with the harmonic mean closest to 0 is preferred. This allowed the determination of whether the addition of the gamma parameter to the model improved its fit to the data (Wiens *et al.*, 2005). Furthermore, I also calculated the Bayes factor for the two Bayesian analyses. The Bayes factor is twice the difference between the two harmonic means of the two Bayesian analyses (Müller & Reisz, 2006). This factor assesses the significance of the difference between two harmonic means. Usually, a Bayes factor of greater than ten indicates strong support (Kass & Raftery, 1995).

Preference between the parsimony strict reduced consensus tree and the chosen Bayesian topology was evaluated using the fit between the stratigraphic ages of hadrosaurid taxa and the order of branching events for each of these two phylogenies. This was accomplished by implementing the Manhattan stratigraphic measure (Siddall, 1998), as modified by Pol & Norell (2001; MSM*). The MSM* has the advantage of not being affected by tree shape and being much more sensitive to the age differences among taxa than other measures, such the Spearman Rank-order Correlation (SRC) (Norell & Novacek, 1992) and

Stratigraphic Consistency Index (SCI) (Huelsenbeck, 1994). Conceptually, the MSM* is analogous with the consistency index (Kluge & Farris, 1969). Calculation of the MSM* is based on the optimization of an age character using a symmetrical Sankoff step matrix of absolute age differences (Tables 3 and 4).

RESULTS

The maximum parsimony analysis resulted in 160 equally most parsimonious trees of 906 steps each. The best score was hit 124 times out of the 10 000 replicates. The consistency index was 0.54 and the retention index was 0.81. Such a relatively low consistency index reflected the high degree of homoplasy present in these data, a fact previously noticed by other authors in, for example, the case of hadrosaurine hadrosaurids (Horner *et al.*, 2004). Implementation of the reduced consensus method (Wilkinson, 2001b) identified a profile of five strict reduced consensus trees, the first of which includes all taxa and corresponds to the strict consensus tree presented in Figure 5. The other four strict reduced consensus trees pruned one taxon in each case (*Claosaurus agilis*, *Barsboldia sicinskii* Maryanska & Osmolska, 1981, *Nipponosaurus sachalinensis* Nagao, 1936, and *Kerberosaurus manakini*). Exclusion of *C. agilis*, *B. sicinskii*, and *N. sachalinensis* produced a nearly completely resolved strict consensus tree (Fig. 6). Most clades were weakly supported, as shown by the low bootstrap proportions and decay indices (Figs 5, 6). The groupings with greater bootstrap proportions were found among the most inclusive clades outside hadrosaurids, and also among those hadrosaurid clades consisting of multispecific genera. A similar pattern of support was shown by the posterior probabilities in the Bayesian consensus trees (Figs 7, 8). The data matrix was subjected to a PTP test implemented in PAUP. This test resulted in a P value of 0.01, indicating that, although weak, given those low support measures, the phylogenetic signal present in the data is significant.

The value of the harmonic mean of the Bayesian analysis without the gamma parameter was –4367.57, whereas that of the analysis with the gamma parameter was –4229.19. Because the latter value is closer to 0, the tree derived from the Bayesian analysis with gamma was preferred. The Bayes factor was 276 (i.e. two times the difference between 4229.19 and 4367.57), which means that the difference between the harmonic means of the two analyses was significant.

Application of the MSM* to the strict reduced consensus derived from the parsimony analysis, and to the tree summarizing the results from the Bayesian analysis with the gamma parameter, produced the following results. For the clade Hadrosauroidea, MSM* was 0.97 ($P = 0.001$) for the parsimony phylogeny, whereas it had a value of 0.91 (P value = 0.015) for the Bayesian tree. When applied to Hadrosauridae, MSM* was 0.91 (P value = 0.008) for the parsimony tree and 0.87 (P value = 0.017) for the Bayesian phylogeny. These figures indicate a greater stratigraphic fit for the parsimony phylogeny. Therefore, the strict reduced consensus tree was used as the framework for the taxonomy and character optimization discussed below (Fig. 9). A time-calibrated tree of this phylogenetic hypothesis can be found in Figure 10.

Summary of hadrosaurid relationships

All the analyses resulted in unbalanced consensus trees showing a series of outgroup taxa to Hadrosauridae (Figs 5–8). The clades stemming from the most distant outgroup taxa to hadrosaurids were well supported in the parsimony and Bayesian analyses, with bootstrap proportions approaching 90 or 100, and posterior probabilities equal or very close to 1, respectively.

In the following sections, characters will be referred to by a number followed by the character state number in brackets. These numbers can be used to find the definition and documentation of the character in the Appendix and in the Morphbank web links. Clade definitions followed the requirements for establishing clade names stated in Article 9 of the PhyloCode (Cantino & de Queiroz, 2007).

In contrast to previous studies implementing parsimony and Bayesian methods on fossil data (Müller & Reisz, 2006; Evans, 2007b), important differences were found among the inferred phylogenies. This was particularly evident when comparing the tree from the Bayesian analysis including gamma and those from the other two analyses. In the phylogenies resulting from the parsimony and Bayesian analysis without gamma (Figs 5–7), hadrosaurids were composed of two major clades. This general pattern is congruent with the most accepted cladistic hypothesis of the relationships of these animals derived from numerous studies over the last two decades (Sereno, 1986; Weishampel & Horner, 1990; Forster, 1997b; Horner *et al.*, 2004). On the other hand, the topology inferred in the Bayesian analysis with gamma (Fig. 8) showed an unbalanced tree with a paraphyletic Hadrosaurinae (Saurolophinae in this paper; see below). This topology is more congruent with the phylogenetic hypotheses of Hopson (1975: 39) and Wagner (2001: 176), suggestive of the derivation of the enclosed nasal passages in lambeosaurines from a common ancestor of *Edmontosaurus* or edmontosaur-like saurolophines.

In all consensus trees presented here the most basal members of Lambeosaurinae were species

Table 3. Coding of the Sankoff age character used in the calculation of the Manhattan Stratigraphic Measure (MSM*; Siddall 1998; Pol & Norell 2001)

Taxa	Age (million years)	State code	Geochronological stage
Edmontosaurus annectens	65	a	Late Maastrichtian
Edmontosaurus regalis	65	a	Late Maastrichtian
Kerberosaurus manakini	65	a	Late Maastrichtian
Wulagasaurus dongi	65	a	Late Maastrichtian
Pararhabdodon isonensis	65	a	Late Maastrichtian
Charonosaurus jiayinensis	65	a	Late Maastrichtian
Olorotitan ararhensis	65	a	Late Maastrichtian
Amurosaurus riabinini	65	a	Late Maastrichtian
Sahaliyania elunchunorum	65	a	Late Maastrichtian
Telmatosaurus transsylvanicus	68	b	Early Maastrichtian
Saurolophus osborni	68	b	Early Maastrichtian
Saurolophus angustirostris	68	b	Early Maastrichtian
Barsboldia sicinskii	68	b	Early Maastrichtian
Hypacrosaurus altispinus	68	b	Early Maastrichtian
Bactrosaurus johnsoni	70	c	Late Campanian–early Maastrichtian
Gilmoreosaurus mongoliensis	70	c	Late Campanian–early Maastrichtian
Kritosaurus navajovius	70	c	Late Campanian–early Maastrichtian
Salitral Moreno OTU	70	c	Late Campanian–early Maastrichtian
Secernosaurus koerneri	70	c	Late Campanian–early Maastrichtian
Hadrosaurus foulkii	74	d	Late Campanian
Two Medicine OTU	74	d	Late Campanian
Maiasaura peeblesorum	74	d	Late Campanian
Brachylophosaurus canadensis	74	d	Late Campanian
Sabinas OTU	74	d	Late Campanian
Prosurolophus maximus	74	d	Late Campanian
Big Bend UTEP OTU	74	d	Late Campanian
Gryposaurus notabilis	74	d	Late Campanian
Gryposaurus monumentensis	74	d	Late Campanian
Parasaurolophus walkeri	74	d	Late Campanian
Parasaurolophus tubicen	74	d	Late Campanian
Parasaurolophus cyrtocristatus	74	d	Late Campanian
Lambeosaurus magnicristatus	74	d	Late Campanian
Lambeosaurus lambei	74	d	Late Campanian
Hypacrosaurus stebingeri	74	d	Late Campanian
Corythosaurus casuarius	74	d	Late Campanian
Corythosaurus intermedius	74	d	Late Campanian
Velafrons coahuilensis	74	d	Late Campanian
Lambeosaurus laticaudus	74	d	Late Campanian
Tanius sinensis	80	e	Early Campanian
Shantungosaurus giganteus	80	e	Early Campanian
Gryposaurus latidens	80	e	Early Campanian
Tsintaosaurus spinorhinus	80	e	Early Campanian
Lophorhothon atopus	83	f	Late Santonian–early Campanian
Aralosaurus tuberiferus	83	f	Late Santonian–early Campanian
Nipponosaurus sachalinensis	83	f	Late Santonian–early Campanian
Jaxartosaurus aralensis	84	g	Santonian
Claosaurus agilis	86	h	Late Coniacian
Protohadros byrdi	95	i	Middle Cenomanian
Eolambia caroljonesa	98	j	Early Cenomanian
Probactrosaurus gobiensis	110	k	Albian
Equijubus normani	125	l	Early Aptian
Mantellisaurus atherfieldensis	125	l	Early Aptian
Iguanodon bernissartensis	127	m	Barremian–early Aptian

Table 4. Sankoff step matrix of the age character used in the calculation of the Manhattan Stratigraphic Measure (MSM*)

	a	b	c	d	E	f	g	h	i	J	k	l	m
a	0	3	5	9	15	18	19	21	30	33	45	60	62
b	i	0	2	6	12	15	16	18	27	30	42	57	59
c	i	i	0	4	10	13	14	16	25	28	40	55	57
d	i	i	i	0	6	9	10	12	21	24	36	51	53
e	i	i	i	i	0	3	4	6	15	18	30	45	47
f	i	i	i	i	I	0	1	3	12	15	27	42	44
g	i	i	i	i	I	i	0	2	11	14	26	41	43
h	i	i	i	i	I	i	i	0	9	12	24	39	41
i	i	i	i	i	I	i	i	i	0	3	15	30	32
j	i	i	i	i	I	i	i	i	i	0	12	27	29
k	i	i	i	i	I	i	i	i	i	I	0	15	17
l	i	i	i	i	I	i	i	i	i	I	i	0	2
m	i	i	i	i	I	i	i	i	i	I	i	i	0

from Eurasia, such as *Aralosaurus tuberiferus*, *Jaxartosaurus aralensis*, *Tsintaosaurus spinorhinus* Young, 1958, and *Pararhabdodon isonensis* (Figs 5–8). *Aralosaurus tuberiferus* was inferred to be the most basal lambeosaurine, in agreement with recent studies (Evans & Reisz, 2007; Gates *et al.*, 2007; Godefroit *et al.*, 2008). The following more exclusive clades were present in all phylogenies resulting from parsimony and Bayesian analyses: the *Sahaliyania–Amurosaurus* clade, the *Charonosaurus–Parasaurolophus* clade, the *Pararhabdodon–Tsintaosaurus* clade, and the *Corythosaurus–Lambeosaurus* clade (with or without a monophyletic *Hypacrosaurus* as sister taxon).

Parsimony and Bayesian analysis with no gamma parameter recovered a monophyletic Saurolophinae (Figs 6, 7). Likewise, two clades were always present: one composed of *Kritosaurus*, *Gryposaurus*, *Secernosaurus*, and the Salitral Moreno and Big Bend UTEP OTUs; and another containing *Prosaurolophus*, *Saurolophus*, and the Sabinas OTU. These two clades were united to form a larger clade. *Edmontosaurus* was placed as sister taxon to the clade including *Gryposaurus* and *Prosaurolophus*. In contrast, the consensus tree derived from the Bayesian analysis with gamma recovered a paraphyletic Saurolophinae (Fig. 8). Following that analysis, the *Prosaurolophus–Saurolophus* clade, *Edmontosaurus*, *Shantungosaurus*, and *Barsboldia* were part of an unbalanced tree leading to Lambeosaurinae.

DISCUSSION

The interrelationships of non-hadrosaurid hadrosauroids

The most inclusive clade considered here was Hadrosauroidea (Sereno, 1986), redefined as *Hadrosaurus foulkii* Leidy, 1858 and all taxa more closely related to it than to *Iguanodon bernissartensis* Boulenger, 1881. Hadrosauroidea was supported by the following unambiguous synapomorphies: at least three teeth per alveoli arranged dorsoventrally at mid-length of the dental battery [2(1)]; ventral deflection of the dentary ocurring rostrally, between 66 and 78% of approximately the length of the dental battery [37(1)]; absence of accessory foramen in the surangular [53(1)]; the rostral end of the rostrodorsal process of the nasal reaching the rostral margin of the narial foramen [79(1)]; centrally located dorsolateral maxillary promontory, base of dorsal process positioned slightly caudal to the mid-length of the maxilla [90(1)]; jugal with orbital and infratemporal margins nearly equal in width [115(1)]; articulation margin of the occipital condyle facing caudally, and divided from the caudal border of the basioccipital by a shallow cleft [152(1)]; absence of supraorbital bone [187(0)]; and ilium with a ratio between the dorsoventral depth of the central plate and the distance between the pubic peduncle and the caudodorsal prominence of the ischial peduncle of 0.8 or greater [234(0)].

Outgroup taxa to Hadrosauridae formed an unbalanced tree of Asian and North American species in both parsimony and Bayesian phylogenies (Figs 5–8). Closer to Hadrosauridae we find a sequence of Eurasian species, *Bactrosaurus johnsoni*, *Gilmoreosaurus mongoiliensis*, and *Telmatosaurus transsylvanicus*, in this order. This result, recovered in of all the phylogenies, is in conflict with previous hypotheses that placed *T. transsylvanicus* as the sister taxon (Weishampel & Horner, 1990; Weishampel *et al.*, 1993; Kirkland, 1998; Horner *et al.*, 2004; Suzuki *et al.*, 2004; Prieto-Márquez *et al.*, 2006a) or among the closest sister taxa (Head, 1998; Hu *et al.*, 2001) to Euhadrosauria. These findings are, however, more

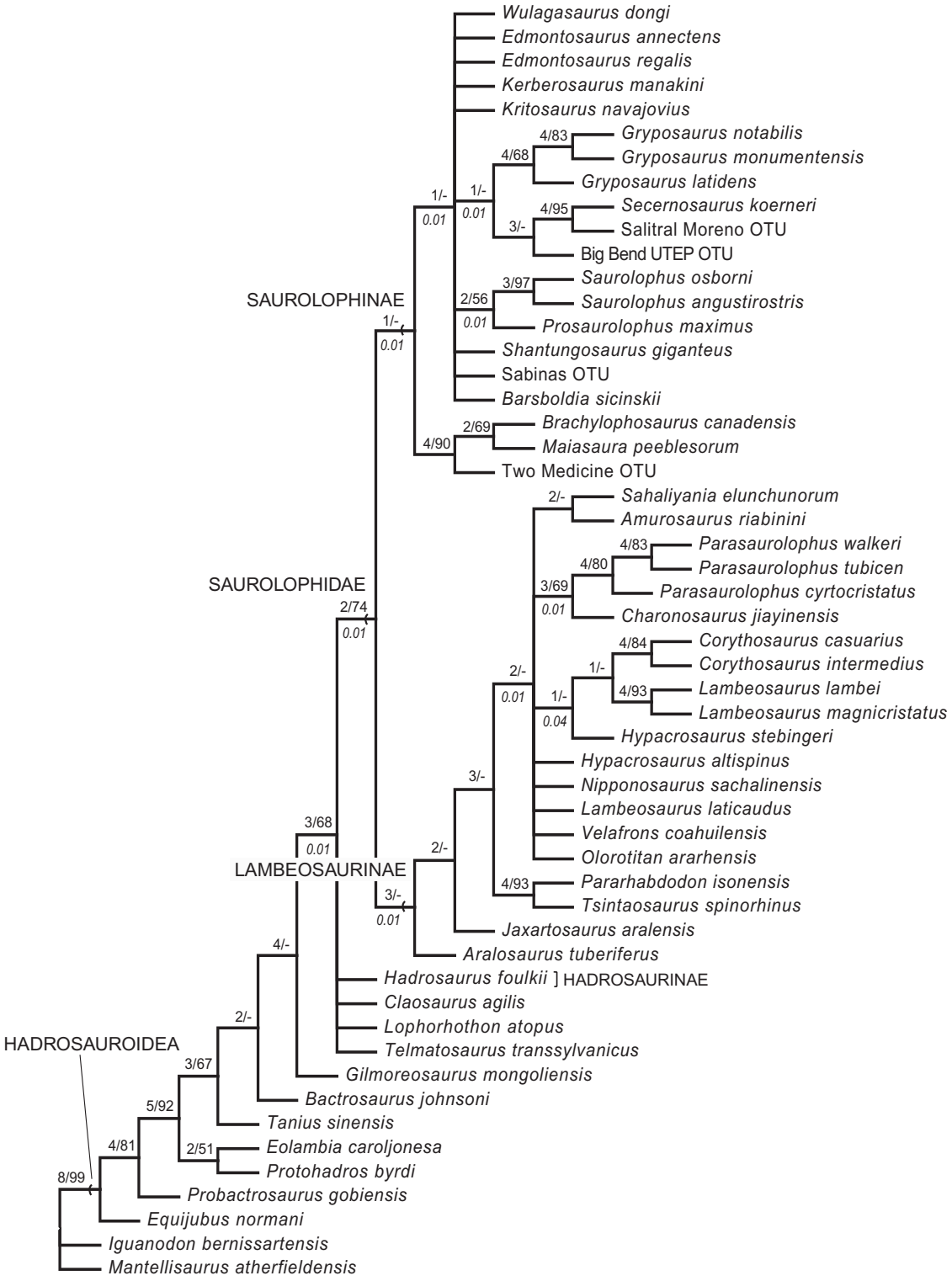

Figure 5. Strict consensus tree of the 160 most parsimonious trees resulting from the parsimony analysis of 53 iguanodontian taxa. At each node, the pair of numbers separated by a slash above a branch represents, from left to right, a decay index and a bootstrap proportion. Bootstrap proportions lower than 50 are indicted by a hyphen. The decimal number in italics that appears below a branch represents the *P* value of topology-dependant permutation tail probability (T-PTP) analysis.

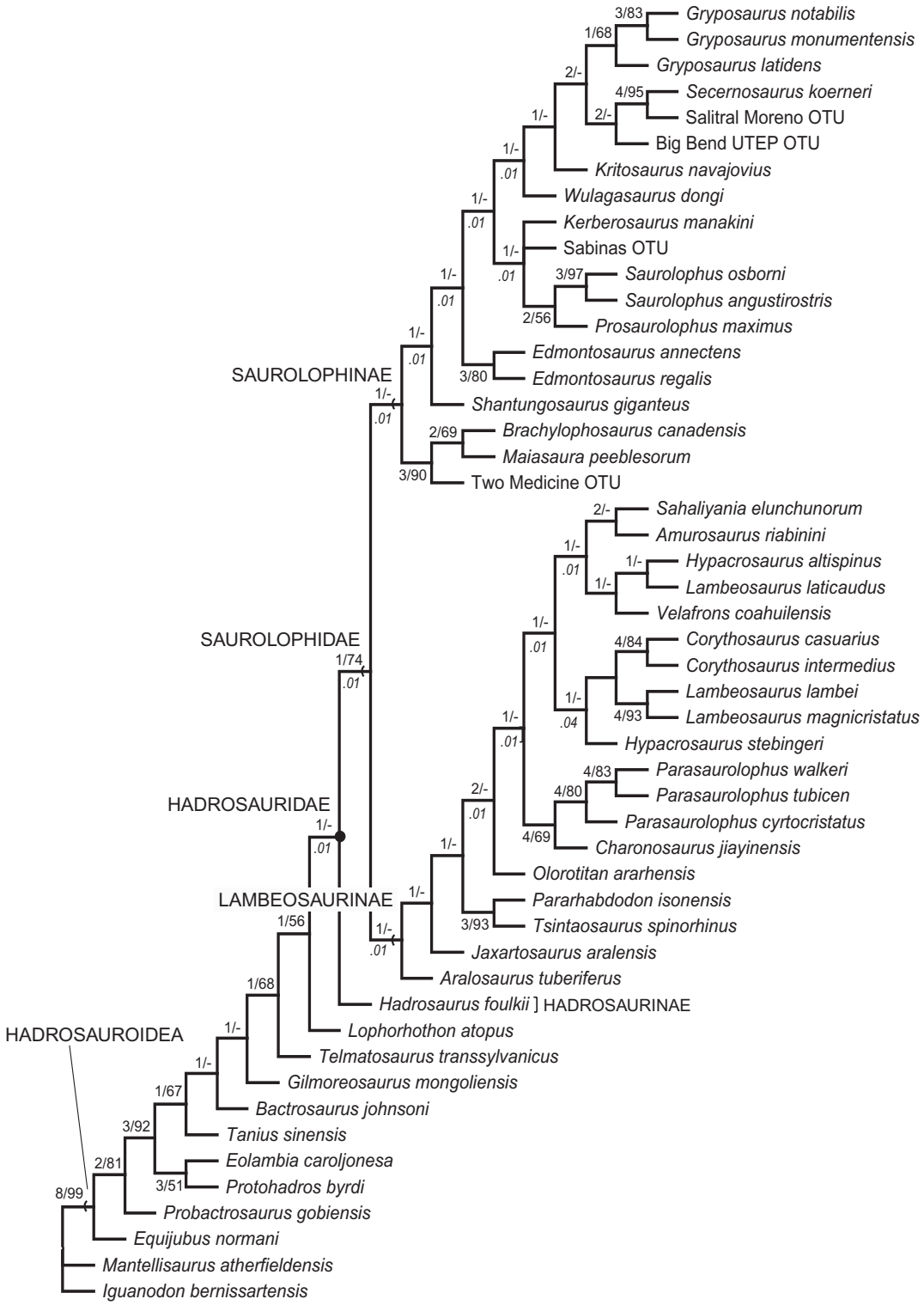

Figure 6. Strict reduced consensus tree of the 160 most parsimonious trees resulting from the parsimony analysis of 53 iguanodontian taxa. Posterior to the analysis, *Claosaurus agilis*, *Barsboldia sicinskii*, and *Nipponosaurus sachalinensis* were pruned from the data after implementation of REDCON 3.0 (Wilkinson, 2001b). At each node, the pair of numbers separated by a slash above or below a branch represents, from left to right, a decay index and a bootstrap proportion. Bootstrap proportions lower than 50 are indicted by a hyphen. The decimal number in italics that appears below a branch represents the *P* value of topology-dependant permutation tail probability (T-PTP) analysis.

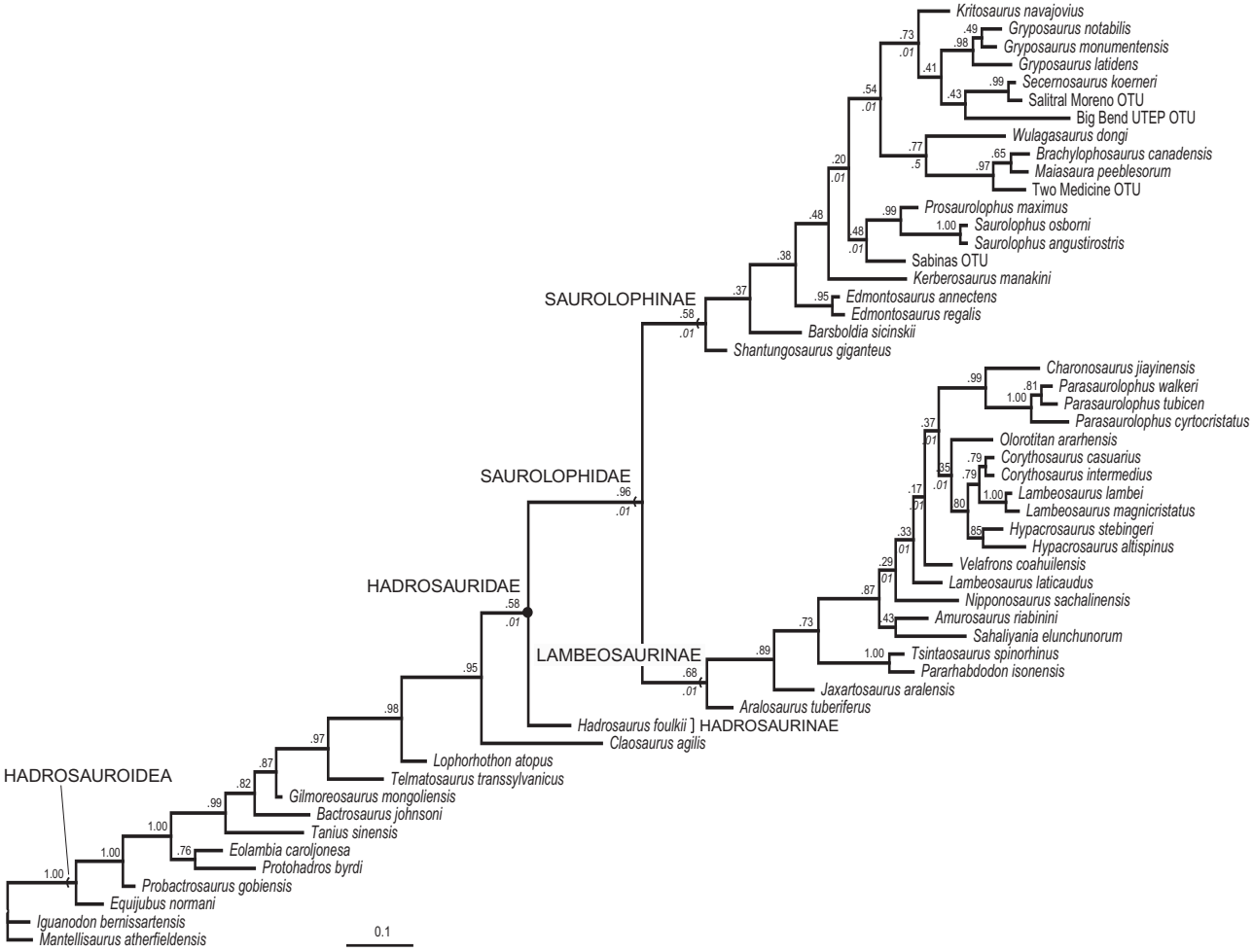

Figure 7. Bayesian consensus tree of the analysis with equal rates of character change showing the phylogenetic relationships of 53 iguanodontians. At each node, the decimal number above a branch indicates a posterior probability, and the decimal number below represents a *P* value of topology-dependant permutation tail probability (T-PTP) analysis.

congruent with the hypothesis of Wagner (2001), who placed *T. transsylvanicus* as a more distantly related species to hadrosaurids. Likewise, in all the analyses the most closely related taxa to Hadrosauridae were two North American species, *Lophorhothon atopus* Langston, 1960 and *Claosaurus agilis* (Figs 5–8).

EUHADROSAURIA

Euhadrosauria was a name erected by Weishampel *et al.* (1993). However, these authors did not provide a definition of this taxon. In published phylogenies, Euhadrosauria has been applied to the clade composed of Hadrosaurinae (Saurolophinae in this paper) + Lambeosaurinae (Weishampel *et al.*, 1993; Kirkland, 1998; Casanovas *et al.*, 1999; Horner *et al.*, 2004; Prieto-Márquez *et al.*, 2006a) or to a more inclusive clade than Lambeosurinae + Saurolophinae (Casanovas *et al.*, 1999; Wagner, 2001; Norman, 2002). Thus, without a definition, what Euhadrosauria is remains open to interpretation: it is either equivalent in its content to Saurolophidae or it may refer to a clade closer to Saurolophidae than to *Telmatosaurus*. For the clade composed of Saurolophinae + Lambeosaurinae I preferred the use of a new name, Saurolophidae (a derivation of Saurolophinae Brown, 1914), rather than defining Euhadrosauria and applying it for that clade. Under the International Code of Zoological Nomenclature (ICZN; International Commission on Zoological Nomenclature, 1999), any taxon less inclusive than a taxon in the family rank group is a subfamily, tribe, subtribe, genus, or species (Article 35.1). In addition, a taxon name in the family-group rank must be made by adding to the stem or to the entire name of its type genus (ICZN Article 29.1), using a standard sufix (whether subfamily, tribe, or subtribe, as specified in Article 29.2). Euhadrosauria fails on both accounts

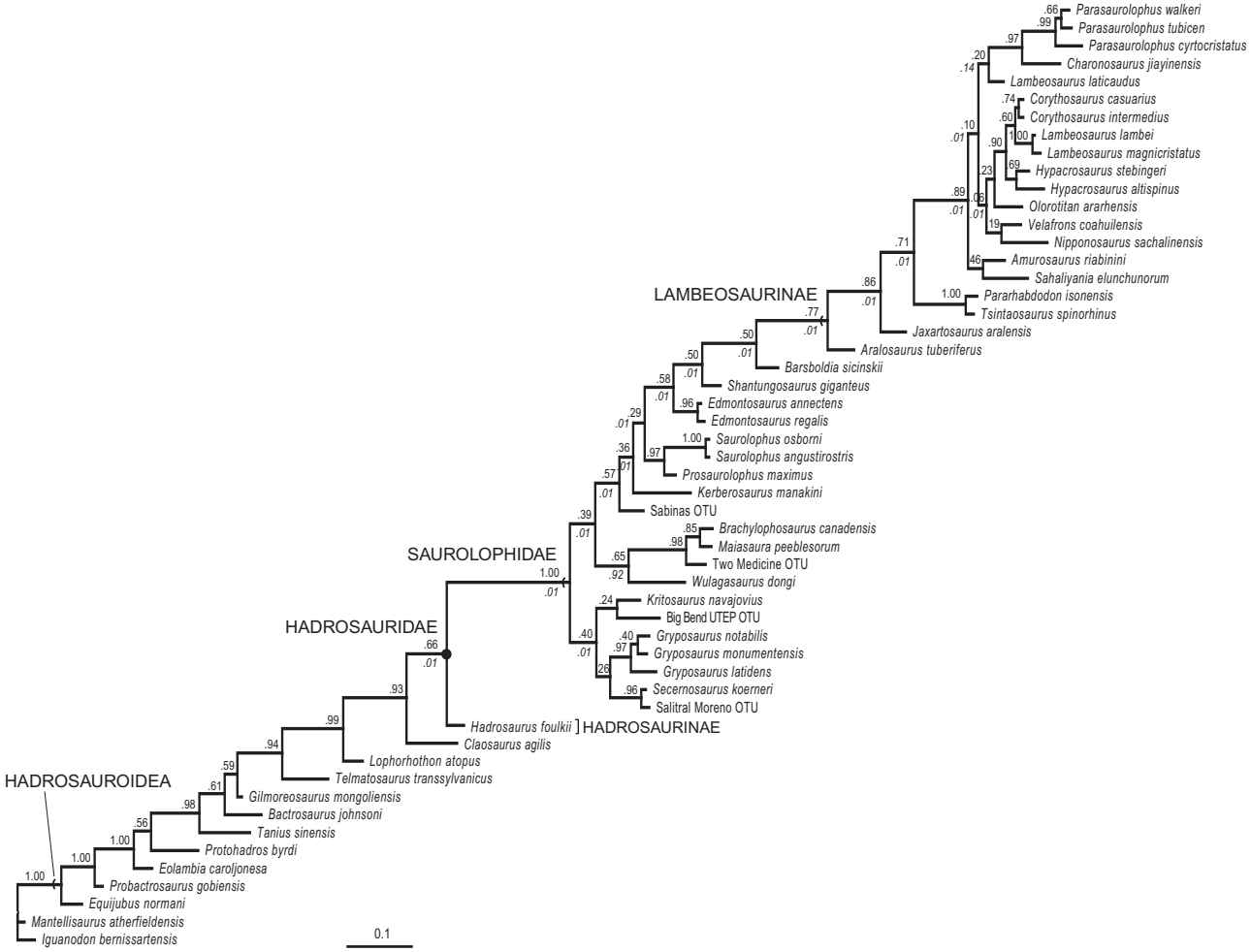

Figure 8. Bayesian consensus tree of the analysis with variable rates of character change showing the phylogenetic relationships of 53 iguanodontians. At each node, the decimal number above a branch indicates a posterior probability, whereas the decimal number below represents a *P* value of topology-dependant permutation tail probability (T-PTP) analysis.

(for example, there is no genus 'Euhadrosaurus', and thus, Euhadrosauria cannot be ranked as any family-group name). In this situation, I considered it more preferable to stretch the ICZN rules by nesting a family name within a family name rather than violting them by using an unranked taxon within a family.

HADROSAURIDAE

This study followed Cope's (1870) original concept of Hadrosauridae, where *Hadrosaurus foulkii* is the type genus and species of the family. Thus, Hadrosauridae was here redefined as the last common ancestor of *Hadrosaurus foulkii* Leidy, 1858, *Edmontosaurus regalis* Lambe, 1917b, *Saurolophus osborni* Brown, 1913, and *Lambeosaurus lambei* Parks, 1923, and all of its descendants (definition emended from Sereno, 1998; Wagner, 2001; Prieto-Marquez, 2008). According to the time-calibrated phylogram based on the strict reduced consensus tree derived from the parsimony analysis, hadrosaurids appeared no later than the Santonian (Fig. 10). Hadrosauridae was supported by four unambiguous synapomorphies: loss of all but the primary ridge of dentary tooth crowns [5(3), convergent in *Eolambia caroljonesa*]; ilium with ventralmost margin of the supra-acetabular process located anterodorsally relative to the caudoventral margin of the lateral ridge of the caudal protuberance of the ischial peduncle [235(1)]; short supra-acetabular process of the ilium, ratio between the breadth of the process across its dorsal region, and the craniocaudal length of the central iliac blade less than 0.55 [237(3), reversed in *Gryposaurus*, the *Secernosaurus* clade, the Sabinas saurolophine, the *Prosaurolophus* clade, *Brachylophosaurus canadensis* Sternberg, 1953, and *Maiasaura peeblesorum* Horner

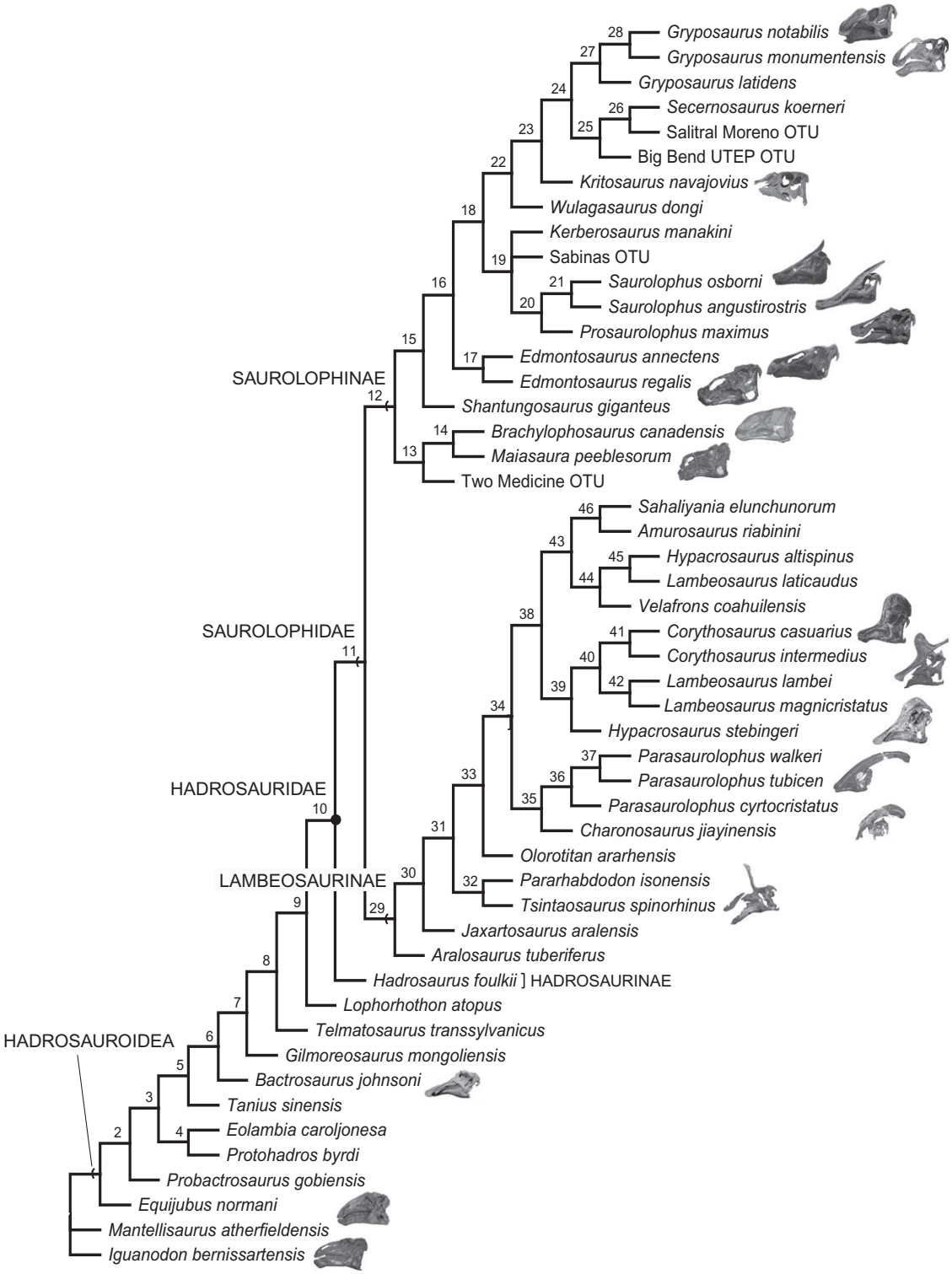

& Makela, 1979]; and ilium with lateral margin of the iliac peduncle progressively disappearing ventrally into the lateral surface of the region adjacent to the acetabular margin [257(1)].

Because the cranium of *Hadrosaurus foulkii* remains unknown (aside from a handful of teeth and a pair of poorly preserved maxillary fragments), numerous additional synapomorphies that might also

Figure 9. Strict reduced consensus tree of the 160 most parsimonious trees derived from maximium parsimony analysis, showing numbers for referring to the different clades of the phylogeny. The following list contains the synapomorphies supporting each clade, which are indicated by a pair of numbers. The number to the left of the dash is the character number corresponding to the list in the Appendix, whereas the number between brackets represents the character state. All the characters represent unambiguous synapomorphies, unless asterisks are present. An asterisk indicates an ambiguous synapomorphy under ACCTRAN. Two asterisks indicate an ambiguous synapomorphy under DELTRAN. Hadrosauroidea: 2(1), 37(1), 53(1), 79(1), 90(1), 115(1), 152(1), 187(0), 234(0). Clade 2: 5(1), 30(1), 41(2), 195(1). Clade 3: 60(1), 85(1), 92(1), 99(1), 232(1), 241(1), 264 (1), 266(1). Clade 4: 4(1), 34(1), 132(0), 257(1). Clade 5: 167(1), 220(1), 237(1), 239(1). Clade 6: 111(1), 161(1), 216(1), 236(1). Clade 7: 38(0), 90(2), 98(1), 242(2). Clade 8: 48(1), 97(2), 121(1), 198(1). Clade 9: 6(1), 89(0). Hadrosauridae: 5(3), 235(1), 237(3), 257(1). Saurolophidae: 7(1), 219(2), 221(1), 248(1). Saurolophinae: 32(1), 60(2), 64(1), 119(2), 191(1), 240(1), 267(2), 269(1). Clade 13: 35(2), 87(1), 98(2), 105(1), 110(2), 112(1), 143(1), 155(1), 158(2), 195(0). Clade 14: 126(1). Clade 15: 1(2), 15(2), 34(1), 220(1), 234(1), 238(1), 265(2), 282(0). Clade 16: 7(0), 123(1), 136(1), 200(0), 260(0), 270(0). Clade 17 (*Edmontosaurus*): 10(2), 29(1), 41(3), 65(1), 67(1), 77(2), 113(2), 130(2), 131(0), 160(1), 166(1), 168(0), 195(0). Clade 18: 33(1), 62(2), 85(0), 96(0), 109(0), 217(1), 253(4), 259(2), 284(1). Clade 19: 108(1)*, 158(0)*. Clade 20: 8(1)**, 41(3)**, 77(2)**, 78(2)**, 102(1)**, 113(0)**, 119(1)**, 120(0)**, 125(1)**, 170(2)**, 172(2)**, 180(1)**, 243(2)**. Clade 21 (*Saurolophus*): 60(1), 70(1), 123(0), 128(1), 131(2), 135(1), 136(2), 141(1), 143(2), 184(3), 201(1), 217(0), 220(2), 223(X), 262(1). Clade 22: 1(1), 35(1), 213(0). Clade 23: 33(0), 34(0), 36(2). Clade 24: 15(2), 35(2), 90(3). Clade 25: 206(1), 244(1), 245(3), 246(1). Clade 26: 200(1), 207(0), 238(0), 240(0), 270(2). Clade 27 (*Gryposaurus*): 33(2), 184(1), 243(2). Clade 28: 60 (1), 83(1). Lambeosaurinae: 84(1), 91(1), 193(1). Clade 30: 144(1), 147(0). Clade 31: 145(1), 150(1). Clade 32: 37(2), 40(0), 92(3). Clade 33: 5(3), 23(1), 24(3), 27(1), 35(1), 55(1), 56(1), 62(1), 73(2), 88(1), 122(2), 238(1). Clade 34: 103(2), 192(2). Clade 35: 115(0), 141(1), 145(2), 228(0), 243(0), 272(1), 274(1). Clade 36 (*Parasaurolophus*): 2(2), 218(1), 223(0), 236(3). Clade 37: 129(2), 131(0). Clade 38: 69(1), 80(1), 90(2), 131(0), 140(1), 173(1). Clade 39: 11(1), 22(0), 73(1). Clade 40: 34(1), 171(0), 262(1). Clade 41 (*Corythosaurus*): 214(1). Clade 42 (*Lambeosaurus*): 27(0), 72(1), 77(3), 80(0), 127(1), 159(1), 183(2). Clade 43: 9(2), 156(0), 278(0). Clade 44: 34(1), 244(1), 245(2). Clade 45: 270(2). Clade 46: 33(2), 36(2), 37(2), 150(2).

be diagnostic for hadrosaurids could only be ambiguously reconstructed. When the accelerated transformation option (ACCTRAN) was applied to the ancestral state reconstructions the following characters also became synapomorphic for Hadrosauridae: up to 32 tooth positions in the maxillary tooth row [15(1), convergent in *Protohadros byrdi*]; relatively elevated lateral surface of the rostrodorsal region of the maxilla [89(1), reversed in the *Brachylophosaurus* clade]; anterior apex of the rostral process of the jugal wedge-shaped, pointed, but not excessively elongated, with the dorsal magin of the apex forming a relatively steep angle with the horizontal [103(1), reversed in the *Brachylophosaurus* clade]; caudodorsal margin of the rostral process of the jugal that is 60–90% as deep as the rostral jugal constriction, and dorsally or slightly recurved caudodorsally, forming the rostroventral corner of the orbital rim [104(1)]; caudoventral apex of the rostral jugal process located ventral to the caudal margin of the lacrimal process (106[1], reversed in all saurolophines except the *Brachylophosaurus* clade); medial articular surface of the rostral process of the jugal facing medially, the articular surface is bounded only caudally by a rim of bone [107(1)]; squamosal buttress on the caudal margin of the dorsal end of the quadrate absent or poorly developed as a gentle convexity [120(0)]; extensive intersquamosal joint present at the midline, parietal completely excluded from the sagittal plane of the skull at that particular spot (in adults) [136(2)]; absence of frontal fontanelle [139(0), convergent in *Iguanodon bernissartensis*, *Mantellisaurus atherfieldensis*, and *Equijubus normani*]; coracoid reduced in size relative to the scapula [205(1)]; angle between the lateral margins of the facet for scapular articulation and the glenoid up to 115° [207(1), reversed in *Secernosaurus koerneri*, the Salitral Moreno OTU, *Tsintaosaurus spinorhinus*, and *Pararhabdodon isonensis*); concave anteromedial margin of the coracoid, associated with a relatively large and lateroventrally-projected biceps tubercle [208(1)]; moderately long 'hook-like' ventral process of the coracoid, ratio between the dorsoventral depth and the breadth of the process between 0.65 and 0.80 [209(1)]; recurved and caudoventrally directed ventral process of the coracoid [210(1), reversed in *Shantungosaurus giganteus*); curved and dorsally convex dorsal margin of the scapula, curvature originating at the level of the dorsal margin of the pseudoacromion process, and being most pronounced over the dorsoventral constriction [211(1), convergent in *Tanius sinensis* Wiman, 1929, and reversed in the Sabinas OTU]; relatively long scapula, ratio between its anteroposterior length and the dorsoventral depth of its proximal end greater than 4 [212(1), reversed in the *Kritosaurus navajovius* clade and *S. giganteus*); elongation of metacarpal V, so that it is more than twice as long as it is proximally wide [228(1), reversed in

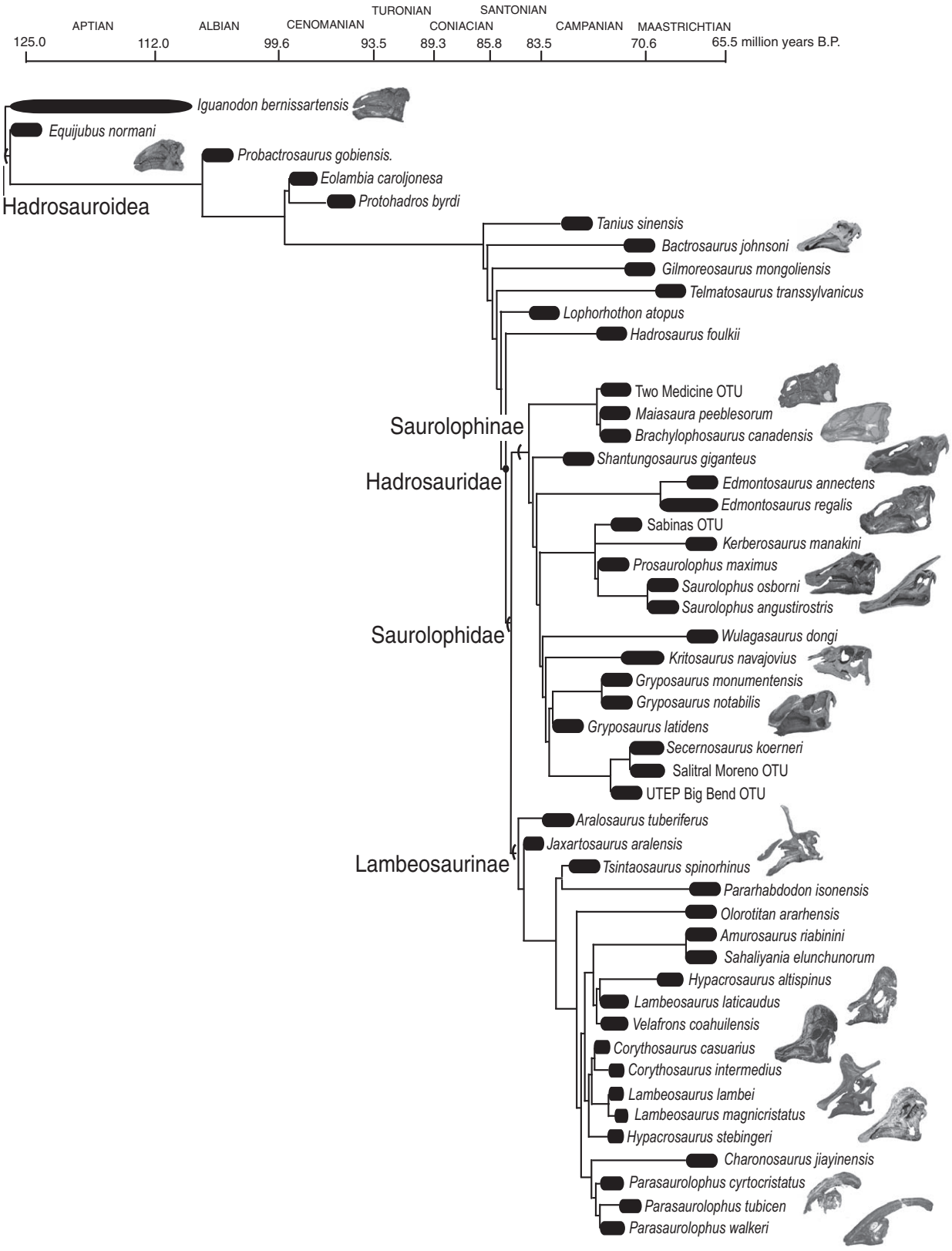

Figure 10. Time-calibrated phylogram based on the strict reduced consensus tree derived from maximum parsimony analysis of hadrosaurid relationships. The geochronological ages are taken from Gradstein, Ogg & Smith (2004).

Charonosaurus jiayinensis Godefroit *et al.*, 2000 and *Parasaurolophus*]; and mediolaterally broad and proximodistally shortened pedal unguals, rounded shield or hoof-like shaped, with reduced or absent claw grooves [285(1), convergent in *Bactrosaurus johnsoni*). On the other hand, the following ambiguous synapomorphy also supported Hadrosauridae when the delayed transformation option (DELTRAN) was applied to the ancestral state reconstructions: dorsoventrally thick and continuous lateral emargination of the ectopterygoid shelf, gradually thicker caudally than rostrally [99(2)].

Saurolophidae

This clade is defined as the last common ancestor of *Saurolophus osborni* Brown, 1913, *Lambeosaurus lambei* Parks, 1923, and all of its descendants (definition emended from Wagner, 2001; Prieto-Marquez, 2008). This clade represents the major split within Hadrosauridae into the hollow-crested lambeosaurines and all other forms that include flat-headed and solid-crested species. This split occurred no later than the Santonian, according to the time-calibrated phylogram based on the strict reduced consensus tree derived from the parsimony analysis (Fig. 10). Saurolophidae was supported by four unambiguous synapomorphies: presence of sinuous primary ridge in dentary tooth crowns [7(1), reversed in saurolophines except in the *Brachylophosaurus* clade and *Gryposaurus latidens* Horner, 1992]; long deltopectoral crest, with the ratio between the proximodistal length of the crest and the proximodistal length of the humerus greater than 0.55 [219(2), reversed in saurolophines except the Salitral Moreno OTU, *Saurolophus*, *Edmontosaurus*, and *Shantungosaurus giganteus*]; deltopectoral crest of the humerus extending abruptly from the humeral shaft to give a distinct angular profile [221(1)]; and caudodorsally oriented dorsal margin of the postacetabular proces of the ilium, rising dorsally relative to the acetabular margin [248(1), reversed in the Big Bend UTEP saurolophine].

Numerous ambiguous synapomorphies also supported Saurolophidae under DELTRAN, which are not documented because of poor preservation in the most immediate outgroup taxa, *Claosaurus agilis*, *Lophorhothon atopus*, and *Hadrosaurus foulkii*: three functional teeth throughout most of the dental battery, gradually decreasing to two near the rostral and caudal ends of the dentary [3(2)]; 33–44 tooth positions in the maxilla [15(1), convergent in *Protohadros byrdi*]; two functional teeth throughout most of the dental battery length, gradually changing to one near the rostral and caudal ends of the maxilla [17(2)]; predentary with an angle between its rostral surface and the dorsal margin of the lateral process of 40–55° [24(2), reversed in *Gryposaurus monumentensis* Gates & Sampson, 2007, *Kritosaurus navajovius*, and *Edmontosaurus*); subrectangular to rectangular predentary denticles [25(1), reversed in *Gryposaurus notabilis*]; predentary denticles limited to the rostral margin [28(1), convergent in *Bactrosaurus johnsoni*]; dorsal keel-like process of the predentary with well-developed ridge on the lingual surface of the rostral segment of the predentary, from which the former extends further caudally to lie dorsal to the dentary symphysis [31(1), convergent in *Protohadros byrdi*]; angle between the dentary symphysis and the lateral side of the rostral half of the dentary up to 15° [39(1), convergent in *P. byrdi*); dentary coronoid process rostrally inclined with an angle up to 68° [42(2)]; well-developed expansion of both the caudal and, especially, the rostral margin of the dorsal region of the coronoid process of the dentary [43(1)]; well-developed expansion of the lateral side of the dentary ventral to the coronoid process, with an angle between the lateral surface of the dentary and that of the region caudoventral to the coronoid process up to 165° [46(1)]; longitudinal axis of the dentary occlusal plane axis parallel with the lateral side of the dentary [47(1)]; caudal end of the dental battery located posterior to the caudal edge of the coronoid process [49(2)]; rostrodorsal process of the surangular reduced in thickness rostrocaudally, strap-like, and wedging dorsally into a thin sliver that becomes concealed in lateral view by the dorsal half of the caudal margin of the coronoid process [51(1)]; convex side of the lateral lap and the lateroventral surface of the main body of the surangular facing more ventrally than laterally [54(1)]; premaxillary oral margin very strongly deflected ventrally, so that, approximately, the dorsoventral distance between the occlusal plane and the level of the premaxillary oral margin is equal to or larger than the mean depth of the dentary [61(1), convergent in *P. byrdi*]; premaxillary oral margin with a 'double layer' morphology consisting of an external denticle-bearing layer and an internal layer of thickened bone set back slightly from the oral margin, and separated from the denticular layer by a deep sulcus bearing vascular foramina [63(1), convergent in *Bactrosaurus johnsoni*]; subtriangular articular surface for the jugal that is more laterally than dorsally facing, with a lateroventrally-directed pointed corner that is located adjacent and slightly dorsal to the proximal end of the lateral ridge of the ectopterygoid shelf [92(2)]; six or less maxillary foramina ventral and rostral to the jugal articulation (excluding large rostrodorsal or rostrolateral foramen) [94(1)]; dorsoventrally deep, with the caudodorsal margin of the rostral process of the jugal about 60–90% as deep as the rostral jugal constriction,

dorsally or slightly recurved caudodorsally, and forming the rostroventral corner of the orbital rim [104(1), convergent in *P. byrdi*]; medial articular surface of the rostral process of the jugal facing medially, being bounded only caudally by a rim of bone [107(1)]; elongated orbit, dorsoventrally deeper than it is wide [188(1)]; subtriangular occiput, with the quadrates laterally splayed distally [196(1)]; 12 or more cervical vertebrae [199(1)]; eight or more co-ossified vertebrae in the sacrum [202(1), convergent in *Iguanodon bernissartensis*]; coracoid reduced in size relative to the scapula [205(1)]; concave craniomedial margin of the coracoid, with a relatively large and lateroventrally-projected biceps tubercle [208(1)]; recurved ventral process of the coracoid, so that it is caudoventrally directed [210(1), reversed in *Shantungosaurus giganteus*]; curved dorsal margin of the scapula, dorsally convex, with the curvature originating at the level of the dorsal margin of the pseudoacromion process, most pronounced over the dorsoventral constriction [211(1), convergent in *Tanius sinensis* and reversed in the Sabinas saurolophine]; relatively long scapula, ratio between its anteroposterior length and the depth of the proximal region greater than 4 [212(1), reversed in the *Secernosaurus–Gryposaurus* clade and in *S. giganteus*]; ratio between the depth of the distal end of the scapular blade and the depth of the proximal region of the scapula, 1 or greater [213(1), convergent in *B. johnsoni* and reversed in the *Secernosaurus–Gryposaurus* clade and *S. giganteus*]; number of carpal bones reduced to a maximum of two unfused elements [225(1)]; absence of manual digit I [226(1)]; elongation of metacarpal V, so that it is more than twice as long as it is proximally wide [228(1), reversed in the *Charonosaurus–Parasaurolophus* clade]; and absence of distal tarsals II and III [280(1)]. Under ACCTRAN, Saurolophidae was also supported by an ambiguous synapomorphy: the presence of dentary marginal denticles with three or more indentations at the apex [10(0)].

Saurolophinae and a revised Hadrosaurinae

As explained before, historically, one of the two major subclades of hadrosaurids, Hadrosaurinae, included all forms with or without solid crests, and hypertrophied nasal passages with more or less developed circumnarial fossae exposed on the lateral side of the skull (Lull & Wright, 1942; Weishampel & Horner, 1990; Horner *et al.*, 2004). The clade was recovered in the consensus trees derived from all analyses except the Bayesian analysis with gamma. However, in all the phylogenies inferred in this study the name-bearing type of Hadrosaurinae, *Hadrosaurus foulkii*, was excluded from this clade. Articles 29.3 and 63 state that the stem of the family-group names must be based on the name of its type genus. Consequently, Hadrosaurinae must include the genus *Hadrosaurus*. Given the phylogenetic results of this study (Figs 5–8), this restricts the use of Hadrosaurinae to the lineage formed by *H. foulkii*. The sister clade to Lambeosaurinae was here given the name Saurolophinae, a term originally coined by Brown (1914). Saurolophinae is here defined as *Saurolophus osborni* and all taxa more closely related to it than to *Lambeosaurus lambei* or *Hadrosaurus foulkii* (definition emended from Wagner, 2001; Prieto-Marquez, 2008) (Fig. 9). According to the time-calibrated phylogram based on the strict reduced consensus tree derived from the parsimony analysis, saurolophine hadrosaurids appeared no later than the Lower Campanian (Fig. 10).

Numerous unambiguous synapomorpies supported Saurolophinae: predentary ventral process with long indentation and shallow undivided portion, with the splitting originating at a distance from the predentary ventral margin that is less than the mediolateral width of the process [32(1), reversed in *Gryposaurus notabilis* and *Gryposaurus monumentensis*]; very wide premaxilla, ratio between the maximum mediolateral width of the element and the minimum width at its narrowest point (post-oral constriction) greater than 2 [60(2), reversed in *G. notabilis* and *G. monumentensis*, and in *Saurolophus*]; presence of premaxillary foramen located rostrally and ventrolaterally to the anterior margin of the external naris [64(1)]; quadrate with wide arcuate and symmetrical quadratojugal notch, the ventral half of the notch being rostroventrally-directed and nearly straight, as it is the dorsal half [119(2), reversed in the *Prosaurolophus–Saurolophus* clade]; subtriangular infratemporal fenestra, with a dorsal margin that is narrower than the ventral one [191(1), reversed in the *Kritosaurus* clade]; supra-acetabular process of the ilium with a caudodorsal margin that is poorly defined and appears discontinuous with the dorsal margin of the proximal region of the postacetabular process because of the lack of a well-demarcated caudodorsal ridge [240(1), reversed in *Gryposaurus latidens*, *Secernosaurus koerneri*, the Salitral Moreno saurolophine, and *Prosaurolophus maximus*]; pubic peduncle of the ischium oriented parallel with the ischial shaft [267(2), reversed in *Saurolophus*]; and ischium with dorsal acetabular margin of the pubic peduncle set dorsal to the dorsal margin of the ischial shaft [269(1), reversed in *Saurolophus angustirostris* Rozhdestvensky, 1952 and the Salitral Moreno saurolophine].

In addition, the following ambiguous synapomorphies supported Saurolophinae under ACCTRAN: dentary marginal denticles absent or reduced to small

papillae along the apical half of the dorsal half of the tooth crown [9(2), convergent in *Bactrosaurus johnsoni*]; rostrocaudally constricted dorsal region of the infratemporal fenestra, caused by the presence of a nearly straight and oblique caudoventral margin of the caudodorsal region of the postorbital (dorsal region of infratemporal fenestra typically subtriangular) [129(1), reversed in the *Kritosaurus–Gryposaurus* clade]; relatively long parietal, maximum length/minimum width ratio greater than 2.35 [147(2)]; proximal caudal vertebrae with chevrons longer than the neural spines [203(1)]; and scapula with dorsoventrally deep and craniocaudally long deltoid ridge, with a well-demarcated ventral margin of the deltoid ridge [218(1), convergent in *B. johnsoni*, *Gilmoreosaurus mongoliensis*, *Parasaurolophus*, and reversed in *Shantungosaurus giganteus*).

Under DELTRAN, Saurolophinae was supported by the following ambiguous synapomorphies: predentary where the separation between two consecutive denticles is smaller than the basal width of each individual denticle, but larger than 25% of its basal breadth [26(1)]; presence of premaxillary foramen located rostrally and ventrolaterally to the rostral margin of the external naris [64(1), convergent in *Tsintaosaurus spinorhinus* and reversed in the Salitral Moreno saurolophine]; large rostral maxillary foramen opening on the rostrolateral body of the maxilla, within the dorsal half of the rostrodorsal margin of the element, and exposed in lateral view [95(1)]; angle between the ventral margins of the basispterygoid processes of the basisphenoid, 100° or greater [154(1), convergent in *Tanius sinensis*, *T. spinorhinus*, and reversed in *Kerberosaurus manakini*]; caudal margin of the functional external naris composed entirely by the nasal [177(1)]; pseudoacromion process of the scapula horizontal, occasionally with minor and subtle dorsal or ventral curvatures, so that the cranial region is cranially or mostly cranially directed [215(1), convergent in *Lophorhothon atopus*]; and relatively long ulna, up to 20% longer than the humerus [224(1), convergent in the *Charonosaurus–Parasaurolophus* clade].

The position of the Brachylophosaurus clade

Previous analyses have regarded the clade including *Brachylophosaurus canadensis* and *Maiasaura peeblesorum* as most closely related to *Gryposaurus* (Weishampel & Horner, 1990; Weishampel *et al.*, 1993; Kirkland, 1998; Hu *et al.*, 2001; Gates & Sampson, 2007), as sister clade to *Edmontosaurus* (Horner *et al.*, 2004), as sister clade to a monophyletic group composed of *Gryposaurus*, *Saurolophus*, and *Prosaurolophus* (Prieto-Márquez, 2005; Prieto-Márquez *et al.*, 2006a), or as a basal saurolophine (Horner, 1992; Godefroit *et al.*, 2008). A close relationship between the *Brachylophosaurus* clade and *Gryposaurus* was only supported in the phylogeny derived from the Bayesian analysis without the gamma parameter (Fig. 7). The other two analyses (Bayesian with gamma and parsimony) supported a basal position of the *Brachylophosaurus* clade within Saurolophinae. In particular, both the strict (Fig. 5) and reduced strict (Fig. 6) consensus trees of the preferred (parsimony) phylogeny recovered the *Brachylophosaurus* clade as the sister clade to all other saurolophines. Unambiguous synapomorphies present in all saurolophines, with the exception of the *Brachylophosaurus* clade, include: more than 42 tooth positions in the dentary dental battery [1(2)]; 45 or more tooth positions in the maxillary dental battery [15(2)]; angle between the dentary proximalmost edentulous slope and the occlusal plane of 150° or more [34(1)]; moderately expanded deltopectoral crest of the humerus, with ratio between the width of the humerus across the distal fourth of the deltopectoral crest and the width of the distal shaft at the point of maximum curvature between 1.65 and 1.90 [220(1)]; ratio between the depth of the central plate of the ilium and the distance between the pubic peduncle and the caudodorsal prominence of the ischial peduncle less than 0.8 [234(1)]; long iliac peduncle of the ischium, ratio between the proximodistal length and the craniocaudal width of the distal margin greater than 2 [265(2)]; and length/width ratio of metatarsal III less than 4.5 [282(0)].

The position of the Prosaurolophus–Saurolophus clade

The relationship of *Prosaurolophus* and *Saurolophus* within saurolophines represents one of the most notable cases of character conflict among hadrosaurids. On one hand, the facial anatomy of *Prosaurolophus* and *Saurolophus* shares a number of characters with *Edmontosaurus*, such as the elongated mandible with more than 50 alveolar positions per tooth row, and the deeply excavated caudal region of the circumnarial fossa. On the other hand, several other characters are shared between the *Prosaurolophus–Saurolophus* clade and *Gryposaurus*, such as a thin and reflected premaxillary oral margin and a prepubic blade with a squared dorsal margin. Thus, previous analyses have shown that the *Prosaurolophus–Saurolophus* clade was either closely related to *Edmontosaurus* (Weishampel & Horner, 1990; Weishampel *et al.*, 1993; Kirkland, 1998; Gates & Sampson, 2007; Godefroit *et al.*, 2008) or to *Gryposaurus* (Prieto-Márquez, 2005; Prieto-Márquez *et al.*, 2006a). None of the phylogenetic analyses of this study supported the close relationship of the *Prosaurolophus–Saurolophus* clade with *Edmontosaurus*. Instead, all but the Bayesian analysis with

gamma recovered *Prosaurolophus* and Saurolophus as being most closely related to a clade including *Gryposaurus* and *Kritosaurus* (Figs 5–7). In the preferred phylogeny (Fig. 6), unambiguous synapomorphies uniting the *Prosaurolophus–Saurolophus* clade with the clade including *Gryposaurus* are: ratio between the length of the proximal edentulous slope of the dentary and the distance between the rostralmost tooth position and the caudal margin of the coronoid process between 0.20 and 0.31 [33(1)]; oral premaxillary margin folded caudodorsally into a thin recurved edge [62(2)]; lack of lateral exposure of the rostrodorsal process of the maxilla through the narial foramen [85(0)]; maxilla–lacrimal contact present externally [96(0)]; wide and shallow embayment forming the ventral margin of the jugal, between the caudoventral flange and the rostral process [109(0)]; relatively short craniodorsal region of the scapula [217(1)]; rectangular to subrectangular prepubic process of the pubis, craniocaudally longer than dorsoventrally tall, nearly straight profiles of the dorsal and ventral proximal margins [253(4)]; pubis with proximal constriction and distal expansion of approximately the same length [255(1)]; length/width ratio of the ischial peduncle of the pubis, 3 or more [259(2)]; and disc-shaped pedal phalanges III2 and III3 being more than three times wider than they are proximodistally long [284(1)].

The position of Barsboldia sicinskii

This poorly known hadrosaurid from the Nemegt Formation of Mongolia has long been considered a lambeosaurine (Maryanska & Osmolska, 1981; Weishampel & Horner, 1990; Horner *et al.*, 2004), based on the great elongation of the neural spines of the sacral and anterior caudal vertebrae (Maryanska & Osmolska, 1981). However, the lambeosaurine affinities of *Barsboldia sicinskii* were not supported in the present study. In contrast, in both the Bayesian and parsimony consensus trees, this species was recovered as a member of Saurolophinae (Figs 5, 7, 8). Unambiguous synapomorphies supporting the inclusion of *B. sicinskii* within Saurolophinae in the strict consensus tree of the parsimony analysis include an ilium with caudodorsal margin that is poorly defined and appears discontinuous with the dorsal margin of the proximal region of the postacetabular process, because of the lack of a well-demarcated caudodorsal ridge [240(1)].

Lambeosaurinae

The clade of 'hollow-crested' hadrosaurids was redefined here as *Lambeosaurus lambei* Parks, 1923 and all taxa more closely related to it than to *Hadrosaurus foulkii* Leidy, 1858, *Saurolophus osborni* Brown, 1913, or *Edmontosaurus regalis* Lambe, 1917b (definition emended from Sereno, 1998; Wagner, 2001; Prieto-Marquez, 2008). According to the time-calibrated phylogram based on the strict reduced consensus tree derived from the parsimony analysis, lambeosaurine hadrosaurids appeared no later than the Santonian (Fig. 10). Lambeosaurine monophyly was supported by the following unambiguous synapomorphies: absence of rostrodorsal process of the maxilla, so that the rostral end of the element forms a ventrally sloping rostrodorsal shelf that underlies the premaxilla [84(1)]; dorsal process of the maxilla dorsoventrally taller than it is wide, with a peaked and caudally inclined apex [91(1)]; and oval supratemporal fenestra, with the long axis directed rostrolaterally [193(1)].

The incompletely known *Aralosaurus tuberiferus* caused the following characters to be ambiguous synapomorphies, and these characters also supported Lambeosaurinae when ACCTRAN was applied to the ancestral state reconstructions: subsquared rostrolateral corner of the predentary [29(1), convergent in *Protohadros byrdi*, *Eolambia caroljonesa*, and *Edmontosaurus*); elongate caudodorsal process of the premaxilla that extends caudally to meet the caudoventral process, forming the caudal margin of the external naris [68(1)]; large rostral maxillary foramen opening on the dorsal surface of the maxilla along the maxilla–premaxilla contact, not exposed laterally [95(2)]; triangular adult lacrimal, rostrocaudally abbreviated with a relatively shorter and thinner rostral process [101(1)]; ventrally projected, triangular, and narrow caudoventral margin of the rostral process of the jugal, at least twice as deep as it is wide, sharply pointed and often recurved caudally [105(2)]; caudal margin of the dorsal half or third of the quadrate that is strongly curved caudally relative to the ventral half of the element, showing an angle of less than 150° [116(1), convergent in *Iguanodon bernissartensis* and *Shantungosaurus giganteus*]; midpoint of the quadratojugal notch of the quadrate located near the mid-length of the element, ratio between the distance from the mid-length of the notch to the qudadrate head and the dorsoventral length of the element less than 0.60 [117(0), convergent in *Iguanodon bernissartensis*, *Mantellisaurus atherfieldensis*, *Equijubus normani*, and *Eolambia caroljonesa*); frontal completely excluded from the orbital margin by an extensive articulation between the prefrontal and postorbital [143(2), convergent in *Saurolophus*]; sharp annular ridge of the frontal [146(1)], [148(1), convergent in *Saurolophus osborni*]; nasal passage nearly or completely enclosed by bone and formation of internal cavities and passages (such as lateral diverticula and a common median chamber) [169(1)]; nasal passage

not extending caudally to the occiput, with a nasal vestibule that flanks a common median chamber [176(1)]; caudal margin of the functional external naris composed entirely by the premaxilla [177(2)]; absence of circumnarial fossa on the lateral surface of the facial region of the skull, circumnarial fossa entirely enclosed [178(0)]; slightly elongated neural spines in the cranial dorsal vertebrae, forming a 'wither-like' region above the pectoral girdle [201(1), convergent in *Saurolophus* and *Saurolophus giganteus*]; recurved pseudoacromion process of the scapula, so that the cranial region is dorsally or craniodorsally directed [215(0), convergent in *I. bernissartensis*, *M. atherfieldensis*, *E. normani*, *E. caroljonesa*, *P. byrdi*, *Tanius sinensis*, *Bactrosaurus johnsoni*, and *Gilmoreosaurus mongoliensis*]; greatly expanded deltopectoral crest of the humerus, ratio between the width of the humerus across the distal fourth of the deltopectoral crest and the width of the distal shaft greater than 1.90 [220(2), convergent in *Wulagasaurus dongi* and *Saurolophus*]; ulna more than 20% longer than the humerus [224(2), reversed in the *Charonosaurus–Parasaurolophus* clade and *Brachylophosaurus canadensis*]; prepubic process of the pubis with subsquared distal dorsal margin, expansion dorsoventrally taller than cranioventrally long, very pronounced proximal dorsal concavity and nearly straight distal ventral margin [253(1)]; presence of a well-developed curvature in the posterodorsal corner of the distal margin of the iliac peduncle of the ischium, so that the peduncle appears 'thumb-like' in lateral and medial profiles [263(2)]; ventrally expanded distal end of the ischial shaft, forming a large 'foot' or 'boot-like' process [271(1), convergent in *I. bernissartensis*, *M. atherfieldensis*, *E. normani*, *E. caroljonesa*, *P. byrdi*, *T. sinensis*, *B. johnsoni*, and *G. mongoliensis*); club-shaped distal end of the fibula, with a concave cranial margin and prominent cranial expansion [278(1), convergent in *T. sinensis* and reversed in the *Hypacrosaurus altispinus–Amurosaurus* clade]; short medial platform of the astragalus, wedging laterally, underlying only part of the medial malleolus of the tibia [279(1)]; pedal phalanges III2 and III3 more than three times wider than they are proximodistally long [284(1), convergent in saurolophines except the *Brachylophosaurus* clade, *Shantungosaurus giganteus*, and *Edmontosaurus*). No ambiguous synapomorphies were found under DELTRAN.

The position of Olorotitan ararhensis

This species of lambeosaurine was described by Godefroit *et al.* (2003) from material collected in Maastrichtian strata near Kundur, in the Amur region of Far Eastern Russia. Previous phylogenies have shown *Olorotitan ararhensis* as most closely allied to the *Corythosaurus* clade (Godefroit *et al.*, 2003; Evans & Reisz, 2007; Gates *et al.*, 2007; Godefroit *et al.*, 2008). In this study, this hypothesis was supported in both Bayesian analyses, where *O. ararhansis* was recovered as the sister taxon to a clade composed of *Corythosaurus*, *Lambeosaurus*, and *Hypacrosaurus* (Figs 7, 8). In contrast, the strict reduced consensus tree of the parsimony analysis recovered *O. ararhensis* as a basal species, the sister taxon to a clade including all lambeosaurines except *Tsintaosaurus spinorhinus*, *Pararhabdodon isonensis*, *Jaxartosaurus aralensis*, and *Aralosaurus tuberiferus*. Unambiguous synapomorphies uniting *O. ararhensis* to the clade composed of all lambeosaurines except *T. spinorhinus*, *P. isonensis*, *J. aralensis*, and *A. tuberiferus* include: dentary tooth crowns with a primary ridge and one or two faint and shorter ridges [5(2)]; ratio between the dorsoventral depth of the predentary rostral face (excluding the median ventral process) and the length of the lateral process of 0.38 or less [23(1)]; angle of the predentary rostral surface relative to the dorsal margin of the lateral process of 40° or less, gently rounded rostral surface [24(3)]; presence of six predentary denticles in adult individuals lateral to the median denticle [27(1)]; angle between the proximal slope of the edentulous margin of the dentary that articulates with the predentary and the horizontal between 113° and 128° [35(1)]; presence of lateral curvature of the caudal process of the surangular [55(1)]; angle between the medial margin of the proximal region of the surangular and the medial margin of the proximal region of the caudal process of the element up to 148° [56(1)]; premaxilla with moderately expanded oral margin, becoming thinner towards the parasagittal plane of the snout [62(1)]; triangular and rostrocaudally compressed lateral surface of the rostrodorsal region of the maxilla [88(1)]; dorsomedial margin of the prefrontal developed into a caudodorsally oriented crest, which extends caudally over the dorsal surface of the frontal and above the prefrontal–postorbital articulation in lateral view in adults [122(2)]; and iliac supra-acetabular process symmetrical or with a slightly caudally skewed profile [238(1)]. Likewise, the following two unambiguous synapomorphies are lacking in *O. ararhensis*, but are present in all lambeosaurines except *T. spinorhinus*, *P. isonensis*, *J. aralensis* Riabinin, 1939, and *A. tuberiferus*: rostral apex of the rostral process of the jugal greatly reduced to a blunt convexity [103(2)]; and dorsal margin of the infratemporal fenestra lying slightly or substantially below the level of the dorsal margin of the orbit, with the caudal region of the skull roof being subhorizontal or slightly sloping caudoventrally relative to the frontal plane [192(2)].

The position of Hypacrosaurus stebingeri

Horner, Varricchio & Goodwin (1992) originally regarded this species from the late Campanian of the Two Medicine Formation of Montana, USA, and the Oldman Formation of Alberta, Canada, as having evolved anagenetically from a taxon closely related to *Lambeosaurus* spp. These authors pointed out that *Hypacrosaurus stebingeri* had a cranial crest mostly composed of premaxillae, as in *Lambeosaurus*, and a reduced narial opening, as in *Hypacrosaurus altispinus*. From this, they deduced that *H. stebingeri* was a metaspecies, a taxon that had evolved through anagenesis from a species of *Lambeosaurus*. However, examination of the type skull of *H. stebingeri*, MOR 549, supports Evans, Forster & Reisz (2005) and Evans & Reisz (2007) in that the narial opening is very elongated and not restricted, as in species of *Lambeosaurus* and *Corythosaurus*. Furthermore, although the premaxilla forms a large part of the crest in *H. stebingeri*, its contribution in no way approaches the condition in *Lambeosaurus*. Nevertheless, *H. stebingeri* also have greatly elongated dorsal vertebral neural spines, as in *H. altispinus*.

Two recent phylogenetic analyses inferred the position of *H. stebingeri* as the sister taxon to *H. altispinus* (Evans & Reisz, 2007; Gates *et al.*, 2007), whereas other studies could not resolve its position beyond its being a lambeosaurine hadrosaurid (Suzuki *et al.*, 2004; Prieto-Márquez *et al.*, 2006a). In the present study, all the analyses supported *H. stebingeri* as being closely related to the *Lambeosaurus–Corythosaurus* clade. However, the parsimony analysis recovered a paraphyletic *Hypacrosaurus*, with *H. stebingeri* as the sister taxon to the *Lambeosaurus–Corythosaurus* clade (Figs 5, 6). Unambiguous synapomorphies supporting *H. stebingeri* as the sister taxon to the *Lambeosaurus–Corythosaurus* clade in the preferred parsimony strict reduced consensus tree are: dentary tooth crowns with mesial margin having larger denticles than the distal one [11(1)]; ratio between the predentary maximum mediolateral width and the maximum rostrocaudal length along the lateral process less than 1.2 [22(0)]; and triangular and very long external naris (length/width ratio greater than 2.85), with a caudal constriction gradually closing caudodorsally [73(1)]. In contrast, both Bayesian analyses showed a monophyletic *Hypacrosaurus* (composed of *H. altispinus* and *H. stebingeri*) as the sister clade to the *Lambeosaurus–Corythosaurus* clade (Figs 7, 8). Unambiguous synapomorphies supporting the monophyly of *Hypacrosaurus*, shared by *H. altispinus* and *H. stebingeri* in both Bayesian trees, are: height/width ratio of the dentary tooth crowns greater than 3.3 [4(3)]; very long dorsal and sacral neural spines, ratio of the height of the neural spine relative to that of the centrum of the tallest posterior dorsal or sacral vertebrae greater than 3.25 [200(2)]; and length/width ratio of metatarsal III less than 4.5 [282(0)].

The position of Nipponosaurus sachalinensis

This taxon is known from a partially preserved juvenile specimen collected from the Late Santonian–Early Campanian Upper Yezo Group of South Sackhalin, Russia (Nagao, 1936; Suzuki *et al.*, 2004). Previous analyses have hypothesized a close relationship between *Nipponosaurus sachalinensis* and *Hypacrosaurus altispinus* (Suzuki *et al.*, 2004) or positioned the former species as the sister taxon to a clade formed by *Corythosaurus*, *Lambeosaurus*, and *Hypacrosaurus* (Evans & Reisz, 2007). In contrast to Suzuki *et al.* (2004) and Evans & Reisz (2007), I did not score *N. sachalinensis* as having an angular ventral flange of the jugal (character 21 in Suzuki *et al.*, 2004). This is because the presence of such a character in *N. sachalinensis* is ambiguous at best, as previously noted by Evans (2007b). Figure 3 of Suzuki *et al.* (2004) shows that the ventral flange of the jugal in UHR 6590 is incomplete. Reconstruction of the ventral margin of the flange as angular is only one of the many possible profiles that this region of the jugal may have had. A more rounded ventral margin is also possible, given the amount of bone missing in the jugal flange in this exemplar. Thus, an angular ventral flange of the jugal was only observed with certainty in specimens of *H. altispinus* (e.g. ROM 702), and thus constitutes an autapomorphy of this species. In this study, the position of *N. sachalinensis* could not be resolved using parsimony, reflecting the labile phylogenetic placement of this taxon recognized by Evans & Reisz (2007). The strict consensus tree of the parsimony analysis showed *N. sachalinensis* as part of a clade including all lambeosaurines, to the exception of *Tsintaosaurus spinorhinus*, *Pararhabdodon isonensis*, *Jaxartosaurus aralensis*, and *Aralosaurus tuberiferus* (Fig. 5). In contrast, the position of *N. sachalinensis* could be resolved in the two Bayesian analyses, although it differed between the two Bayesian analyses. Thus, in the tree summarizing the results of the Bayesian analysis without gamma, *N. sachalinensis* was positioned outside the clade including *Corythosaurus* and *Parasaurolophus* (Fig. 7). This position was unambiguously supported by the presence of sinuous primary ridges on maxillary tooth crowns [20(1)]. Finally, the tree derived from the Bayesian analysis without gamma recovered *N. sachalinensis* as the sister taxon to *Velafrons coahuilensis*, with both taxa forming a basal clade within the *Corythosaurus* clade. This position of the *N. sachalinensis–V. coahuilensis* clade was unambiguously supported by an angle between the dentary proximalmost edentulous slope and the tooth row of

150° or greater [34(1)], and subrectangular dorsal margin of the infratemporal fenestra, with a dorsal infratemporal margin that is approximately as wide as the ventral margin [191(0)].

The status of Lambeosaurus laticaudus Morris, 1981

This lambeosaurine was described from partial cranial and postcranial elements collected in Campanian deposits of El Gallo Formation in Baja California, Mexico (Morris, 1981). None of the phylogenetic analyses conducted in the present study supported the inclusion of *Lambeosaurus laticaudus* in the genus *Lambeosaurus*. However, no consensus was found regarding the phylogenetic position of this taxon among all the phylogenies resulting from this study. Thus, *L. laticaudus* was recovered as a member of the *Hypacrosaurus* clade in the strict reduced consensus of the parsimony analysis (Fig. 6), as a relatively basal lambeosaurine in the Bayesian analysis without gamma (Fig. 7), and as a basal member of the Parsaurolophus clade in the Bayesian analysis with gamma (Fig. 8). In the strict reduced consensus tree of the preferred parsimony, unambiguous synapomorphies supporting the inclusion of *L. laticaudus* in a clade with *Velafrons coahuilensis* and *Hypacrosaurus altispinus* are: angle between the dentary proximalmost edentulous slope and the horizontal of between 113° and 128° [34(1)]; presence of brevis shelf at the base of the postacetabular process of the ilium [244(1)]; and presence of a well-defined ridge on the medial side of the postacetabular process, forming the medial margin of a medioventrally-facing shelf, with a postacetabular process that is progressively expanded mediolaterally towards the caudal end [245(2)]. Likewise, a single unambiguous synapomorphy supported *L. laticaudus* as the sister taxon to *H. altispinus*: a very thick ischial shaft, of thickness greater than 7.5% the length of the shaft [270(2)].

CONCLUSIONS

Parsimony and Bayesian analyses (Mk model with and without the gamma parameter) were conducted on a complete taxonomic sample of hadrosaurid species. Hadrosauridae was redefined as the clade stemming from the most recent common ancestor of *Hadrosaurus foulkii* and *Parasaurolophus walkeri*. Parsimony and Bayesian analysis using the Mk model without the gamma parameter confirmed the evolution of hadrosaurids into Saurolophinae (Hadrosaurinae of most previous authors) and Lambeosaurinae. Saurolophines consisted of *Edmontosaurus*, *Shantungosaurus giganteus*, *Barsboldia sicinskii*, and a speciose clade composed of the *Prosaurolophus–Saurolophus* and the *Kritosaurus–Gryposaurus–Secernosaurus* subclades. Lambeosaurines consisted of a succession of Eurasian taxa leading to a speciose clade composed of the *Parasaurolophus* and the *Hypacrosaurus altispinus–Corythosaurus* subclade. The *Brachylophosaurus* clade was recovered as the most basal saurolophine clade in the strict and strict reduced consensus trees derived from parsimony analysis, whereas it was positioned as a sister clade to the *Kritosaurus–Gryposaurus–Secernosaurus* clade in the consensus tree derived from the Bayesian analysis without gamma. In contrast, the topology derived from the Bayesian analysis using the Mk model with the gamma parameter resulted in an unbalanced hadrosauroid tree containing a paraphyletic Saurolophinae. Saurolophines such as *Edmontosaurus*, *Shantungosaurus giganteus*, and *Barsboldia sicinskii* were recovered as successively closer sister taxa to Lambeosaurinae. In general, the interrelationships among lambeosaurine taxa did not differ substantially in the latter analysis, with the recovery of a speciose clade composed of the *Parasaurolophus* and *Corythosaurus* subclades.

ACKNOWLEDGEMENTS

This study represents the main subject of my doctoral dissertation conducted in the graduate program of the Department of Biological Science at Florida State University. I am especially grateful to my advisor G.M. Erickson and committee members W.C. Parker, S.J. Steppan, D.L. Swofford, and F. Ronquist. I am also thankful to everyone who allowed access to specimens in their care: P. Barrett, B. Battail, M. Brett-Surman, D. Brinkman, K. Carpenter, S. Chapman, J. Cheng, L. Chiappe, Z. Csiki, R. Culbertson, T. Culver, P. Currie, T. Daeschler, R. Dante, C. Delgado, J. Desojo, B. Espinosa, D. Evans, Z. Fang, M. Feuerback, R. Gaete, A. Galobart, E. García, J. Gardner, T. Gates, M. Getty, P. Godefroit, M. del R. Gómez, M. Goodwin, D. Goujet, D. Grigorescu, A. Heckert, A. Henrici, R. Hernández, P. Holroyd, J. Horner, B. Iwama, B. Jacobs, L. Jacobs, Y. Jun, J. Kobalynski, A. Kramarz, M. Lamanna, J. Lamb, W. Langston, T. Lehman, C. de León, L. Liping, J. Li-Young, S. Lucas, E. Lund, K. Madalena, S. Maganuco, P. Makovicky, B. McLeod, C. Mehling, M. Montellano, I. Morrison, C. Muñoz, L. Murray, M. Norell, H. Osmolska, P. Owen, J. Padilla, J. Peel, M. del C. Perrillat, M. Pierce, G. Plodowski, Z. Qin, R. Reisz, L. Rinehart, T. Rowe, K. Sabath, G. Salinas, C. Dal Sasso, C. Serrano, K. Seymour, K. Shepherd, W. Simpson, E. Steurbaut, S. Stuenes, L. Tao, P. Taquet, D. Vineyard, O. Vogel, D. Weishampel, C. Weißbrod, D. Winkler, X. Xu, L. Zanno, R. Zapata, K. Zhang, L. Zhong, and R. Zúñiga. K. Seltmann assisted in the use of Morphbank. J.R. Wagner, D. Evans, T. Gates, G. Salinas, and M.

Guenter provided enlightening advice and discussions on hadrosaurid anatomy. M. Marzin, G. Salinas, P.J. Makovicky, T. and I. Krupa, L. and B. Jacobs, Z. Csiki, R. Hernández, R. Gaete, P.J. Currie, and M. del Rosario Gómez provided logistical assistance during travel for specimen-based reseach. I am also grateful to the advice provided by J.R. Wagner, P. Barrett, D.C. Evans, T. Gates, L. Zanno, R.J. Butler, J. Müller, M. Wilkinson, J. Carpenter, and J. Conrad in various aspects of this research. This study owes much to the generosity of T. and M. Kohler, who provided most of the financial support through a Charlotte and Walter Kohler Charitable Trust. Additional funds were provided by the Department of Biological Science at Florida State University, the National Science Foundation (EAR 0207744 and DBI 0446224 grants presented to Gregory M. Erickson), The Field Museum, and a grant (CGL2005-07878-C02-01) from the Ministry of Education and Science of Spain presented to A. Galobart.

REFERENCES

Abramoff MD, Magelhaes PJ, Ram SJ. 2004. Image processing with ImageJ. *Biophotonics International* **11:** 36–42.

Apesteguia S. 2005. A late Campanian sphenodontid (Reptilia, Diapsida) from northern Patagonia. *Comptes Rendus Palevol* **4:** 663–669.

Averianov AO. 2007. Theropod dinosaurs from Late Cretaceous deposits in the northeastern Aral Sea region, Kazakhstan. *Cretaceous Research* **28:** 532–544.

Averianov AO, Nessov L. 1995. A new Cretaceous mammal from the Campanian of Kazakhstan. *Neues Jahrbuch Für Geologie Und Paläontologie, Montshefte* **1995:** 65–74.

Bolotsky Y, Kurzanov SK. 1991. The hadrosaurs of the Amur Region [in Russian]. In: Moiseyenko VG, ed. *[*Geology of the Pacific Ocean border*]*. Blagoveschensk: Amur KNII, 94–103 [In Russian].

Bolotsky YL, Godefroit P. 2004. A new hadrosaurine dinosaur from the Late Cretaceous of Far Eastern Russia. *Journal of Vertebrate Paleontology* **24:** 351–365.

Bonaparte JF, Franchi MR, Powell JE, Sepulveda EG. 1984. [The Alamitos Formation (Campanian-Maastrichtian) from southeastern Rio Negro, with description of *Kritosaurus australis* n. sp. (Hadrosauridae). Paleogeographical meaning of the vertebrates]. *Revista de la Asociacion Geologica de Argentina* **39:** 284–299 [In Spanish].

Bookstein FL, Chernoff BC, Elder RL, Humphries JM, Smith GR, Strauss RE. 1985. Morphometrics in evolutionary biology. *Academy of Natural Sciences of Philadelphia Special Publication* **15:** 1–277.

Bremer K. 1988. The limits of amino acid sequence data in angiosperm phylogenetic reconstruction. *Evolution* **42:** 795–803.

Brett-Surman MK. 1975. The appendicular anatomy of hadrosaurian dinosaurs. Master's thesis, University of California, Berkeley.

Brett-Surman MK. 1979. Phylogeny and palaeobiogeography of hadrosaurian dinosaurs. *Nature* **277:** 560–562.

Brett-Surman MK. 1989. *A revision of the Hadrosauridae (Dinosauria: Ornithischia) and their evolution during the Campanian and Maastrichtian*. 272 pp. Unpublished PhD dissertation, George Washington University, Washington, DC.

Brett-Surman MK, Wagner JR. 2007. Discussion of character analysis of the appendicular anatomy in Campanian and Maastrichtian North American hadrosaurids – variation and ontogeny. In: Carpenter K, ed. *Horns and beaks. Ceratopsian and ornithopod dinosaurs*. Bloomington: Indiana University Press, 135–169.

Brown B. 1910. The Cretaceous Ojo Alamo beds of New Mexico with description of the new dinosaur genus Kritosaurus. *American Museum of Natural History Bulletin* **28:** 267–274.

Brown B. 1912. A crested dinosaur from the Edmonton Cretaceous. *American Museum of Natural History Bulletin* **31:** 131–136.

Brown B. 1913. A new trachodont dinosaur, *Hypacrosaurus*, from the Edmonton Cretaceous of Alberta. *American Museum of Natural History Bulletin* **32:** 395–406.

Brown B. 1914. *Corythosaurus casuarius*, a new crested dinosaur from the Belly River Cretaceous, with provisional classification of the family Trachodontidae. *Bulletin of the American Museum of Natural History* **33:** 559–565.

Brown B. 1916. A new crested trachodont dinosaur *Prosaurolophus maximus*. *Bulletin of the American Museum of Natural History* **35:** 701–708.

Campione N, Evans D, Cuthbertson R. 2007. Anatomy of the atlas-axis complex of hadrosaurid dinosaurs. *Journal of Vertebrate Paleontology* **27:** 55A.

Cantino PD, de Queiroz K. 2007. *PhyloCode. International code of phylogenetic nomenclature. Version 4b*. Available at http://www.ohiou.edu/phylocode.html

Casanovas ML, Pereda-Suberbiola X, Santafé JV, Weishampel DB. 1999. First lambeosaurine hadrosaurid from Europe: palaeobiogeographical implications. *Geological Magazine* **136:** 205–211.

Casanovas-Cladellas ML, Santafé-Llopis JV, Isidro-Llorens A. 1993. [*Pararhabdodon isonense* n.gen. n.sp. (Dinosauria). Morphology, radio-tomographic study and biomechanic considerations]. *Paleontologia I Evolució* **26–27:** 121–131 [In Spanish].

Case JA, Martin JE, Chaney DS, Reguero M, Marenssi SA, Santillana SM, Woodburne MO. 2000. The first duck-billed dinosaur (Family Hadrosauridae) from Antarctica. *Journal of Vertebrate Paleontology* **20:** 612–614.

Chapman RE, Brett-Surman MK. 1990. Morphometric observations on hadrosaurid ornithopod ornithopods. In: Carpenter K, Currie PJ, eds. *Dinosaur systematics: approches and perspetives*. Cambridge: Cambridge University Press, 163–178.

Cootes TF, Taylor CJ, Cooper DH, Graham J. 1995. Active shape models, their training and application. *Computer Vision and Image Understanding* **61:** 38–59.

Cope ED. 1869. Remarks on Holops brevispinus, Ornithotarsus immanis, and Macrosaurus proriger. *Proceedings of the Academy of Natural Sciences of Philadelphia* **21:** 123.

Cope ED. 1870. Synopsis of the extinct Batracia, Reptilia and Aves of North America. *Transactions of the American Philoshopical Society* **14:** 1–252.

Cope ED. 1883. On the characters of the skull in the Hadrosauridae. *Proceedings of Rhe Academy of Natural Sciences of Philadelphia* **35:** 97–107.

Currie PJ, Nadon GC, Lockley MG. 1991. Dinosaur footprints with skin impressions from the Cretaceous of Alberta and Colorado. *Canadian Journal of Earch Sciences* **28:** 102–115.

Dalla Vecchia F. 2006. *Telmatosaurus* and the other hadrosaurids of the Cretaceous European Archipelago. An overview. *Natura Nascosta* **32:** 1–55.

Dalla Vecchia F. 2007. European hadrosauroids. *IV Jornadas Internacionales Sobre Dinosaurios y su Entorno, Salas de los Infantes* 25–28.

Davies KL. 1983. Hadrosaurian dinosaurs of Big Bend National Park. 231 pp. Unpublished Master's Thesis, university of Texas at Austin, Austin.

Dodson P. 1971. Sedimentology and taphonomy of the Oldman Formation (Campanian), Dinosaur Provincial Park, Alberta (Canada). *Palaeogeography, Palaeoclimatology, Palaeoecology* **10:** 21–74.

Donoghue MJ, Olmstead RG, Smith JF, Palmer JD. 1992. Phylogenetic relationships of Dipsacales based on rbcL sequences. *Annals of the Missouri Botanical Garden* **79:** 672–685.

Dryden IL, Mardia KV. 1998. *Statistical shape analysis*. Chichester: John Wiley and Sons.

Evans DC. 2006. Nasal cavity homologies and cranial crest function in lambeosaurine dinosaurs. *Paleobiology* **32:** 109–125.

Evans DC. 2007a. Phylogeny of lambeosaurine dinosaurs using parsimony and Bayesian likelihood approaches. *Journal of Vertebrate Paleontology* **27:** 72A.

Evans DC. 2007b. Ontogeny and evolution of lambeosaurine dinosaurs (Ornithischia: Hadrosauridae). PhD dissertation, University of Toronto, Toronto, Ontario, 497 pp.

Evans DC, Forster CA, Reisz RR. 2005. The type specimen of *Tetragonosaurus erectofrons* (Ornithischia: Hadrosauridae) and the identification of juvenile lambeosaurines. In: Currie PJ, Koppelhus EB, eds. *Dinosaur provincial park: a spectacular ecosystem revealed*. Bloomington: Indiana University Press, 349–366.

Evans DC, Reisz RR. 2007. Anatomy and relationships of *Lambeosaurus magnicristatus*, a crested hadrosaurid dinosaur (Ornithischia) from the Dinosaur Park Formation, Alberta. *Journal of Vertebrate Paleontology* **27:** 373–393.

Everhart MJ, Ewell K. 2006. Shark-bitten dinosaur (Hadrosauridae) caudal vertebrae from the Niobrara Chalk (Upper Coniacian) of western Kansas. *Transactions of the Kansas Academy of Science* **109:** 27–35.

Felsenstein J. 1985. Confidence limits on phylogenies: An approach using the bootstrap. *Evolution* **39:** 783–791.

Fitch WM. 1971. Toward defining the course of evolution: minimum change for a specific tree topology. *Systematic Zoology* **20:** 406–416.

Forster CA. 1997a. Phylogeny of the Iguanodontia and Hadrosauridae. *Journal of Vertebrate Paleontology* **17:** 47A.

Forster CA. 1997b. Hadrosauridae. In: Currie PJ, Padian K, eds. *Encyclopedia of dinosaurs*. San Diego, CA: Academic Press, 293–299.

Forster CA, Sereno PC. 1994. Phylogeneny of the Hadrosauridae. *Journal of Vertebrate Paleontology* **14:** 25A.

Fraley C, Raftery AE. 2002. Model-based clustering, discriminant analysis, and density estimation. *Journal of Rhe American Statistical Association* **97:** 611–630.

Fraley C, Raftery AE. 2003. Enhanced model-based clustering, density estimation and discriminant analysis software: MCLUST. *Journal of Classification* **20:** 263–286.

Fraley C, Raftery AE. 2006. *MCLUST version 3 for R: normal mixture modeling and model-based clustering*. Technical Report no. 504. Seattle: Department of Statistics, University of Washington.

Gates TA. 2007. *Taxonomy, Biogeography, and Paleoecology of North American Hadrosaurid (Ornithopoda) Dinosaurs*. 299 pp. Unpublished PhD dissertation, The University of Utah, Salt Lake City.

Gates TA, Sampson SD. 2007. A new species of *Gryposaurus* (Dinosauria: Hadrosauridae) from the late Campanian Kaiparowits Formation, southern Utah, USA. *Zoological Journal of the Linnean Society* **151:** 351–376.

Gates TA, Sampson SD, Delgado de Jesús CR, Zanno LE, Eberth D, Hernández-Rivera R, Aguillón Martínez MC, Kirkland JI. 2007. *Velafrons coahuilensis*, a new lambeosaurine hadrosaurid (Dinosauria: Ornithopoda) from the late Campanian Cerro del Pueblo Formation, Coahuila, Mexico. *Journal of Vertebrate Paleontology* **27:** 917–930.

Gilmore CW. 1924. A new species of hadrosaurian dinosaur from the Edmonton Formation (Cretaceous) of Alberta, Canada. *Bulletin of the Department of Mines, Geological Survey of Canada (Geological Series 43)* **38:** 13–26.

Gilmore CW. 1933. On the dinosaurian fauna of the Iren Dabasu Formation. *Bulletin of the American Museum of Natural History* **67:** 23–78.

Godefroit P, Alifanov V, Bolotsky Y. 2004b. A re-appraisal of *Aralosaurus tuberiferus* (Dinosauria, Hadrosauridae) from the Late Cretaceous of Kazakhstan. *Bulletin de l'Institute Royal des Sciences Naturelles du Belgique* **74:** 139–154.

Godefroit P, Bolotsky YL, Alifanov V. 2003. A remarkable hollow-crested hadrosaur from Russia: an Asian origin for lambeosaurines. *Comptes Rendus Palevol* **2:** 143–152.

Godefroit P, Bolotsky YL, Van Itterbeeck J. 2004a. The lambeosaurine dinosaur *Amurosaurus riabinini*, from the Maastrichtian of Far Eastern Russia. *Acta Palaeontologica Polonica* **49:** 585–618.

Godefroit P, Dong Z-M., Bultynck P, Li H, Feng L. 1998. Sino-Belgian Cooperative Program. Cretaceous Dinosaurs and Mammals from Inner Mongolia: 1) New *Bactrosaurus* (Dinosauria: Hadrosauroidea) material from Iren Dabasu (Inner Mongolia, P.R. China). *Bulletin de l'Institute Royal des Sciences Naturelles du Belgique* **68:** 1–70.

Godefroit P, Shulin H, Tingxiang Y, Lauters P. 2008. New hadrosaurid dinosaurs from the uppermost Cretaceous of northeastern China. *Acta Palaeontologica Polonica* **53:** 47–74.

Godefroit P, Zan S, Jin L. 2000. *Charonosaurus jiayinensis* n.g., n.sp., a lambeosaurine dinosaur from the Late Cretaceous of northeastern China. *Comptes Rendus de l'Academie des Sciences de Paris, Sciences de la Terre et des Planetes* **330:** 875–882.

Godefroit P, Zan S, Jin L. 2001. The Maastrichtian (Late Cretaceous) lambeosaurine dinosaur *Charonosaurus jiayinensis* from north-eastern China. *Bulletin de l'Institut Royal des Sciences Naturelles du Belgique, Sciences de la Terre* **71:** 119–168.

Goloboff PA, Farris JS, Nixon K. 2003. *TNT: tree analysis using new technologies*. Program and documentation available from the authors and at http://www.zmuc.dk/public/phylogeny

Gradstein FM, Ogg JG, Smith AG. 2004. *A geologic time scale*. Official website of the International Commission of Stratigraphy (ICS). Avaialable at http://www.stratigraphy.org

Head JJ. 1998. A new species of basal hadrosaurid (Dinosauria, Ornithischia) from the Cenomanian of Texas. *Journal of Vertebrate Paleontology* **18:** 718–738.

Head JJ. 2001. A reanalysis of the phylogenetic position of *Eolambia caroljonesa* (Dinosauria, Iguanodontia). *Journal of Vertebrate Paleontology* **21:** 392–396.

Hillis DM. 1996. Inferring complex phylogenies. *Nature* **383:** 130–131.

Hong J, Miyata T. 1999. Strike-slip origin of Cretaceous Mazhan Basin, Tan-Lu fault zone, Shandong, east China. *The Island Arc* **8:** 80–91.

Hopson JA. 1975. The evolution of cranial display structures in hadrosaurian dinosaurs. *Paleobiology* **1:** 21–43.

Horner JR. 1982. Evidence of colonial nesting and 'site fidelity' among ornithischian dinosaurs. *Nature* **297:** 675–676.

Horner JR. 1985. Evidence of polyphyletic origination of the Hadrosauridae (Reptilia: Ornithischia). *Proceedings of the Pacific Division of the American Association for the Advancement of Science* **4:** 31–32.

Horner JR. 1988. A new hadrosaur (Reptilia, Ornithischia) from the Upper Cretaceous Judith River Formation of Montana. *Journal of Vertebrate Paleontology* **8:** 314–321.

Horner JR. 1990. Evidence of diphyletic origination of the hadrosaurian (Reptilia: Ornithischia) dinosaurs. In: Carpenter K, Currie PJ, eds. *Dinosaur systematics: perspectives and approaches*. New York: Cambridge University Press, 179–187.

Horner JR. 1992. Cranial morphology of *Prosaurolophus* (Ornithischia: Hadrosauridae) with descriptions of two new hadrosaurid species and an evaluation of hadrosaurid phylogenetic relationships. *Museum of the Rockies, Occasional Paper* **2:** 1–119.

Horner JR. 2000. Dinosaur reproduction and parenting. *Annual Review of Earth and Planetary Sciences* **28:** 19–45.

Horner JR, Currie PJ. 1994. Embryonic, neonatal morphology and ontogeny of a new species of *Hypacrosaurus* (Ornithischia, Lambeosauridae) from Montana and Alberta. In: Carpenter K, Hirsch KF, Horner JR, eds. *Dinosaur eggs and babies*. Cambridge: Cambridge University Press, 312–336.

Horner JR, Makela R. 1979. Nest of juveniles provides evidence of family structure among dinosaurs. *Nature* **282:** 296–298.

Horner JR, Varricchio DJ, Goodwin MB. 1992. Marine transgressions and the evolution of cretaceous dinosaurs. *Nature* **358:** 59–61.

Horner JR, Weishampel DB, Forster CA. 2004. Hadrosauridae. In: Weishampel DB, Dodson P, Osmólska H, eds. *The dinosauria*, 2nd edn. Berkeley, CA: University of California Press, 438–463.

Hu C. 1972. A new hadrosaur from the Cretaceous of Chucheng, Shantung. *Acta Geologica Sinica* **2:** 179–206.

Hu C, Zhengwu C, Qiqing P, Xiaosi F. 2001. *Shantungosaurus giganteus*. 135 pp. Beijing, China: Hauyu Nature Trade.

Huelsenbeck JP. 1994. Comparing the stratigraphic record to estimates of phylogeny. *Paleobiology* **20:** 470–483.

Huelsenbeck JP, Ronquist F. 2001. MRBAYES: Bayesian inference of phylogeny. *Bioinformatics* **17:** 754–755.

von Huene F. 1908. Die dinosaurier der Europäischen triasformation mit brücksichtigung der Aussereuropäischen vorkommnisse. *Geologische und Palaeontologische Abhandlungen Supplement* **1:** 1–419.

von Huene F. 1956. *Paläontologie und Phylogenie der Niederen Tetrapoden*. 716 pp. Jena, Germany: Veb Gustav Fischer Verlag.

Hunt AP, Lucas SG. 1993. Cretaceous vertebrates of New Mexico. *New Mexico Museum of Natural History and Science Bulletin* **2:** 77–91.

Ihaka R, Gentleman R. 1996. 'R': a language for data analysis and graphics. *Journal of Computational and Graphical Statistics* **5:** 299–314.

International Commission on Zoological Nomenclature. 1999. *International code of zoological nomenclature*, 4th edn. London: The International Trust for Zoological Nomenclature.

Kass RE, Raftery AE. 1995. Bayes factor. *Journal of the American Statistical Association* **90:** 773–795.

Kirkland JI. 1998. A new hadrosaurid from the upper cretaceous cedar mountain formation (Albian-Cenomanian: Cretaceous) of Eastern Utah – the oldest known hadrosaurid (Lambeosaurinae?). *New Mexico Museum of Natural History and Science Bulletin* **14:** 283–295.

Kirkland JI, Hernández-Rivera R, Gates T, Paul GS, Nesbitt S, Inés-Serrano C, Garcia-de la Garza JP. 2006. Large hadrosaurine dinosaurs form the latest Campanian of Coahuila, Mexico. *New Mexico Museum of Natural History and Science Bulletin* **35:** 299–315.

Klassen E, Srivastava A, Mio W, Joshi S. 2004. Analysis of planar shapes using geodesic paths on shape spaces. *Institute of Electrical and Electronic Engineers, Transactions on Pattern Analysis and Machine Intelligence* **26:** 372–383.

Kluge AG, Farris JF. 1969. Quantitative phyletics and the evolution of anurans. *Systematic Zoology* **18:** 1–32.

Kobayashi Y, Azuma Y. 2003. A new Iguanadontian (Dinosauria: Ornithopoda) from the lower Cretaceous Kitadani Formation of Fukut Prefecture, Japan. *Journal of Vertebrate Paleontology* **23:** 166–175.

Kordikova EG, Polly PD, Alifanov VA, Rocek Z, Gunnell GF, Averianov AO. 2001. Small vertebrates form the late Cretaceous and early Tertiary of the northeastern Aral Sea Region, Kazakhstan. *Journal of Paleontology* **75:** 390–400.

Lambe LM. 1902. On Vertebrata of the Mid-Cretaceous of the North West Territory. 2. New genera and species from the Belly River Series (Mid-Cretaceous). *Geological Survery of Canada, Contributions to Canadian Paleontology* **3:** 23–81.

Lambe LM. 1914. On *Gryposaurus notabilis*, a new genus and species of trachodont dinosaur from the Belly River Formation of Alberta. *Ottawa Naturalist* **27:** 145–155.

Lambe LM. 1917a. On Cheneosaurus tolmatensis, a new genus and species of trachodont dinosaur from Edmonton Cretaceous of Alberta. *Ottawa Naturalist* **30:** 117–123.

Lambe LM. 1917b. A new genus and species of crestless hadrosaur from the Edmonton Formation of Alberta. *Ottawa Naturalist* **31:** 65–73.

Lambe LM. 1920. The hadrosaur *Edmontosaurus* from the Upper Cretaceous of Alberta. *Geological Survey Memoir, Canada Department of Mines* **120:** 1–79.

Langston WD. 1960. The vertebrate fauna of the Selma Formation of Alabama. Part 6: the dinosaurs. *Fieldiana: Geology Memoirs* **3:** 313–363.

LaRock JW. 2000. *Sedimentology and taphonomy of a dinosaur bonebed from the Upper Cretaceous (Campanian) Judith River Formation of North Central Montana*. 61 pp. Unpublished Master's thesis, Montana State University, Bozeman.

Lee MSY. 2005. Molecular evidence and marine snake origins. *Biological Letters* **1:** 227–230.

Leidy J. 1856a. Notices of remains of extinct reptiles and fishes, discovered by Dr. F. V. Hayden in the badlands of Judith River, Nebraska Territory. *Proceedings of the Academy of Natural Sciences of Philadelphia* **8:** 72–73.

Leidy J. 1856b. Notices of extinct Vertebrate discovered by Dr. F. V. Hayden during the expedition to the Sioux country under the command of Lieut. G. K. Warren. *Proceedings of the Academy of Natural Sciences of Philadelphia* **8:** 311–312.

Leidy J. 1858. *Hadrosaurus foulkii*, a new saurian from the Cretaceous of New Jersey, related to *Iguanodon*. *Proceedings of the Academy of Natural Sciences of Philadelphia* **10:** 213–218.

Lewis PO. 2001. A likelihood approach to estimating phylogeny from discrete morphological character data. *Systematic Biology* **50:** 913–925.

López-Martínez N, Canudo JI, Ardévol L, Pereda Suberbiola X, Orue-Etxebarría X, Cuenca-Bescós G, Ruiz Omeñaca JI, Murelaga X, Feist M. 2001. New dinosaur sites correlated with Upper Maastrichtian pelagic deposits in the Spanish Pyrenees: implications for the dinosaur extinction pattern in Europe. *Cretaceous Research* **22:** 41–61.

Lucas S, Spielmann JA, Sullivan RM, Hunt AP, Gates TA. 2006. *Anasazisaurus*, a hadrosaurian dinosaur from the Upper Cretaceous of New Mexico. *New Mexico Museum of Natural History and Science Bulletin* **35:** 293–297.

Lull RS, Wright NE. 1942. Hadrosaurian dinosaurs of North America. *Geological Society of America Special Papers* **40:** 1–242.

Lund EK, Gates TA. 2006. A historical and biogeographical examination of hadrosaurian dinosaurs. In: Lucas SG, Sullivan RM, eds. *Late Cretaceous vertebrales from the Western Interior. New Mexico Museum of Natural History and Science Bulletin* **35:** 263–276.

Maddison DR, Maddison WP. 2003. *Macclade version 4.0*. Sunderland, MA: Sinauer Associates, Inc.

Maddison WP, Donoghue MJ, Maddison DR. 1984. Outgroup analysis and parsimony. *Systematic Zoology* **33:** 83–103.

Marsh OC. 1872. Notice on a new species of *Hadrosaurus*. *American Journal of Science* third series **3:** 301.

Marsh OC. 1890. Description of new dinosaurian reptiles. *American Journal of Science* third series **39:** 81–86.

Marsh OC. 1892. Notice of new reptiles from the Laramie Formation. *American Journal of Science* third series **257:** 449–453.

Maryanska T, Osmolska H. 1981. First lambeosaurine dinosaur from the Nemegt Formation, Upper Cretaceous, Mongolia. *Acta Palaeontologica Polonica* **26:** 243–255.

Matthew WD. 1920. Canadian dinosaurs. *Natural History* **20:** 536–544.

Mio W, Srivastava A, Joshi SH. 2007. On shape of plane elastic curves. *International Journal of Computer Vision* **73:** 307–324.

Morris WJ. 1970. Hadrosaurian dinosaur bills – morphology and function. *Contributions in Science of Los Angeles County Museum* **193:** 1–14.

Morris WJ. 1981. A new species of hadrosaurian dinosaur form the Upper Cretaceous of Baja California –? *Lambeosurus laticaudus*. *Journal of Paleontology* **55:** 453–462.

Müller J, Reisz RR. 2006. The phylogeny of early eurepties: comparing parsimony and Bayesian approaches to the investigation of a basal fossil clade. *Systematic Biology* **55:** 503–511.

Murphy NL, Trexler D, Thompson M. 2007. 'Leonardo', a mummified *Brachylophosaurus* (Ornithischia: Hadrosauridae) from the Judith River Formation of Montana. In: Carpenter K, ed. *Horns and beaks: ceratopsian and ornithopod dinosaurs*. Bloomington: Indiana University Press, 117–133.

Nagao T. 1936. Nipponosaurus sachalinensis, a new genus and species of Trachodont dinosaur from Japanese Saghalien. *Journal of Faculty Science of Hokkaido Imperial University* **4:** 185–220.

Nopcsa F. 1900. Dinosaurierreste aus Siebenbürgen. I. Schädel von *Limnosaurus transsylvanicus* nov. gen. et

spec. *Denkschriften der Königlichen Akademie der Wissenschaften, Wien* **68:** 555–591.

Nopcsa F. 1903. *Telmatosaurus*, new name for the dinosaur Limnosaurus. *Geological Magazine* **10:** 94–95.

Nopcsa F. 1928. The genera of reptiles. *Palaeobiologica* **1:** 163–188.

Norell MA, Novacek MJ. 1992. Te fossil record and evolution: comparing cladistic and paleontologic evidence for vertebrate history. *Science* **255:** 1690–1693.

Norman DB. 1984. On the cranial morphology and evolution of ornithopod dinosaurs. *Symposium of the Zoological Society of London* **52:** 521–547.

Norman DB. 1998. On Asian ornithopods (Dinosauria: Ornithischia). 3. A new species of iguanodontid dinosaur. *Zoological Journal of the Linnean Society* **122:** 291–348.

Norman DB. 2002. On Asian ornithopods (Dinosauria: Ornithischia). 4. *Probactrosaurus* Rozhdestvensky, 1966. *Zoological Journal of the Linnean Society* **136:** 113–144.

Nylander JAA, Ronquist F, Huelsenbeck J, Nieves-Aldrey JL. 2004. Bayesian phylogenetic analysis of combined data. *Systematic Biology* **53:** 47–67.

Osborn HF. 1912. Integument of the iguanodont dinosaur *Trachodon*. *Memoirs of the American Museum of Natural History* New Series **1:** 35–54.

Ostrom JH. 1961. Cranial morphology of the hadrosaurian dinosaurs of North America. *Bulletin of the American Museum of Natural History* **122:** 33–186.

Ostrom JH. 1962. The cranial crests of hadrosaurian dinosaurs. *Postilla* **62:** 1–29.

Parks WA. 1919. Preliminary description of a new species of trachodont dinosaur of the genus *Kritosaurus*, *Kritosaurus incurvimanus*. *Transactions of the Royal Society of Canada, Series 3* **13:** 51–59.

Parks WA. 1920. The osteology of the trachodont dinosaur *Kritosaurus incurvimanus*. *University of Toronto Studies, Geological Series* **11:** 1–74.

Parks WA. 1922. *Parasaurolophus walkeri*, a new genus and species of crested trachodont dinosaur. *University of Toronto Studies, Geological Series* **13:** 1–32.

Parks WA. 1923. *Corythosaurus intermedius*, a new species of trachodont dinosaur. *University of Toronto Studies, Geological Series* **15:** 5–57.

Paul GS. 2008. A revised taxonomy of the iguanodont dinosaur genera and species. *Cretaceous Research* **29:** 192–216.

Persoon E, Fu KS. 1986. Shape discrimination using Fourier descriptors. *Institute of Electrical and Electronic Engineers, Transactions on Pattern Analysis and Machine Intelligence* **8:** 388–397.

Pol D, Norell MA. 2001. Comments on the Manhattan Stratigraphic Measure. *Cladistics* **17:** 285–289.

Powell JE. 1987. [Finding of a hadrosaurid dinosaur (Ornithischia, Ornithopoda) in the Allen Formation (Upper Cretaceous) of Salitral Moreno, Rio Negro Province, Argentina]. *Décimo Congreso Geologico Argentino, San Miguel de Tucuman, Actas* **3:** 149–152 [In Spanish].

Prieto-Márquez A. 2005. New information on the cranium of *Brachylophosaurus canadensis* (Dinosauria: Hadrosauridae) with a revision of its phylogenetic position. *Journal of Vertebrate Paleontology* **25:** 144–156.

Prieto-Márquez A. 2008. Phylogeny and historical biogeography of hadrosaurid dinosaurs. PhD dissertation, Florida State University, Tallahassee, Florida, 936 pp.

Prieto-Márquez A, Gaete R, Rivas G, Galobart A, Boada M. 2006a. Hadrosauroid dinosaurs from Western Europe: *Pararhabdodon isonensis* revisited and *Koutalisaurus kohlerorum* n. gen. et sp. *Journal of Vertebrate Paleontology* **26:** 929–943.

Prieto-Márquez A, Gignac PM, Joshi S. 2007. Neontological evaluation of pelvic skeletal attributes purported to reflect sex in extinct non-avian archosaurs. *Journal of Vertebrate Paleontology* **27:** 603–609.

Prieto-Márquez A, Weishampel DB, Horner JR. 2006b. The hadrosaurid dinosaur *Hadrosaurus foulkii* from the Campanian of the East coast of North America, with a review of the genus. *Acta Palaeontologica Polonica* **51:** 77–98.

Riabinin AN. 1930. [*Mandschurosaurus amurensis*, nov. gen., nov. sp., a hadrosaurian dinosaur from the Upper Cretaceous of Amur River]. *Mémoires de la Société Paléontologique de Russie* **59:** 1–36 [In Russian].

Riabinin AN. 1939. [The upper cretaceous vertebrate fauna of south Kazakhstan. I. part 1. Ornithischia.]. *Centralnyj Naucno-Issledovatelnyj Geologiceskij Institut, Trudy* **118:** 1–40 [In Russian].

Rozhdestvensky AK. 1952. The unveiling of an Iguanodon in Mongolia. *Comptes Rendus of the Academy of Sciences of Moscow* **84:** 1243–1246.

Rozhdestvensky AK. 1966. New iguanodonts from Central Asia: phylogenetic and taxonomic relationships between late Iguanodontidae and early Hadrosauridae. *Paleontological Journal* **1966:** 103–116.

Rozhdestvensky AK. 1968. [Hadrosaurs of Kazakhstan]. In: Tatarinov LP, ed. *[*Upper paleozoic and mesozoic amphibians and reptiles*]*. Moscow: Akademia Nauk S.S.S.R., 97–141 [In Russian].

Salgado L, Coria RA, Magalhaes Ribeiro CM, Garrido A, Rogers R, Simón ME, Arcucci AB, Curry-Rogers K, Carabajal AP, Apesteguia S, Fernandez M, Garcia RA, Televi M. 2007. Upper Cretaceous dinosaur nesting sites of Río Negro (Salitral Ojo de Agua and Salinas de Trapalcó-Salitral de Santa Rosa), northern Patagonia, Argentina. *Cretaceous Research* **28:** 392–404.

Seitz V, Garcia SO, Liston A. 2000. Alternative coding strategies and the inapplicable data coding problem. *Taxon* **49:** 47–54.

Sereno PC. 1986. Phylogeny of the bird-hipped dinosaurs (Order Ornithischia). *National Geographic Research* **2:** 234–256.

Sereno PC. 1998. A rationale for phylogenetic definitions, with application to the higher-level taxonomy of Dinosauria. *Neues Jahrbuch Fur Geologie und Paläontology, Abhandlungen* **210:** 41–83.

Siddall ME. 1998. Stratigraphic fit to phylogenies: a proposed solution. *Cladistics* **14:** 201–208.

Snively E, Russell AP, Powell GL. 2004. Evolutionary morphology of the coelurosaurian arctometatarsus: descriptive, morphometric and phylogenetic approaches. *Zoological Journal of the Linnean Society* **142:** 525–553.

Srivastava A, Joshi SH, Kaziska D, Wilson DC. 2005. Planar shape analysis and its applications in image-based inferences. In: Paragios N, Chen Y, Faugeras O, eds. *Matematical models of computer vision: the handbook*. New York: Springer-Verlag, 189–203.

Sternberg CM. 1926. A new species of *Thespesius* from the Lance Formation of Saskatchewan. *Bulletin of the Department of Mines, Geological Survey of Canada* **44:** 73–84.

Sternberg CM. 1935. Hooded hadrosaurs of the Belly River Series of the Upper Cretaceous: a comparison, with descriptions of new species. *Bulletin of the National Museum of Canada* **52:** 1–37.

Sternberg CM. 1954. Classification of North American duck-billed dinosaurs. *Journal of Paleontology* **28:** 382–383.

Strong EE, Lipscomb D. 1999. Character coding and inapplicable data. *Cladistics* **15:** 363–371.

Sullivan RM. 1999. *Nodocephalosaurus kirtlandiensis* gen. et sp. nov., a new ankylosaurid dinosaur (Ornithischia: Ankylosauria) from the Upper Cretaceous (Late Campanian) Kirtland Formation of New Mexico. *Journal of Vertebrate Paleontology* **19:** 126–139.

Sullivan RM, Williamson TE. 1999. A new skull of *Parasaurolophus* (Dinosauria: Hadrosauridae) from the Kirtland Formation of New Mexico and a revision of the genus. *New Mexico Museum of Natural History and Science* **15:** 1–52.

Suzuki D, Weishampel DB, Minoura N. 2004. *Nipponosaurus sachalinensis* (Dinosauria: Ornithopoda): anatomy and systematic position within Hadrosauridae. *Journal of Vertebrate Paleontology* **24:** 145–164.

Swofford DL. 2002. *PAUP*. Phylogenetic analysis using parsimony (*and other methods). Version 4.0b10*. Sunderland, MA: Sinauer Associates.

Swofford DL, Olsen GJ, Wadell PJ, Hillis DM. 1996. Phylogenetic inference. In: Hillis DM, Moritz C, Mable B, eds. *Molecular systematics*, 2nd edn. Sunderland: Sinauer Associates, 407–514.

Tang F, Luo ZX, Zhou ZH, You HL, Georgi A, Tang ZL, Wang XZ. 2001. Biostratiography and palaeonvironment of the dinosaur-bearing sediments in Lower Cretaceous of Mazongshan area, Gansu Province, China. *Cretaceous Research* **22:** 115–129.

Taquet P. 1976. [Geology and paleontology of the Gadoufaoua fossil locality. Aptian of Niger]. Paris: *Cahiers de Paleontologie*. [In French].

Therrien F. 2005. Palaeoenvironments of the latest Cretaceous (Maastrichtian) dinosaurs of Romania: insights from fluvial deposits and paleosols of the Transylvanian and Hateg basins. *Palaeogeography, Palaeoclimatology, Palaeoecology* **218:** 15–56.

Trexler DL. 1995. A detailed description of newly-discovered remains of *Maiasaura peeblesorum* (Reptilia: Ornithoschia) and a revised diagnosis of the genus. Unpublished master's thesis. Calgary: University of Calgary.

Van Itterbeek JV, Horne DJ, Bultynck P, Vandenberghe N. 2005. Stratigraphy and palaeonvironment of the dinosaur-bearing Upper Cretaceous Iren Dabasu Formation, Inner Mongolia, People's Republic of China. *Cretaceous Research* **26:** 699–725.

Varricchio DJ, Horner JR. 1993. Hadrosaurid and lambeosaurid bone beds from the upper cretaceous two medicine foramtion on Montana; taphonomic and biologic implications. *Canadian Journal of Earth Sciences* **30:** 997–1006.

Wagner JR. 2001. The hadrosaurian dinosaurs (Ornithischia: Hadrosauria) of Big Bend National Park, Brewster County, Texas, with implications for Late Cretaceous Paleozoogeography. 417 pp. Unpubished Master's Thesis, Texas Tech University, Austin.

Wagner JR. 2004. Hard-tissue homologies and their consequences for interpretation of the canial crests of lambeosaurine dinosaurs (Dinosauria: Hadrosauria). *Journal of Vertebrate Paleontology* **24:** 125A–126A.

Weishampel DB. 1981. The nasal cavity of lambeosaurine hadrosaurids (Reptilia: Ornithischia): comparative anatomy and homologies. *Journal of Paleontology* **55:** 1046–1057.

Weishampel DB, Horner JR. 1990. Hadrosauridae. In: Weishampel DB, Dodson P, Osmólska H, eds. *The dinosauria*. Berkeley, CA: University of California Press, 534–561.

Weishampel DB, Norman DB, Grigorescu D. 1993. *Telmatosaurus transsylvanicus* from the Late Cretaceous of Romania: the most basal hadrosaurid. *Palaeontology* **36:** 361–385.

Wiens JJ. 1998. Does adding characters with missing data increase or decrease phylogenetic accuracy? *Systematic Biology* **47:** 625–640.

Wiens JJ. 2003. Incomplete taxa, incomplete characters, and phylogenetic accuracy: is there a missing data problem? *Journal of Vertebrate Paleontology* **23:** 297–310.

Wiens JJ, Bonett RM, Chippindale PT. 2005. Ontogeny discombobulates phylogeny: paedomorphosis and higher-level salamander reationships. *Systematic Biology* **54:** 91–110.

Wiens JJ, Reeder TW. 1995. Combining data sets with different numbers of taxa for phylogenetic analysis. *Systematic Biology* **44:** 548–558.

Wiley EO. 1981. *Phylogenetics: the theory and practice of phylogenetic systematics*. 439 pp. New York: John Wiley & Sons.

Wilkinson M. 1995. More on reduced consensus methods. *Systematic Biology* **44:** 435–439.

Wilkinson M. 2001a. *TAXEQ3: software and documentation*. London: The Department of Zoology, Natural History Museum. Available at http://www.nhm.ac.uk/research-curation/projects/software/mwphylogeny.html

Wilkinson M. 2001b. *REDCON 3.0: software and documentation*. London: The Department of Zoology, Natural History Museum. Available at http://www.nhm.ac.uk/research-curation/projects/software/mwphylogeny.html

Wilkinson M. 2003. Missing trees and multiple trees: instability, relationships, and support in parsimony analysis. *Journal of Vertebrate Paleontology* **23:** 311–323.

Williamson TE. 2000. Review of Hadrosauridae (Dinosauria: Ornithischia) from the San Juan Basin. *New Mexico Museum of Natural History and Science Bulletin* **17:** 191–213.

Wilson JA. 2005. Redescription of the Mongolian sauropod *Nemegtosaurus mongoliensis* Nowinski (Dinosauria: Saurischia) and comments on late Cretaceous sauropod diversity. *Journal of Systematic Palaeontology* **3:** 283–318.

Wiman C. 1929. Die Kreide. Dinosaurier aus Shantung. *Palaeontologia Sinica, Series C* **6:** 1–67.

Wiman C. 1931. *Parasaurolophus tubicen* (n. sp.) aus der Kreide in New Mexico. *Nova Acta Regiae Societatis Scientiarum Upsaliensis* **7:** 1–11.

You HL, Luo Z, Shubin NH, Witmer LM, Tang ZL, Tang F. 2003. The earliest-known duck-billed dinosaur from deposits of late Early Cretaceous age in northwestern China and hadrosaur evolution. *Cretaceous Research* **24:** 347–355.

Young CC. 1958. The dinosaurian remains of Laiyang, Shantung. *Palaeontologica Sinica, New Series C* **16:** 53–138.

Young FW. 1985. Multidimentional scaling. In: Kotz S, Johnson NL, eds. *Encyclopedia of Statistical Sciences, volume 5*. New York: John Wiley and Sons, 649–658.

Zelditch ML, Swiderski DL, Fink WL. 2000. Discovery of phylogenetic characters in morphological data. In: Wiens JJ, ed. *Phylogenetic analysis of morphological data*. Washington: Smithsonian Institution Press, 37–83.

APPENDIX

List of the characters used for inferring the phylogenetic relationships of hadrosaurid dinosaurs. The list is organized by anatomical region. Characters are illustrated and documented online using graphs and photographs deposited in http://www.morphbank.net. There are two ways to access the images. On one hand, a link is provided for an entire anatomical region to a collection of images documenting its entire set of characters. One can then browse among these images representing all the characters for a given anatomical region. On the other hand, I have provided direct links for each individual character. Each one of these links will display a window with the image record for a particular character in Morphbank. Figure captions, including specimen numbers for each illustrated example, were included as annotations: these are revealed by clicking on 'Display Information' at the bottom left corner of the Annotation Record window. Taxon abbreviations in the boxplots documenting various quantitative characters in Morphbank are as follows: Am, *Amurosaurus riabinini*; Ar, *Aralosaurus tuberiferus*; Ba, *Bactrosaurus johnsoni*; Bb, *Barsboldia sicinskii*; Br, *Brachylophosaurus canadensis*; Ch, *Charonosaurus jiayinensis*; Cl, *Claosaurus agilis*; Co, *Corythosaurus* sp.; Coi, *Corythosaurus intermedius*; Cos, *Corythosaurus casuarius*; Ed, *Edmontosaurus* sp.; Eda, *Edmontosaurus annectens*; Edr, *Edmontosaurus regalis*; Eo, *Eolambia caroljonesa*; Eqn, *Equijubus normani*; Gi, *Gilmoreosaurus mongoliensis*; Gr, *Gryposaurus* sp.; Grl, *Gryposaurus latidens*; Grm, *Gryposaurus monumentensis*; Grn, *Gryposaurus* notabilis; Hd, *Hadrosaurus foulkii*; Hy, *Hypacrosaurus altispinus*; Hys, *Hypacrosaurus stebingeri*; Ig, *Iguanodon* sp.; Iga, *Mantellosaurus atherfieldensis*; Igb, *Iguanodon bernissartensis*; Jx, *Jaxartosaurus aralensis*; Kb, *Kerberosaurus manakini*; Kr, *Kritosaurus navajovius*; Lc, *Lambeosaurus laticaudus*; Lh, *Lophorhothon atopus*; Lm, *Lambeosaurus lambei*; Lmm, *Lambeosaurus magnicristatus*; Ma, *Maiasaura peeblesorum*; Ol, *Olorotitan ararhensis*; Ou, *Ouranosaurus nigeriensis*; Pa, *Parasaurolophus* sp.; Pac, *Parasaurolophus walkeri*; Pat, *Parasaurolophus tubicen*; Paw, *Parasaurolophus walkeri*; Pb, *Probactrosaurus gobiensis*; Ph, *Pararhabdodon isonensis*; Pr, *Prosaurolophus maximus*; Pt, *Protohadros byrdi*; Saa, *Saurolophus angustirostris*; Sal, Salitral Moreno OTU; Sao, *Saurolophus osborni*; Sh, *Shantungosaurus giganteus*; Sy, *Sahaliyania elunchunorum*; Se, *Secernosaurus koerneri*; Ta, *Tanius sinensis*; Te, *Telmatosaurus transsylvanicus*; Ts, *Tsintaosaurus spinorhinus*; Ve, *Velafrons coahuilensis*; Wu, *Wulagasaurus dongi*; ×, Hadrosauridae indeterminate. In the list below, the codes in capital letters (e.g. DTTH1, MX7, etc.) are labels that designate characters documented in Morphbank and also in Prieto-Márquez (2008).

Dental characters (http://www.morphbank.net/myCollection/index.php?collectionId=461022)

1. Maximum number of tooth positions in the dentary dental battery (DTTH1, http://www.morphbank.net/Show/?id=460667; modified from Horner *et al.*, 2004: character 1): 30 or less (sample mean of 22 alveolar positions) (0); 31–42 (sample mean of 37 alveolar positions) (1); more than 42 (sample mean of 49 alveolar positions) (2).
2. Minimum number of teeth per alveoli arranged dorsoventrally at mid length of the dental battery (DTTH3, http://www.morphbank.net/Show/?id=461202; modified from Horner *et al.*, 2004: character 2): two (0); three (1); four; (2) five or more (3).
3. Maximum number of functional teeth exposed on the dentary occlusal plane (DTTH4, http://www.morphbank.net/Show/?id=461203; modified from Horner *et al.*, 2004, character 3): one (0); one functional tooth rostrally and caudally, and

up to two teeth at and approaching the middle of the dental battery (1); three functional teeth throughout most of the dental battery, gradually decreasing to two near the rostral and caudal ends of the dentary (2).

4. Height/width ratio of the dentary tooth crowns in lingual aspect (DTTH5, http://www.morphbank.net/Show/?id=461204): ratio up to 1.95 (sample mean ratio of 1.6) (0); ratio from 1.95 to 2.7 (sample mean ratio of 2.4) (1); ratio from 2.8 to 3.3 (sample mean ratio of 3.0) (2); ratio greater than 3.3 (sample mean ratio of 3.7) (3).
5. Maximum number of ridges on the enamelled lingual side of dentary tooth crowns (DTTH6, http://www.morphbank.net/Show/?id=461205; modified Horner *et al.*, 2004, character 6): presence of a primary major ridge extending from the ventral to the dorsal end of the crown, a rostral and slightly shorter secondary ridge, and several (three or more) subdisidary, faintly developed, and short tertiary ridges (0); presence of primary, secondary, and one or two tertiary ridges (1); presence of a primary ridge and one or two faint and shorter ridges (2); loss of all but the primary ridge (3).
6. Dentary tooth crowns, position of the primary ridge (DTTH7, http://www.morphbank.net/Show/?id=461207; modified from You *et al.*, 2003, character 39): well offset caudally from the midline (0); median for most teeth, although some teeth within the same dental battery may display a slight caudal offset of the primary ridge (1).
7. Shape of the primary ridge of dentary tooth crowns (DTTH8, http://www.morphbank.net/Show/?id=461208; modified from Godefroit *et al.*, 2000 character 23): straight in all teeth within the same dentition (0); straight for some crowns and sinuous for others (1). In those taxa with teeth with sinuous primary ridges, the proportion in which these crowns occur in the dentition is variable. For example, whereas most tooth crowns bear sinuous ridges in the *Corythosaurus* specimen TMP 82-37-01, Godefroit *et al.* (2004a) reported that the sinuous carina are present only on the mesial crowns of *Amurosaurus riabinini*.
8. Angle between the crown and the root of dentary teeth (DTTH9, http://www.morphbank.net/Show/?id=461209; modified from Godefroit *et al.*, 2000, character 24): up to 110° (sample mean angle of approximately 105°), curved root (0); more than 110° and up to 135° (sample mean angle of approximately 125°), straight root (1); more than 135° (sample mean angle of approximately 140°), straight root.
9. Overall morphology of the dentary marginal denticles (DTTH10, http://www.morphbank.net/Show/?id=461210; Norman, 2002: character 31): wedge to tongue-shaped (0); curved and mammillated asymmetrical ledge (1); absent or very reduced to small papillae along the apical half of the dorsal half of the crown (2).
10. Structure of the dentary marginal denticles (DTTH11, http://www.morphbank.net/Show/?id=461211): denticles with three or more indentations at the apical margin of the denticle (0); denticles with three separate and rounded knobs aligned labiomesially (1); each denticle consisting of a single and rounded knob (2). In all taxa under consideration denticles become smaller and more densely packed at the apex of the crown. Thus, the character states listed above concern the morphology of the denticles along the margins of the dorsal half of the crown, to the exclusion of the apex itself.
11. Denticle size (DTTH12-13, http://www.morphbank.net/Show/?id=461212): the denticles of both mesial and distal margins are equal in size (0); the mesial margin has larger denticles than the distal one (1).
12. Imbrication of dentary tooth crowns (DTTH12-13, http://www.morphbank.net/Show/?id=461212): absent (0); present, the mesial margin overlaps the distal one of the adjacent crown (1).
13. Morphology of the alveolar sulci (DTTH14, http://www.morphbank.net/Show/?id=461214; Norman, 2002: character 33): shaped by dentary crowns (0); narrow and parallel-sided sulci (1).
14. Distribution of the enamel of dentary crowns (Norman, 2002: character 30): presence of a thin veneer labially, thick lingually (0); only present lingually (1).
15. Maximum number of tooth positions in the maxillary dental battery (MXTH1, http://www.morphbank.net/Show/?id=461215; modified from Horner *et al.*, 2004: character 1): up to 32 tooth positions (sample mean of 23 teeth) (0); from 33 to 44 tooth positions (sample mean of 40 teeth) (1); 45 or more tooth positions (sample mean of 49 teeth) (2).
16. Increase in the number of tooth positions in the maxilla relative to the dentary (MXTH3, http://www.morphbank.net/Show/?id=461217; modified from Wagner, 2001): absent (0); present, maxillary dental battery with 5–20% more tooth positions than the dentary one (1).
17. Maximum number of functional teeth per alveolus in the maxillary occlusal plane (MXTH4, http://www.morphbank.net/Show/?id=461218; modified from Horner *et al.*, 2004: character 3): one (0); one tooth for most of the dental battery, with the sporadic presence of a second tooth forming the occlusal plane (1); two functional

teeth throughout most of the dental battery length, gradually changing to one near the rostral and caudal ends of the maxilla (2).

18. Maximum number of ridges on the enamelled labial side of maxillary tooth crowns (MXTH5, http://www.morphbank.net/Show/?id=461219; Horner *et al.*, 2004: character 7): presence of a primary major ridge and three or more much fainter ridges (0); loss of all but the primary ridge in all or, at least, most of the crowns (in the latter situation a few crowns show a fainter secondary ridge) (1).
19. Maxillary tooth crowns, position of the primary ridge (MXTH6, http://www.morphbank.net/Show/?id=461220 and http://www.morphbank.net/Show/?id=461221; modified from You *et al.*, 2003: character 36): the dental battery contains a mixture of teeth with primary ridge positioned caudally and teeth with the ridge at the centre of the crown (0); the majority of teeth in the dental battery have a primary ridge positioned at the midline of the crown (1).
20. Shape of the primary ridge of maxillary tooth crowns (MXTH7, http://www.morphbank.net/Show/?id=461222; modified from Godefroit *et al.*, 2000: character 23): straight in all teeth within the same dentition (0); straight for some crowns and sinuous for others (1).
21. Overall morphology of the maxillary marginal denticles (MXTH8, http://www.morphbank.net/Show/?id=461223; Norman, 2002: character 30): wedge- to tongue-shaped (0); curved and mammillated asymmetrical ledge (1); absent or reduced to small papillae along the apical half of the dorsal half of the crown (2).

Mandibular characters (http://www.morphbank.net/myCollection/index.php?collectionID=461021)

22. Predentary. Ratio between the predentary maximum mediolateral width and the maximum rostrocaudal length along the lateral process (PDT1, http://www.morphbank.net/Show/?id=461224; modified from Horner *et al.*, 2004: character 13): less than 1.2 (sample mean ratio of 1) (0); between 1.2 and 1.75 (sample mean ratio of 1.5) (1); more than 1.75 (sample mean ratio of 2) (2).
23. Predentary. Ratio between the dorsoventral depth of the predentary rostral face (excluding the median ventral process) and the length of the lateral process (PDT2, http://www.morphbank.net/Show/?id=461225): ratio greater than 0.38 (sample mean ratio of 0.43) (0); ratio of 0.38 or less (sample mean ratio of 0.33) (1).
24. Predentary. Orientation of the rostral surface relative to the dorsal margin of the lateral process (PDT3, http://www.morphbank.net/Show/?id=461226; modified from Horner *et al.*, 2004: character 14): angle of 75° or greater (sample mean angle of 81°) (0); angle between 56° and 74° (sample mean angle of 66°) (1); angle between 40° and 55° (sample mean angle of 47°) (2); angle of 40° or less, gently rounded rostral surface (sample mean angle of 34°) (3).
25. Predentary. Shape of the denticles of the predentary oral margin (PDT4, http://www.morphbank.net/Show/?id=461227; modified from Horner *et al.*, 2004: character 13): triangular and pointed (0); subrectangular to rectangular (1). Denticle shape could only be appreciated in a fraction of the preserved predentaries because in most exemplars the oral margin is abraded or incompletely preserved. In the cases where denticles could be observed these were often only partially preserved. Most complete articulated skulls have predentaries with oral margins so abraded that denticles are missing. However, the finding of disarticulated predentaries of taxa for which articulated skulls are recorded showed that denticles were indeed present in all hadrosaurids (contra Weishampel *et al.*, 1993 and Wagner, 2001). In several cases denticle shape appeared subtriangular with truncated tips (e.g. *Brachylophosaurus canadensis*, MOR 1071-7-28-98-299). However, it was very difficult to assess how breakage and abrasion modified denticle morphology. For this reason, I decided to consider only the two states described above.
26. Predentary denticle spacing (i.e. distance between the mid height of two consecutive denticles (PDT5, http://www.morphbank.net/Show/?id=461227; modified from Prieto-Márquez *et al.*, 2006a: character 2): the separation between two consecutive denticles is larger than or equal to the basal width of each individual denticle (0); the separation between two consecutive denticles is smaller than the basal width of each individual denticle, but larger than 25% of its basal breadth (1); denticles are tightly arranged, with no substantial separation between their bases (less than or with a separation equal to 25% of the basal denticle width) (2).
27. Predentary. Number of predentary denticles in adult individuals lateral to the median denticle (not included in the count) (PDT6, http://www.morphbank.net/Show/?id=461228, http://www.morphbank.net/Show/?id=461229, and http://www.morphbank.net/Show/?id=461230): maximum of five (0); six (1); more than six (2). The number of predentary denticles appeared to

increase slightly through ontogeny, at least in some taxa. For example, undescribed juvenile *Edmontosaurus* remains from Alaska have only three or four denticles lateral to the median one (adults probably had a minumum of five denticles, as in CMN 8399). However, this ontogenetic variation may not be present in all hadrosaurids: for example, both juveniles (TMP 83-64-3) and adults or larger subadults referable to *Prosaurolophus maximus* have four denticles in their predentaries.

28. Predentary. Extension of the predentary denticulate margin (PDT7, http://www.morphbank.net/Show/?id=461228, http://www.morphbank.net/Show/?id=461229, and http://www.morphbank.net/Show/?id=461230): denticles extending into the lateral process (0); denticles limited to the rostral margin (1).
29. Predentary. Morphology of the predentary rostrolateral corner (PDT8, http://www.morphbank.net/Show/?id=461228, http://www.morphbank.net/Show/?id=461229, and http://www.morphbank.net/Show/?id=461230; modified from Horner *et al.*, 2004: character 13): gently rounded and continuous with the lateral process, giving the predentary an arcuate dorsal profile (0); subsquared rostrolateral corner (1); subsquared, very broad, and rostrolaterally projected (2).
30. Predentary. Development of a lateral shelf on the dorsal side of the predentary lateral process (PDT9, http://www.morphbank.net/Show/?id=460672, http://www.morphbank.net/Show/?id=460673, and http://www.morphbank.net/Show/?id=460674; modified from Wagner, 2001): absence of shelf, presence of a rostrocaudally short and shallow groove limited to the distal region of the lateral process, bounded by a tall lateral wall (0); short and shallow shelf limited to the laterocaudal region of the lateral process (1); short and well-incised shelf that is wider near the rostrolateral corner of the predentary (2); shelf extremely narrow mediolaterally and very long rostrocaudally (3); shelf rostrocaudally long, deeply incised, and mediolaterally broad, forming half of the mediolateral breadth of the lateral process and becoming wider distally (4).
31. Predentary. Ridge on the dorsal lingual, keel-like process of the predentary (PDT11, http://www.morphbank.net/Show/?id=461232): the process lacks a prominent median ridge on the lingual side of the rostral region of the predentary, and, if present, the former forms and projects caudally from the caudal margin of the predentary rostral region (0); the process has a well-developed ridge on the lingual surface of the rostral segment of the predentary, from which the former extends further caudally to lie dorsal to the dentary symphysis (1).
32. Predentary. Ventral median process, degree of indentation of the split of the process into two distinct lobes (PDT13, http://www.morphbank.net/Show/?id=461234): short indentation and deep undivided portion, the splitting originates at a distance from the predentary ventral margin that equals approximately half of the mediolateral width of the ventral process (0); long indentation and shallow undivided portion, the splitting originates at a distance from the predentary ventral margin that is less than the mediolateral width of the process (1).
33. Dentary. Ratio between the length of the proximal edentulous slope of the dentary and the distance between the rostralmost tooth position and the caudal margin of the coronoid process (DT1, http://www.morphbank.net/Show/?id=461235): less than 0.20 (sample mean ratio of 0.11) (0); ratio between 0.20 and 0.31 (sample mean ratio of 0.27) (1); ratio between 0.32 and 0.45 (sample mean ratio of 0.35) (2); ratio greater than 0.45 (sample mean ratio of 0.54) (3).
34. Dentary. Angle between the dentary proximalmost edentulous slope and the horizontal (DT2, http://www.morphbank.net/Show/?id=461236): less than 150° (sample mean angle of 144°) (0); 150° or greater (sample mean angle of 156°) (1).
35. Dentary. Angle between the proximal slope of the edentulous margin of the dentary that articulates with the predentary and the horizontal (DT3, http://www.morphbank.net/Show/?id=461237): greater than 128° (sample mean angle of 137°) (0); between 113° and 128° (sample mean angle of 121°) (1); less than 113° (sample mean angle of 107°) (2).
36. Dentary. Angle of deflection of the rostral ventral margin of the dentary (DT4, http://www.morphbank.net/Show/?id=461238): less than 17° (sample mean angle of 13°) (0); between 17° and 25° (sample mean angle of 22°) (1); greater than 25° (sample mean angle of 33°) (2).
37. Dentary. Location of the origin of the ventral deflection of the dentary (measured as the ratio between the distance from the caudal margin of the coronoid process to the inflection point of the ventral margin, and the distance from the caudal margin of the coronoid process to the rostralmost alveolus) (DT5, http://www.morphbank.net/Show/?id=461239): the deflection occurs near the rostral end of the dentary, ratio greater than 0.78 (sample mean ratio of 0.87) (0); ratio between 0.66 and 0.78 (sample mean ratio of 0.72) (1); deflection originating near the middle of the dental battery, ratio of 0.65 or less (sample mean ratio of 0.59) (2).

38. Dentary. Lingual projection symphyseal region of the dentary (measured as a ratio between the labiolingual extension of the symphyseal region and the maximum labiolingual width of the dentary) (DT6, http://www.morphbank.net/Show/?id=471319): ratio up to 1.65 (sample mean ratio of 1.47) (0); ratio greater than 1.65 and up to 2.85 (sample mean ratio of 1.87) (1); extremely elongated rostral end of the dentary, ratio greater than 2.85 (sample mean ratio of 3.03) (2).
39. Dentary. Orientation of the dentary symphysis (measured as the angle formed by this surface and the lateral side of the rostral half of the dentary) (DT7, http://www.morphbank.net/Show/?id=461241): angle greater than 15° (sample mean angle of 23°) (0); angle up to 15° (sample mean angle of 10°) (1).
40. Dentary. Medial or lateral profile of the dorsal margin of the rostral edentulous region of the dentary for articulation with the predentary (DT9, http://www.morphbank.net/Show/?id=461243): ranging from having a very subtle concavity (almost straight) to straight, or even displaying a subtle convexity (0); having a well-pronounced concavity (1).
41. Dentary. Bulging of the ventral lateral margin of the dentary (DT10, http://www.morphbank.net/Show/?id=461244; modified from Wagner, 2001): ventral dentary margin expanded ventral to the coronoid process (0); margin straight along the caudal half of the dentary and slightly bowed along the rostral half (1); margin straight or slightly bowed rostral to the coronoid process (2); margin with a wide and well-developed ventral bulge rostral to the coronoid process (3).
42. Dentary. Angle between the long axis of the coronoid process and the dorsal margin of the alveolar sulci of the dental battery (DT11, http://www.morphbank.net/Show/?id=461245): coronoid process subvertical or caudally inclined, angle greater than 82° (sample mean angle of 101°) (0); process rostrally inclined with an angle between 69° and 82° (sample mean angle of 73°) (1); coronoid process rostrally inclined with an angle up to 68° (sample mean angle of 66°) (2).
43. Dentary. Morphology of the apex of the coronoid process (in adults) (DT12-13, http://www.morphbank.net/Show/?id=461246; modified from Horner *et al.*, 2004: character 17): slightly expanded rostrocaudally, with very limited development of rostral and caudal expansions resulting in an apex that is taller than wider (0); well-developed expansion of both the caudal and, especially, the rostral margins (1). This character may be variable ontogenetically. For example, large dentaries of *Edmontosaurus* have more expanded processes than undescribed juvenile exemplars recently collected in Alaska. Lambeosaurines appeared to display a less pronounced caudal margin of the process than other hadrosaurids. However, signs of abrasion and breakage were practically always present, so that it remained uncertain whether lambeosaurines possessed a caudally less expanded coronoid process than, for example, saurolophines such as *Edmontosaurus*.
44. Dentary. Caudodorsal margin of the coronoid process projected dorsally into a sharp point (DT12-13, http://www.morphbank.net/Show/?id=461246): absent (0); present (1).
45. Dentary. Thick and dorsoventrally elongated ridge on the medial side of the coronoid process, located near the caudal margin of the process (DT14, http://www.morphbank.net/Show/?id=461247): absent, presence of fine striations (0); present, the ridge forms the rostral boundary of a depressed facet for attachment of the rostrodorsal process of the surangular; coarse striations present rostral to the ridge (1).
46. Dentary. Lateral expansion of the caudal region of the dentary, ventral to the base of the coronoid process (measured as the angle between the lateral surface of the dentary and that of the region caudoventral to the coronoid process) (DT15, http://www.morphbank.net/Show/?id=461248): the lateral side of the dentary is only sightly expanded laterally ventral to the coronoid process, with an angle greater than 165° (sample mean angle of 171°) (0); well-developed expansion of the lateral side of the dentary ventral to the coronoid process, with an angle of up to 165° (sample mean angle of 154°) (1).
47. Dentary. Orientation of the longitudinal axis of the dentary occlusal plane relative to the lateral side of the bone (as seen dorsally and caudal to the edentulous region) (DT16, http://www.morphbank.net/Show/?id=461249): diagonal axis, directed rostrolaterally and forming approximately 15° with the lateral side of the dentary (0); axis parallel with the lateral side of the dentary (1).
48. Dentary. Lingual arching of the occlusal plane (DT17, http://www.morphbank.net/Show/?id=461250; Horner *et al.*, 2004: character 12): present, lingually convex occlusal plane (0); absent, rostrocaudally straight occlusal plane (1).
49. Dentary. Caudal extension of the dental battery (DT18, http://www.morphbank.net/Show/?id=461251; modified from Horner *et al.*, 2004: character 10): the caudal end of the dental battery is found rostral to the caudal margin of the coronoid process (0); the caudal end of the dental

battery is found flush with the caudal margin of the coronoid process (1); the caudal end of the dental battery is found caudal to the caudal margin of the coronoid process (2).

50. Dentary. Separation between the dentary tooth row and the coronoid process (DT19, http://www.morphbank.net/Show/?id=461252; Norman, 2002: character 26): the coronoid process is laterally offset (but nearly in contact) with the tooth row, lacking a platform in between the tooth row and the base of the process (0); the coronoid process is laterally offset relative to the tooth row, with the presence of a concave platform or, in some cases, a laterodorsal concave slope separating the base of the process from the dental battery (1).
51. Surangular. Morphology of the rostrodorsal process of the surangular (SA1, http://www.morphbank.net/Show/?id=461253; modified from Wagner, 2001): rostrocaudally thick process, slightly reduced in thickness rostrally, extensively exposed in lateral view (0); rostrocaudally reduced in thickness, strap-like, and wedging dorsally into a thin sliver that becomes concealed in lateral view by the dorsal half of the caudal margin of the coronoid process (1).
52. Surangular foramen (SA2, http://www.morphbank.net/Show/?id=461254; Norman, 2002: character 27): present (0); absent (1).
53. Surangular. Accessory foramen located rostrodorsal to the main surangular foramen (SA3, http://www.morphbank.net/Show/?id=461255; Kobayashi & Azuma, 2003: character 15): present (0); absent (1).
54. Surangular. Orientation of the convex side of the lateral lap and the lateroventral surface of the main body of the surangular (SA4, http://www.morphbank.net/Show/?id=461256): facing more laterally than ventrally (0); facing more ventrally than laterally (1).
55. Surangular. Lateral curvature of the caudal process of the surangular (SA5, http://www.morphbank.net/Show/?id=461257): absent, process nearly straight rostrocaudally (0); present, process laterally recurved (1).
56. Surangular. Angle between the medial margin of the proximal region of the surangular and the medial margin of the proximal region of the caudal process of the element (SA6, http://www.morphbank.net/Show/?id=461258): angle greater than 148° (sample mean angle of 157°) (0); angle up to 148° (sample mean angle of 139°) (1).
57. Angular. Position of the angular in the mandible (ANG, http://www.morphbank.net/Show/?id=461259; Weishampel *et al.*, 1993: character 26): positioned ventrally and slightly medially, exposed in lateral view (0); positioned medially, not exposed in lateral view (1).
58. Coronoid bone attached to the medial, dorsal, and part of the lateral sides of the distal end of the dentary coronoid process (COB, http://www.morphbank.net/Show/?id=461260; Wagner, 2001): absent (0); present (1).
59. Prearticular bone (PRAR, http://www.morphbank.net/Show/?id=461261): absent (0); present (1).

Facial characters (http://www.morphbank.net/myCollection/index.php?collectionID=461198 and http://www.morphbank.net/myCollection/index.php?collectionID=461199)

60. Premaxilla. Mediolateral expansion of the premaxillary oral margin (measured as the ratio between the maximum mediolateral width of the premaxilla and the minimum width at the narrowest point or post-oral constriction) (PMX1, http://www.morphbank.net/Show/?id=461264; modified from Horner *et al.*, 2004: character 22): relatively narrow, ratio less than 1.65 (mean ratio of 1.45) (0); ratio between 1.65 and 2 (mean ratio of 1.84) (1); very wide, with a ratio greater than 2 (mean ratio of 2.22) (2).
61. Premaxilla. Position of the premaxillary oral margin relative to the occlusal plane of the dentition (PMX2, http://www.morphbank.net/Show/?id=461265; modified from Norman, 2002): premaxillary margin slightly ventrally offset from occlusal plane (approximately, the dorsoventral distance between the occlusal plane and the level of the premaxillary oral margin is less than the mean depth of the dentary) (0); very strongly deflected ventrally (approximately, the dorsoventral distance between the occlusal plane and the level of the premaxillary oral margin is equal to or larger than the mean depth of the dentary) (1).
62. Premaxilla. Degree of expansion and folding of the oral margin of the premaxilla (modified from Horner *et al.*, 2004: character 22): moderately expanded border, dorsoventrally thicker towards the parasagittal plane of the snout, and slightly deflected ventrally (PMX3, http://www.morphbank.net/Show/?id=461266) (0); moderately expanded border, becoming thinner towards the parasagittal plane of the snout (http://www.morphbank.net/Show/?id=461267) (1); folded caudodorsally into a thin recurved margin (http://www.morphbank.net/Show/?id=461268) (2); ventrally deflected and dorsoventrally expanded, forming a very broad 'lip-like'

margin (http://www.morphbank.net/Show/?id=461269) (3).

63. Premaxilla. Premaxillary oral margin with a 'double layer' morphology consisting of an external denticle-bearing layer and an internal layer of thickened bone, set back slightly from the oral margin, and separated from the denticular layer by a deep sulcus bearing vascular foramina (PMX5, http://www.morphbank.net/Show/?id=461271; Horner *et al.*, 2004: character 25): absent (0); present (1).
64. Premaxilla. Premaxillary foramen located rostrally and ventrolaterally to the rostral margin of the external naris (PMX6, http://www.morphbank.net/Show/?id=461272; Horner *et al.*, 2004: character 23): absent (0); present (1).
65. Premaxilla. Premaxillary accessory foramen entering rostrally through the outer (rostral) narial fossa, located rostral to the premaxillary foramen (PMX7, http://www.morphbank.net/Show/?id=461273; Horner *et al.*, 2004: character 24): absent (0); present, empties into a common chamber with the premaxillary foramen (1).
66. Premaxilla. Premaxillary accessory narial fossa located rostral to the circumnarial depression (PMX8, http://www.morphbank.net/Show/?id=461274; Horner *et al.*, 2004: character 26): absent (0); present, separated from circumnarial depression by a rostrocaudally wide ridge (1).
67. Premaxilla. Premaxillary additional accessory fossa located lateral to the rostral accessory fossa and rostrolateral to the circumnarial depression, parallel with the lateral border of the oral margin (PMX9, http://www.morphbank.net/Show/?id=461275): absent (0); present (1).
68. Premaxilla. Elongation of premaxillary caudodorsal process (PMX10, http://www.morphbank.net/Show/?id=461276; modified from Horner *et al.*, 2004: character 27): the premaxillary caudodorsal process does not meet the caudoventral process caudally (0); elongate caudodorsal process that extends caudally to meet the caudoventral process, forming the caudal margin of the external naris (1).
69. Premaxilla. Vertical groove on the caudoventral process of the premaxilla, located rostral to the dorsal process of the maxilla and extending ventrally from a small opening between the two premaxillary caudal processes; the groove is bounded rostrally by a triangular ventral projection of the caudolateral process of the premaxilla (PMX11, http://www.morphbank.net/Show/?id=461277; Evans & Reisz, 2007: character 5): absent (0); present (1).
70. Premaxilla. Elongation of the caudoventral process of the premaxilla (in adults) (PMX12, http://www.morphbank.net/Show/?id=461278; modified from Suzuki *et al.*, 2004: character 4): relatively short, the caudoventral process extends caudodorsally to end dorsal to the lacrimal, or medidodorsal to the rostral end of the prefrontal (0); long, the caudoventral process extends to end medial to the dorsal region of the prefrontal (1); very long, the caudoventral process extends caudodorsal to the prefrontal (2).
71. Premaxilla. Morphology of the caudal region of the caudoventral process of the adult premaxilla: mediolaterally compressed and triangular (PMX13, http://www.morphbank.net/Show/?id=461279) (0); dorsoventrally broad and directed caudally, or caudally and slightly dorsally (http://www.morphbank.net/Show/?id=461280) (1); triangular and dorsoventrally expanded, laterally convex lobe, directed rostrodorsally (http://www.morphbank.net/Show/?id=461281) (2).
72. Premaxilla. Premaxillary caudodorsal process has an accessory rostroventral flange that overlaps the lateral surface of the nasal in the rostral region of a supracranial crest (PMX14, http://www.morphbank.net/Show/?id=461282); Evans & Reisz, 2007: character 18): absent (0); present (1).
73. Premaxilla. Laterodorsal profile of the caudodorsal and caudoventral margins of the external bony naris (PMX15, http://www.morphbank.net/Show/?id=461283 and http://www.morphbank.net/Show/?id=461285; modified from Evans & Reisz, 2007: character 4): subrectangular to subellipsoidal (0); triangular and very long (length/width ratio greater than 2.85), caudal constriction gradually closing caudodorsally (1); triangular and moderately long (length/width ratio greater than 2.85), caudal constriction gradually closing caudodorsally (length/width ratio between 1.85 and 2.85) (2); lacriform (length/width ratio less than 1.85), caudal constriction occurs abruptly and is primarily composed of a lateroventral expansion of the caudodorsal premaxillary process (3); lacriform (length/width ratio less than 1.85), caudal constriction occurs abruptly and is primarily composed of a dorsal expansion of the caudoventral process of the premaxilla (4).
74. Premaxilla. Dorsolateral flange at approximately mid-length of the mediolaterally compressed caudoventral process of the premaxilla (PMX16, http://www.morphbank.net/Show/?id=461286;

Gates & Sampson, 2007): absent (0); present (1).

75. Nasal. Location of the nasal bone and nasal cavity in the adult skull (NS1, http://www.morphbank.net/Show/?id=461287; modified from Horner *et al.*, 2004: character 33, and partially from Evans & Reisz, 2007: character 7): the nasal extends from the rostral region of the skull roof to the rostrodorsal region of the snout, with the nasal cavity rostromedial to the orbit (0); nasal retracted caudal to the rostrum and occupying a supracranial position in the skull, with the ventral region of the nasal meeting the prefrontal rostral to the orbit, resulting in a crest that extends supraorbitally (1); retracted caudal to the rostrum and occupying a supracranial position in the skull, with the ventral region of the nasal meeting the prefrontal caudal to the rostral margin of the orbit, resulting in a convoluted narial passage and hollow crest that extend supraorbitally (2).
76. Nasal. Curvature of the caudodorsal region of the nasal (NS2, http://www.morphbank.net/Show/?id=461288; modified from Wagner, 2001 and partially from Evans & Reisz, 2007: character 7): absent, nasal straight caudodorsally (0); present, nasal rotated and folded caudodorsally (1).
77. Nasal. Morphology of the rostral end of the nasal at the contact with the dorsal process of the premaxilla (NS3, http://www.morphbank.net/Show/?id=461289 and http://www.morphbank.net/Show/?id=461290; states 3 and 4 modified from Evans & Reisz, 2007: character 17): long and wedge-shaped rostral process, gradually decreasing in width rostrally to a sharp point (0); hook-like process, it becomes abruptly deep near its rostral end and then wedges rostrally (1); long and subrectangular process, with slightly rounded corners (2); small rostral process of the nasal fits along the ventral edge of the premaxilla, with the latter briefly overlapping the nasal (3); the nasal bifurcates to meet the premaxilla in a W-shaped interfingering suture, a long and finger-like process of the nasal has an extensive overlapping joint with the caudodorsal process of the premaxilla, and an additional, more caudally-located shorter process of the nasal abuts the premaxilla (4).
78. Nasal. Morphology of the nasal contact with the caudodorsal region of the caudoventral premaxillary process at the caudal margin of the narial foramen (NS4, http://www.morphbank.net/Show/?id=461291): the nasal forms a subrectangular flange exposed dorsal to the premaxillary caudoventral process (0); the nasal forms a large hook-like rostroventral process, exposed dorsal to the premaxillary caudoventral process (1); the nasal forms a greatly shortened and dorsoventrally narrow hook-like rostroventral process, exposed dorsal to the premaxillary caudoventral process (2).
79. Nasal. Location of the rostral end of the dorsal process of the nasal relative to the rostral margin of the narial foramen (NS5, http://www.morphbank.net/Show/?id=461292): the rostral end of the rostrodorsal process of the nasal does not reach the rostral margin of the narial foramen (0); the rostral end of the rostrodorsal process of the nasal reaches the rostral margin of the narial foramen (1).
80. Nasal. Caudoventral region of the nasal ventrally recurved and hook-shaped, with a rostral process that inserts under the caudoventral process of the premaxilla (NS6, http://www.morphbank.net/Show/?id=461293): absent (0); present (1).
81. Nasal. Caudal end of the nasals forming a pair of finger-like processes on top of the frontals, and centered around the sagittal plane of the skull roof (NS7, http://www.morphbank.net/Show/?id=461294; Gates & Sampson, 2007: character 65, in part): absent (0); present (1).
82. Nasal. Caudal end of the nasals forming a pair of small and short processes that insert between the frontals at the sagittal plane of the skull roof (NS8, http://www.morphbank.net/Show/?id=461295; Gates & Sampson, 2007: character 65, in part): absent (0); present (1).
83. Nasal. Position of the summit of the nasal arch crest relative to the caudodorsal margin of the narial foramen (NS9, http://www.morphbank.net/Show/?id=461296): summit located dorsal to the caudal margin of the narial foramen (0); summit located caudodorsal to the caudal margin of the narial foramen (1).
84. Maxilla. Rostrodorsal process that is medially offset from the body of the maxilla, and also extends medial to the caudovenventral process of the premaxilla to form part of the medial floor of the external naris (MX1, http://www.morphbank.net/Show/?id=461297; partially after Wagner, 2001 and Horner *et al.*, 2004: character 42): present (0); absent, the rostral end of the maxilla forms a ventrally sloping rostrodorsal shelf that underlies the premaxilla (1).
85. Maxilla. Lateral exposure of the medial rostrodorsal process (MX2, http://www.morphbank.net/Show/?id=461298; Gates & Sampson, 2007:

character 45): not exposed through the narial foramen in lateral view (0); exposed through the narial foramen in lateral view (1). The only *Gryposaurus notabilis* skull where this character was observable was ROM 873. In this specimen, the laterodorsal flange of the caudoventral process of the premaxilla was incomplete at the level of the rostrodorsal process of the maxilla. If complete, the flange would have concealed the rostrodorsal process of the maxilla. Based on this, the character was scored as absent in *Gryposaurus notabilis*.

86. Maxilla. Pendant rostral end of the rostroventral process of the maxilla (MX3, http://www.morphbank.net/Show/?id=461299): absent (0); present (1).
87. Maxilla. Angle between the dorsal margin of the rostroventral process or shelf of the maxilla and the rostral segment of the tooth row (MX4, http://www.morphbank.net/Show/?id=461300): rostrodorsal region of the maxilla subconical in shape, dorsoventrally narrow, forming an angle of 25° or less with the rostral tooth row (mean angle of 20°) (0); dorsoventrally thicker, forming an angle greater than 25°, and up to 39°, with the rostral tooth row (mean angle of 31°) (1); rostroventral process dipping steeply ventrally, forming an angle of 40° or greater with the tooth row (mean angle of 43°), rostral region of the maxilla appearing dorsally 'swollen' and craniocaudally compressed (2).
88. Maxilla. Geometry of the lateral surface of the rostrodorsal region of the maxilla (MX5, http://www.morphbank.net/Show/?id=461301): arcuate to subrectangular (0); triangular and rostrocaudally compressed (1); subsquared, taller than rostrocaudally wide, with slightly convergent rostral and caudal margins (2).
89. Maxilla. Elevation of the lateral surface of the rostrodorsal region of the maxilla (MX6, http://www.morphbank.net/Show/?id=461302; modified from Weishampel *et al.*, 1993: character 20): relatively low (0); relatively high (1). This character is linked to the elevation of the dorsal maxillary process and the migration of the antorbital fenestra dorsally near the premaxillary articulation surface.
90. Maxilla. Position of the dorsal process and the dorsal margin of the dorsolateral promontory of the maxilla (expressed as the ratio between the distance from its summit to the rostral end of the maxilla and the craniocaudal length of the element) (MX7, http://www.morphbank.net/Show/?id=461303): caudally located dorsolateral promontory (with a ratio greater than 0.57; mean of 0.64), base of dorsal process positioned within the caudal third of the maxilla (0); centrally located dorsolateral promontory (with a ratio between 0.47 and 0.57; mean of 0.51), base of dorsal process positioned slightly caudal to the mid-length of the maxilla (1); dorsolateral promontory located slightly rostral to the mid-length of the maxilla (with a ratio between 0.35 and 0.46; mean of 0.42), base of dorsal process centred around the mid-length of the bone (2); base of dorsal process and dorsolateral promontory located rostral to the mid-length of the maxilla, with a ratio of less than 0.35 (mean of 0.28) for the relative position of the rostrodorsal promontory (3).
91. Maxilla. Morphology of the apex of the dorsal process of the maxilla (MX8, http://www.morphbank.net/Show/?id=461304; modified from Horner *et al.*, 2004: character 48): subtriangular, not dorsoventrally taller than it is rostrocaudally wide (0); dorsoventrally taller than it is wide, with a peaked and caudally inclined apex (1).
92. Maxilla. Morphology of the jugal articulation surface: protruding lateral to the caudal third of the maxilla as a mediolaterally compressed finger-like process directed caudolaterally, separated a short distance from the lateral side of the element (MX9, http://www.morphbank.net/Show/?id=461305) (0); process consisting of a promontory located dorsal and rostral to the ectopterygoid shelf, bearing a concave and subtriangular, dorsolaterally-facing joint surface for the jugal, with a caudolaterally directed corner (http://www.morphbank.net/Show/?id=461306) (1); subtriangular joint surface for the jugal that is more laterally than dorsally facing, with a lateroventrally-directed pointed corner that is located adjacent and slightly dorsal to the proximal end of the lateral ridge of the ectopterygoid shelf (http://www.morphbank.net/Show/?id=461307) (2); dorsally elevated jugal joint (distance between the ventral margin of the jugal joint and ectopterygoid shelf nearly equal to depth of the caudal segment of the maxilla), caudal margin of the joint flush with the caudal margin of the rostrodorsal eminence of the lateral side of the maxilla (http://www.morphbank.net/Show/?id=461308) (3).
93. Maxilla. Arrangement of maxillary foramina ventral and rostral to the jugal articulation (excluding large rostrodorsal or rostrolateral foramen): positioned rostrocaudally and scattered throughout the lateral side of the maxilla (MX10, http://www.morphbank.net/Show/?id=

461309) (0); forming either a row or cluster that is oriented rostrodorsally (http://www.morphbank.net/Show/?id=461310, http://www.morphbank.net/Show/?id=461311, and http://www.morphbank.net/Show/?id=461312) (1).

94. Maxilla. Number of maxillary foramina ventral and rostral to the jugal articulation (excluding large rostrodorsal or rostrolateral foramen) (MX11, http://www.morphbank.net/Show/?id=461313): seven or more (0); six or less (1).
95. Maxilla. Large rostral maxillary foramen (MX12, http://www.morphbank.net/Show/?id=461314 and http://www.morphbank.net/Show/?id=461315; Evans & Reisz, 2007: character 22, modified after Horner *et al.*, 2004: character 44): opening on the rostrolateral body of the maxilla, within the rostral half of the rostrodorsal margin of the element, and exposed in lateral view (0); opening on the rostrolateral body of the maxilla, within the dorsal half of the rostrodorsal margin of the element, and exposed in lateral view (1); opening on the dorsal surface of the maxilla along the maxilla–premaxilla contact, not exposed laterally (2).
96. Maxilla–lacrimal contact (MX13, http://www.morphbank.net/Show/?id=461316 and http://www.morphbank.net/Show/?id=461317; Evans & Reisz, 2007: character 23): present externally (0); largely covered externally by the jugal–premaxilla contact (1).
97. Maxilla. Length of the ectopterygoid shelf relative to the total rostrocaudal length of the alveolar margin of the maxilla (MX14, http://www.morphbank.net/Show/?id=461318; partially after You *et al.*, 2003: character 12): ratio between the length of the ectopterygoid shelf and the length of the rostrocaudal alveolar margin up to 0.25 (mean ratio of 0.20) (0); ratio greater than 0.25 and up to 0.35 (mean ratio of 0.30) (1); ratio greater than 0.35 (mean ratio of 0.45) (2).
98. Maxilla. Slope of the ectopterygoid shelf, measured as the angle between this and the rostrocaudal axis of the caudal segment of the tooth row (MX15, http://www.morphbank.net/Show/?id=461319): steeply inclined caudoventrally, with an angle greater than 21° (mean angle of 29°) (0); shelf inclined with an angle greater than 10° and up to 21° (mean angle of 15°) (1); slightly inclined shelf, with an angle greater than 4° and up to 10° (mean angle of 8°) (2); horizontal shelf, with an angle of up to 4° (3).
99. Maxilla. Morphology of the lateral emargination of the ectopterygoid shelf (MX16, http://www.morphbank.net/Show/?id=461320; modified from Godefroit *et al.*, 2000: character 14): dorsoventrally thin ridge (0); faint or dorsoventrally thin rostrally, then abruptly becoming dorsoventrally thick along the caudal segment of the margin (1); dorsoventrally thick continuous ridge, gradually thicker caudally than rostrally (2).
100. Maxilla. Position of the central region of the arcuate row of special foramina on the medial side of the maxilla (MX17, http://www.morphbank.net/Show/?id=461321): ventral to or at the level of the mid-dorsoventral depth of the maxilla (0); dorsal to the mid-dorsoventral depth of the maxilla (1).
101. Lacrimal. General morphology of the adult lacrimal in lateral view (LC1, http://www.morphbank.net/Show/?id=461325): triangular and rostrocaudally elongated, with a rostral process that is rostrally (and slightly ventrally) directed (0); triangular, rostrocaudally abbreviated with a relatively shorter and thinner rostral process (1).
102. Lacrimal. Ventral margin of the lacrimal with a prominent convexity rostral to the jugal notch (LC2, http://www.morphbank.net/Show/?id=461326): absent (0); present (1).
103. Jugal. Rostral apex of the rostral process of the jugal (J1, http://www.morphbank.net/Show/?id=461327 and http://www.morphbank.net/Show/?id=461328): present, wedge-shaped, elongated, and sharply pointed, positioned at mid distance along the dorsoventral depth of the rostral process (0); present, wedge-shaped, pointed, and less elongated than in (0), positioned within the dorsal half of the rostral process of the jugal, and the dorsal magin of the apex forms a steeper angle with the horizontal than in state (0) (1); greatly reduced to a blunt convexity (2); reduced to a short process, only slightly thinner rostrally, and ending abruptly (3); absent, straight, nearly vertical rostral margin (4).
104. Jugal. Dorsoventral expansion of the caudodorsal margin of the rostral process of the jugal (J2, http://www.morphbank.net/Show/?id=461329; Weishampel *et al.*, 1993: character 15): dorsoventrally narrow, rostrodorsally directed, and forming little of the rostroventral margin of the orbital rim (0); dorsoventrally deep (about 60–90% as deep as the rostral jugal constriction), dorsally or slightly recurved caudodorsally, forming the rostroventral corner of the orbital rim (1).
105. Jugal. Morphology of the triangular caudoventral margin of the rostral process of the jugal (J3, http://www.morphbank.net/Show/?id=461330): shallow and rostrocaudally wide prominence (wider than deep) (0); ventrally pointed, approximately as deep as or slightly deeper as its proximal end is wide (1); ventrally projected

triangular narrow process, at least twice as deep as it is wide, sharply pointed and often recurved caudally (2).

106. Jugal. Location of the caudoventral apex of the rostral process relative to the caudodorsal articulation with the lacrimal (with longitudinal axis of the rostral process oriented horizontally) (J4, http://www.morphbank.net/Show/?id=461333): apex located caudoventral to the caudal margin of the lacrimal process (0); apex located ventral to the caudal margin of the lacrimal process (1).
107. Jugal. Orientation of the medial articular surface of the rostral process of the jugal (J5, http://www.morphbank.net/Show/?id=461332): facing medioventrally, the articular surface forms a deep concavity bounded dorsally and caudally by a laterally offset rim (0); facing medially, the articular surface is bounded only caudally by a rim of bone (1).
108. Jugal. Inclination of the bony rim that bounds caudally the medial articulation surface of the jugal rostral process (this inclination is relative to the rostrocaudal longer axis of the jugal) (J6, http://www.morphbank.net/Show/?id=461334): slightly inclined rostrally (less than 100°) or nearly vertical (0); strongly inclined rostrally, approximately 120° (1).
109. Jugal. Rostrocaudal width of the curvature of the ventral margin of the jugal, between the caudoventral flange and the rostral process (modified from Norman, 2002) (J7, http://www.morphbank.net/Show/?id=461335): relatively wide and shallow embayment (0); relatively narrow and deep embayment (1).
110. Jugal. Ventral expansion of the caudoventral jugal flange (measured as the ratio between the dorsoventral depth of the flange and the minimum depth of the caudal constriction of the jugal) (J8, http://www.morphbank.net/Show/?id=461336; modified from Wagner, 2001): slightly expanded flange, ratio of 1.36 or less (mean ratio of 1.29) (0); moderately expanded flange, ratio greater than 1.36 and up to 1.55 (mean ratio of 1.44) (1); greatly expanded flange, ratio greater than 1.55 (mean ratio of 1.68) (2).
111. Jugal. Lateral profile of the quadratojugal flange (J9, http://www.morphbank.net/Show/?id=461337 and http://www.morphbank.net/Show/?id=461338): subconical, dorsoventrally tall, and rostrocaudally narrow, with a nearly vertical caudal margin (0); auricular in shape, with subparallel concave to nearly straight dorsal and convex ventral margins that converge dorsally into a short, subconical point (1); fan-like, with dorsal and ventral margins that are subparallel and diverge caudodorsally, dorsal and ventral margins can be straight or slightly bowed dorsally (2); auricular in shape, with subparallel concave to nearly straight dorsal and convex ventral margins that converge dorsally into a recurved or dorsally-directed tall subconical extension [this state is similar to (1), but the dorsal region of the flange is rostrocaudally narrower and taller] (3).
112. Jugal. Morphology of the ventral margin located between the caudoventral and quadratojugal flanges (J10, http://www.morphbank.net/Show/?id=461339; modified from Weishampel *et al.*, 1993: character 18): relatively short and shallow concavity (0); relatively wide and well-pronounced concavity (1).
113. Jugal. Relative depth of the caudal and rostral constrictions (in adults) (rostral constriction region located between the rostral and postorbital processes; caudal constriction region located between the postorbital process and the caudoventral flange) (J11, http://www.morphbank.net/Show/?id=461340): deeper rostral constriction, ratio of the depth of the caudal constriction relative to the rostral of 1 or less (mean ratio of 0.93) (0); deeper caudal constriction, with a ratio greater than 1 and less than 1.35 (mean ratio of 1.18, resulting from merging two K-means clusters with mean ratios of 1.13 and 1.24) (1); much deeper caudal constriction, with a ratio greater than 1.35 (mean ratio of 1.43) (2). In hadrosaurid juveniles the orbital margin is wider and the rostral constriction much shallower than the caudal constriction, probably because of the proportionally larger size of the orbit. For example, this could be observed in juveniles of *Lambeosaurus* such as ROM 758 (ratio of 1.40), ROM 869 (ratio of 1.42), and AMNH 5340 (ratio of 1.54). In subadult *Edmontosaurus*, such as CMN 8509, both the rostral and caudal constrictions are shallower than in adults, where the caudal one becomes particularly deep.
114. Jugal, overall robustness (in adults), measured as the ratio between the minimum depth of the caudal constriction and distance between the point of maximum curvature of the infratemporal margin and the caudal margin of the lacrimal process (J12, http://www.morphbank.net/Show/?id=461341; modified from Weishampel *et al.*, 1993: character 13): relatively gracile jugal, ratio less than 0.60 (mean ratio of 0.49) (0); relatively robust jugal, ratio of 0.60 or greater (mean ratio of 0.72) (1). In juveniles of at least *Edmontosaurus*, the above ratio had a lower value relative to that in adults. However, in *Lambeosaurus* there was no substantial change in the robustness of the jugal through ontogeny. For example,

subadults ROM 758 with ratio of 0.69, ROM 869 with 0.70, and AMNH 5340 with 0.67, have ratios within the range of those found in adults.

115. Jugal. Relative width and lateral profiles of the orbital and infratemporal margins of the jugal (J13, http://www.morphbank.net/Show/?id=461342): wider orbital margin and relatively constricted ventral margin of the infratemporal fenestra (0); orbital and infratemporal margins are nearly equally wide (1); wider infratemporal margin (2).
116. Quadrate. Degree of curvature of the caudal margin of the quadrate (Wagner, 2001) (Q1, http://www.morphbank.net/Show/?id=461343): the caudal margin of the dorsal half or third of the quadrate displays a slight curvature relative to the ventral half of the element, with an angle of 150° or greater (mean angle of 161°) (0); the caudal margin of the dorsal half or third of the quadrate is strongly curved caudally relative to the ventral half of the element, with an angle less than 150° (mean angle of 143°) (1).
117. Quadrate. Position of the quadratojugal (paraquadrate) notch along the dorsoventral length of the quadrate (measured as the ratio between the distance from the mid-length of the notch to the qudadrate head and the dorsoventral length of the element) (Q2, http://www.morphbank.net/Show/?id=461344): the midpoint of the notch is located near the mid-length of the quadrate, ratio less than 0.60 (mean ratio of 0.54) (0); the midpoint of the notch is located ventral to the mid-length of the quadrate, ratio of 0.60 or greater (mean ratio of 0.64) (1).
118. Quadrate. Orientation of the dorsal margin of the quadratojugal notch of the quadrate (measured as the angle between this and the caudal margin of the element) (Q3, http://www.morphbank.net/Show/?id=461345): angle greater than 45° (mean angle of 52°) (0); angle up to 45° (mean angle of 28°) (1).
119. Quadrate. Morphology of the lateral profile of the quadratojugal notch of the quadrate (Q4, http://www.morphbank.net/Show/?id=461346): subcircular, with a ventral half of the notch that is recurved and has a horizontal rostral segment (0); wide arcuate and asymmetrical, with the ventral half of the notch having a short horizontal rostral segment (1); wide arcuate and symmetrical, with the ventral half of the notch being rostroventrally-directed and nearly straight, as it is in the dorsal half (2).
120. Quadrate. Development of the squamosal buttress on the caudal margin of the dorsal end of the quadrate (Q5, http://www.morphbank.net/Show/?id=461347): absent or poorly developed as a gentle convexity (0); present, the buttress is a sharp protuberance hanging from the caudal side of the dorsal fourth of the quadrate, near the head of the element (1).
121. Quadrate. Morphology of ventral surface of the quadrate (Q6, http://www.morphbank.net/Show/?id=461349 and http://www.morphbank.net/Show/?id=461348; Weishampel *et al.*, 1993: character 22): mediolaterally broad and rostrocaudally compressed, lateral condyle slightly larger than the medial one (mean ratio between the rostrocaudal width of the lateral condyle and the mediolateral width of the ventral end of the quadrate of 0.59); the ventral surface of the lateral condyle is only slightly offset ventrally relative to the ventral surface of the medial condyle (0); subtriangular in ventral view, lateral condyle rostrocaudally expanded and much larger than the medial one (mean ratio between the rostrocaudal width of the lateral condyle and the mediolateral width of the ventral end of the quadrate of 0.90); the ventral surface of the lateral condyle is well offset ventrally relative to the ventral surface of the medial condyle (1).
122. Prefrontal. Dorsomedial margin of the prefrontal developed into a caudodorsally-oriented crest (PF1, http://www.morphbank.net/Show/?id=461350 and http://www.morphbank.net/Show/?id=461351; Godefroit *et al.*, 2004a: character 16): absent (0); present, not extending caudal to the prefrontal–frontal articulation (1); present, the crest extends caudally over the dorsal surface of the frontal and above the prefrontal–postorbital articulation in lateral view in adults (2).
123. Prefrontal. Lateral profile of the rostrodorsal margin of the prefrontal (PF2, http://www.morphbank.net/Show/?id=461352; modified from Horner *et al.*, 2004: character 50): subarcuate to smoothly curved, the rostral margin is rostroventrally oriented and forms an obtuse angle with the dorsal orbital margin (0); rostromedially broad with subsquared rostrodorsal corner, the rostral margin is ventrally oriented and forms a 90° angle with the dorsal orbital margin (1).
124. Prefrontal. Mediolateral breadth of the exposed rostroventral region of the prefrontal (PF3, http://www.morphbank.net/Show/?id=461353; partially after Horner *et al.*, 2004: character 50): the rostroventral region is mediolaterally expanded (0); the exposed rostroventral region is mediolaterally compressed and narrow (1).
125. Prefrontal. Inclusion of the prefrontal in the circumnarial fossa (PF4, http://www.

morphbank.net/Show/?id=461354 and http://www.morphbank.net/Show/?id=461355; Wagner, 2001): absent (0); present (1).

126. Prefrontal. Outward flaring of the rostrodorsal orbital margin of the prefrontal (PF5, http://www.morphbank.net/Show/?id=461356; Horner *et al.*, 2004: character 49): absent, the prefrontal lies flush with the surrounding lacrimal and postorbital (0); present, the prefrontal flares dorsolaterally forming a thin and everted wing-like rim around the rostrodorsal margin of the orbit (1).
127. Prefrontal. Exposure of the prefrontal–nasal contact in lateral and/or dorsal view (PF6, http://www.morphbank.net/Show/?id=461357; modified from Wagner, 2001): contact totally exposed in lateral and/or dorsal view (0); contact visible in lateral view along the caudal and half of the dorsal margin of the prefrontal (1); contact visible in lateral view only along the caudal region of the prefrontal in adults, because of the invasion of the premaxilla along the medial side of the prefrontal (2).
128. Postorbital. Dorsal promontorium on the rostral process of the postorbital (PO1, http://www.morphbank.net/Show/?id=461359 and http://www.morphbank.net/Show/?id=461358; Godefroit *et al.*, 2004a: character 17): absent, the dorsal surface of the postorbital above the jugal process is horizontal or slightly concave (0); present in adult specimens, the articular margin for the prefrontal is elevated and the dorsal surface of the postorbital above the jugal process is deeply depressed (1). Godefroit *et al.* (2004a) incorrectly reported the absence of this process in *Amurosaurus riabinini*. When a dorsal promontory is present, the dorsal surfaces of the caudal and rostral processes of the postorbital are steeply inclined towards the dorsal surface of the central body of the bone. In *Charonosaurus jiayinensis*, the relatively small size of CUST JIV 1223 indicates that this character is probably present in subadult specimens as well as in adults, although probably not developed in juveniles. However, sudadult individuals do not display a deeply depressed dorsal surface, as in *Lambeosaurus lambei* (ROM 758) and *Corythosaurus casuarius* (CMN 8676). In *Parasaurolophus cyrtocristatus* (UCMP 143270) there is a small dorsal promontorium, and the inclination of the caudal process of the postorbital, although not horizontal, is not as steep as in those taxa with postorbitals with depressed dorsal margins.
129. Postorbital. Rostrocaudal constriction of the dorsal region of the infratemporal fenestra (PO2, http://www.morphbank.net/Show/?id=461360; modified from Evans & Reisz, 2007: character 36): absent, caudal (squamosal) process of the postorbital elongate over the infratemporal fenestra (broad and subrectangular dorsal region of the fenestra) (0); present and caused by the presence of a nearly straight and oblique caudoventral margin of the caudodorsal region of the postorbital (dorsal region of infratemporal fenestra typically subtriangular) (1); present and caused by rostrocaudal shortening of the caudal process of the postorbital (dorsal region of infratemporal fenestra typically oval) (2). This character appeared to be invariable throughout ontogeny, as in, for example, *Saurolophus agustirostris*. In this species state 2 is present in subadults (e.g. ZPAL MgD-I 159) as well as in adults (e.g. MPC-D100/706). In *Edmontosaurus* spp., the constriction of the infratemporal fenestra is further accentuated by the 'swelling' of the postorbital. Notwithstanding this 'swelling', the condition in the genus is as in state 1.
130. Postorbital. Morphology of the central body of the postorbital (PO3, http://www.morphbank.net/Show/?id=461361): triangular, craniocaudally broad, expanded rostroventrally to form a straight and obliquely oriented caudodorsal orbital margin (0); triangular, with a caudodorsal orbital margin that ranges in lateral profile from semicircular to subsquared (1); rostrocaudally expanded, rostrally excavated, and bulging laterally ('inflated'), containing a hollow inner cavity (in adults) (2).
131. Postorbital. Length of the jugal process of the postorbital (PO4, http://www.morphbank.net/Show/?id=461362): relatively short, approximately as long as the craniocaudal width of the orbit, hook-like in lateral profile (0); relatively long, longer than the craniocaudal width of the orbit, nearly straight, only slightly recurved rostrally (1).
132. Postorbital. Morphology of the caudal end of the caudal process of the postorbital at its articulation with the squamosal (PO5, http://www.morphbank.net/Show/?id=461363; Evans & Reisz, 2007: character 35): oblong or wedge-shaped (0); bifid (1).
133. Postorbital. Caudal extension of the caudal ramus of the postorbital that overlaps the laterodorsal surface of the squamosal (PO6, http://www.morphbank.net/Show/?id=461364; modified from Godefroit *et al.*, 2000): the caudal end of the postorbital caudal ramus extends to a point rostral to the quadrate cotylus, and does not overlap the latter (0); the caudal end of the

postorbital caudal ramus extends caudodorsal to the precotyloid process, and over as much as the rostral half of the quadrate cotylus (1); the caudal end of the postorbital caudal ramus completely overlaps the laterodorsal side of the squamosal quadrate cotylus (2).

134. Squamosal. Length of the precotyloid process of the squamosal (measured as the ratio of its length relative to the width of the quadrate cotylus) (SQ1, http://www.morphbank.net/Show/?id=461365): very short precotyloid process, ratio less than 0.95 (mean ratio of 0.74) (0); moderately long precotyloid process, ratio between 0.95 and 1.25 (mean ratio of 1.13) (1); very long precotyloid process, ratio greater than 1.25 (mean ratio of 1.41) (2).
135. Squamosal. Dorsoventral expansion of the caudolateral surface of the squamosal (SQ2, http://www.morphbank.net/Show/?id=461366; Horner *et al.*, 2004: character 64): unexpanded, shallowly exposed in caudal view (0); greatly expanded dorsomedially, forming a deep, near vertical, well-exposed face in caudal view (in adults) (1).
136. Squamosal. Separation of the squamosals at the occipital margin of the skull roof (SQ3, http://www.morphbank.net/Show/?id=461367; Horner *et al.*, 2004: character 63): completely separated by the parietal (0); the squamosal approaches the sagittal plane of the skull, separated by a narrow band of parietal (1); extensive intersquamosal joint present at the midline, parietal completely excluded from the sagittal plane of the skull at that particular spot (in adults) (2).
137. Squamosal. Rostromedial indenture of the medial ramus of the squamosal (SQ4, http://www.morphbank.net/Show/?id=461368; modified from Godefroit *et al.*, 1998): present, medial ramus of the squamosal curves rostromedially, so that the back of the skull appears to be deeply indented rostrally when viewed dorsally (0); absent, medial ramus of the squamosal extends medially, forming a subsquared caudolateral border of the skull roof (1).

Neurocranial characters (http://www.morphbank.net/myCollection/index.php?collectionId=461197)

138. Frontal. Bifurcation of the rostromedial margin of the frontals at the sagittal plane of the skull roof, leaving a V-shaped space in between (F1, http://www.morphbank.net/Show/?id=461369): absent (0); present (1).
139. Frontal fontanelle, present at least at one stage during ontogeny (F2, http://www.morphbank.net/Show/?id=461370; Langston, 1960; Wagner, 2001): absent (0); present (1).
140. Frontal. Nasal articulation surface of the frontal shaped into a rostroventrally-sloping platform (F3, http://www.morphbank.net/Show/?id=461371; Godefroit *et al.*, 2004b: character 7, in part; Evans & Reisz, 2007: character 40, in part): absent (0); present (1).
141. Frontal. Nasal articulation surface of the frontal shaped into a dorsoventrally thickened, tongue-like platform that projects caudodorsally to overhang the parietal in adults (F4, http://www.morphbank.net/Show/?id=461372; Godefroit *et al.*, 2004b: character 7, in part; Evans & Reisz, 2007: character 40, in part, and character 41): absent (0); present (1).
142. Frontal. Median cleft separating the two striated tongues of the frontal platform (F5, http://www.morphbank.net/Show/?id=461373; Evans & Reisz, 2007: character 40, in part): absent (0); present (1).
143. Frontal. Exposure of the frontal along the dorsal margin of the orbit (F6, http://www.morphbank.net/Show/?id=461374; modified from Horner *et al.*, 2004: character 57): frontal exposed, forming part of the dorsal orbital margin in between the prefrontal and postorbital (0); the frontal projects laterally into a triangular narrow apex that inserts in between a narrow gap left by the prefrontal and postorbital (in some exemplars, although the prefrontal and postorbital do not meet at the orbital margin, the apex of the frontal does not reach the lateral margin of the orbit at the same level as the former two elements) (1); frontal completely excluded from the orbital margin by an extensive articulation between the prefrontal and postorbital (2).
144. Frontal, upward doming dorsal to the braincase of subadult hadrosaurids (and perhaps young adult) specimens (F7, http://www.morphbank.net/Show/?id=461375; modified after Horner *et al.*, 2004: character 58): absent (0); present (1).
145. Length/width ratio of the ectocranial surface of the frontal (F8, http://www.morphbank.net/Show/?id=461376; Evans & Reisz, 2007: character 42): relatively elongated ectocranial surface, with a ratio greater than 0.8 (0); relatively short ectocranial surface, with a ratio of 0.8 or less, but greater than 0.4 (1); greatly shortened ectocranial surface, with a ratio less than 0.4 (2).
146. Frontal. Morphology of the ventral annular ridge that defines the rostral extent of the cerebral fossa (F9, http://www.morphbank.net/Show/?id=461377; Evans & Reisz, 2007: character 43):

long, low, and gently rounded in medial view (0); sharp annular ridge (1).

147. Parietal. Maximum length/minimum width proportions of the adult parietal (PAR1, http://www.morphbank.net/Show/?id=461378; modified from Godefroit *et al.*, 2004a: character 2): very short, length/width ratio less than 1.40 (sample mean ratio of 1.19) (0); short, ratio between 1.40 and 2.35 (sample mean ratio of 1.98) (1); relatively long, ratio greater than 2.35 (sample mean ratio of 2.75) (2). This ratio decreases during ontogeny, at least in lambeosaurines such as *Lambeosaurus* spp. For example, the ratio is 1.84 in ROM 758, 1.69 in the larger CMN 8633, and finally reaches 1.16 in ROM 794. Similarly, the subadult *Corythosaurus* ROM 1947 has a long parietal (ratio of 1.90). However, the caudal inclination of the parasagittal crest is consistent through ontogeny. In other hadrosaurids, the parietal appeared to lengthen with ontogeny. For example, in *Brachylophosaurus* MOR 1071-7-13-99-87-I the ratio is 2.04 and increases to 2.50 in the adult specimen UCMP 130139. Horner *et al.* (2004; character 70) and Evans & Reisz (2007; character 45) included the length of the parietal sagittal crest as a phylogenetically informative character. This character is not considered here because it is linked to the length of the entire parietal: shorter parietals have shorter sagittal crests and vice versa. Likewise, no difference in the degree to which the proximal region of the sagittal crest narrows was appreciated among the taxa under study.
148. Parietal. Orientation of the parietal midline crest (PAR2, http://www.morphbank.net/Show/?id=461380; Horner *et al.*, 2004; character 69; Evans & Reisz, 2007: character 44): straight and level with the skull roof or slightly down-warped along its length (0); the sagittal crest deepens caudally and is strongly down-warped (1).
149. Parietal. Morphology of the rostromedian process of the parietal that forms a crenulated suture in between the caudomedian margin of the frontals (PAR3, http://www.morphbank.net/Show/?id=461381): rectangular, rostrocaudally short, and mediolaterally expanded (0); rostrocaudally short and subtriangular to arcuate or absent (1); rostrocaudally elongate and mediolaterally narrow (2).
150. Parietal. Rostral extension of the sagittal crest along the dorsal surface of the parietal (PAR4, http://www.morphbank.net/Show/?id=461382): the sagittal crest extends along the entire length of the parietal, and remains sharp and well defined at the rostral region (0); the sagittal crest extends along the entire length of the parietal, but its sharpness fades away at the rostral region where the parietal is rostrocaudally shorter than it is wide (1); the sagittal crest only extends along the caudal half of the parietal, and the rostral half of the dorsal surface of the parietal is flattened, lacking any ridge or mediolateral compression (2).
151. Basioccipital. Participation of the basioccipital in the ventral margin of the foramen magnum (BO1, http://www.morphbank.net/Show/?id=461383; Weishampel *et al.*, 1993: character 24): absent, the exoccipital condyloids nearly or completely exclude the basioccipital from the ventral margin of the foramen magnum (0); present, the exoccipitals are separated at the sagittal plane of the braincase and allow the basioccipital to become part of the ventral margin of the foramen magnum (1). Exclusion of basioccipital from the foramen magnum is not syanpomrphic for saurolophines; on the contrary, all hadrosaurids have a basioccipital participating in the floor of foramen magnum.
152. Basioccipital. Orientation of the articulation margin of the occipital condyle relative to the convex caudoventral border of the basioccipital (BO2, http://www.morphbank.net/Show/?id=461384; modified from Godefroit *et al.*, 2000: character 1): the articulation margin of the occipital condyle faces caudoventrally, and is continuous with the caudal border of the basioccipital (0); the articulation margin of the occipital condyle faces caudally, and is divided from the caudal border of the basioccipital by a shallow cleft (1).
153. Basioccipital. Length of basioccipital constriction (BO3, http://www.morphbank.net/Show/?id=461385; Godefroit *et al.*, 2001): relatively long and well-developed (0); poorly developed and relatively short (1). Character 80 from Gates & Sampson (2007) was excluded because in all taxa the basisphenoid was found contributing to the delimitation of the trigeminal foramen.
154. Basisphenoid. Orientation of the basipterygoid process of the basisphenoid (measured as the angle between the ventral margins of both processes) (BS1, http://www.morphbank.net/Show/?id=461386; modified from Godefroit *et al.*, 2001: character 2): angle less than 100° (sample mean angle of 79°) (0); angle of 100° or greater (sample mean angle of 111°) (1).
155. Basisphenoid. Developement of the alar process of the basisphenoid (BS2, http://www.morphbank.net/Show/?id=461387): moderately developed (0); very well developed, relatively large in size (1).

156. Basisphenoid. Ventral transverse caudal ridge between the basipterygoid processes of the basisphenoid (BS3, http://www.morphbank.net/Show/?id=461388; Gates & Sampson, 2007: character 78): absent or very poorly developed (0); present, sharply defined ridge (1).
157. Basisphenoid. Short median ventral process located between the basipterygoid processes of the basisphenoid (BS4, http://www.morphbank.net/Show/?id=461389; Gates & Sampson, 2007: character 79): absent (0); present, ventrally or rostroventrally inclined (1).
158. Basisphenoid. Development of the rostral constriction of the basisphenoid, caudal to the basipterygoid processes (measured as the ratio between the minimum mediolateral width of the rostral constriction and the maximum width of the basisphenoid across the spheno-occipital tubercles) (BS5, http://www.morphbank.net/Show/?id=471320): very thick constriction, ratio less than 1.45 (sample mean ratio of 1.37) (0); moderately developed constriction, ratio between 1.45 and 1.90 (sample mean ratio of 1.72) (1); very thin constriction, ratio greater than 1.90 (sample mean ratio of 2.25) (2).
159. Laterosphenoid. Complete lateral osseous closure of the ophthalmic sulcus (V_1) of the laterosphenoid (LS1, http://www.morphbank.net/Show/?id=461391; Evans & Reisz, 2007: character 51): absent (0); present (1).
160. Laterosphenoid. Extreme reduction of the length of the postorbital process of the laterosphenoid to 25% or less of the length of the mediodorsal flange of this element (LS2, http://www.morphbank.net/Show/?id=461392; modified from Prieto-Márquez *et al.*, 2006a: character 76): absent (0); present (1).
161. Supraoccipital. Orientation of the caudal surface of the supraoccipital (SO1, http://www.morphbank.net/Show/?id=461393; Horner *et al.*, 2004: character 65): nearly vertical (0); rostrally inclined and facing caudodorsally (1).
162. Supraoccipital. Lateroventral corner of the supraoccipital deeply inset into the exoccipital, so that the latter is 'locked' between two short flanges that project medially above lateral end of the supraoccipital–exoccipital contact (SO2, http://www.morphbank.net/Show/?id=461394; Horner *et al.*, 2004: character 66): absent (0); present (1).
163. Exoccipital. Caudal extension of the exoccipital–supraoccipital shelf above the foramen magnum (EX1, http://www.morphbank.net/Show/?id=461395; modified from Godefroit *et al.*, 2004b: character 24): very short rostrocaudal length, approximately less than half the diameter of the foramen magnum (0); moderately long, approximately more than half of, but less than, the diameter of the foramen magnum (1); very long, substantially longer (often twice or more) than the diameter of the foramen magnum (2).
164. Exoccipital-opisthotic. Orientation of the distal portion of the paroccipital process (EX2, http://www.morphbank.net/Show/?id=461396; Horner *et al.*, 2004: character 62): ventrally directed (0); rostroventrally directed (1).
165. Pterygoid. Elevation of the proximodorsal region of the quadrate wing of the pterygoid (PLT1, http://www.morphbank.net/Show/?id=461397; Prieto-Márquez *et al.*, 2006a: character 72): absent (0); present (1).
166. Pterygoid. Ventral extension of the lamina located ventral to the central buttress of the pterygoid (PLT2, http://www.morphbank.net/Show/?id=461398; Prieto-Márquez *et al.*, 2006a: character 75): lamina of moderate size, a relatively large portion of the ventral quadrate process and the rostroventral process extends beyond the ventral margin of the lamina (0); extensive lamina, only a relatively small portion of the ventral quadrate process and the rostroventral process extends beyond the ventral margin of the lamina (1).
167. Ectopterygoid–jugal contact (PLT3, http://www.morphbank.net/Show/?id=461399; Godefroit *et al.*, 2001: character 12): present, the ectopterygoid contacts the medial side of the jugal (0); absent, the jugal lacks an articular facet for the ectopterygoid (1).

Regional cranial characters (http://www.morphbank.net/myCollection/index.php?collectionID=461162)

168. Angle between the dorsal margin of the rostrum parallel with the long axis of the external naris and the maxillary tooth row (adults only) (RST2, http://www.morphbank.net/Show/?id=461401): angle up to 30° (sample mean angle of 27°) (0); angle greater than 30° and up to 40° (sample mean angle of 34°) (1); angle greater than 40° (sample mean angle of 47°) (2).
169. Exposure of the nasal passage (NPS1, http://www.morphbank.net/Show/?id=461402; modified from Norman, 2002: character 5): present, nasal passage open and exposed on the lateral side of the rostrum (0); absent, nasal passage nearly or completely enclosed by bone and formation of internal cavities and passages (such as lateral diverticula and a common median chamber) (1). I differentiated between the narial foramen (Wagner, 2001) and the bony naris

(Evans, 2006). Functionally, both structures formed the external naris. The iguanodontoidean narial foramen was regarded as homologous with the common median chamber of lambeosaurines (Hopson, 1975; Wagner, 2004). Because of the caudodorsal migration of the external passage to become enclosed in a supracranial crest forming the common median chamber in lambeosaurines, what remained on the laterodorsal surface of the premaxilla (the bony naris) in the latter group was not regarded as structurally homologous with the narial foramen.

170. Lateral profile of the narial foramen (NPS2, http://www.morphbank.net/Show/?id=461403 and http://www.morphbank.net/Show/?id=461404): broad and subellipsoidal in lateral profile (0); narrow and subellipsoidal in lateral profile (1); extremely narrow, cleft-like, in lateral profile (2).
171. Degree of closure of the nasal passage on the lateral crest surface between the caudoventral process of the premaxilla and the nasal (NPS3, http://www.morphbank.net/Show/?id=461405; Evans, 2007b: character 15): present, premaxilla–nasal fontanellae persist into late ontogenetic stages (0); absent, fontanellae completely closed in adults (1).
172. Ratio between the length of the narial foramen and the distance between the rostroventral corner of the premaxilla and the rostroventral margin of the prefrontal (NPS4, http://www.morphbank.net/Show/?id=461406): very short narial foramen, ratio up to 0.40 (sample mean ratio of 0.32) (0); moderately long narial foramen, ratio greater than 0.40 but less than 0.60 (sample mean ratio of 0.49) (1); elongated narial foramen, ratio between 0.60 and 0.65 (sample mean ratio of 0.62) (2); extremely long narial foramen, ratio greater than 0.65 (sample mean ratio of 0.72) (3).
173. Nasal vestibule folded into an S-loop in the enclosed premaxillary passages rostral to the dorsal process of the maxilla (Weishampel, 1981; Evans, 2007b: character 8): absent (Weishampel, 1981, Fig. 6) (0); present (Weishampel, 1981, Figs 4, 5) (1).
174. Location of the lateral diverticulum relative to the common median chamber (Weishampel, 1981): lateral to the common median chamber (Weishampel, 1981, Fig. 4 and 6) (0); rostral to the common median chamber (Weishampel, 1981, Fig. 10) (1); caudodorsal to the common median chamber (Weishampel, 1981, Fig. 8) (2).
175. Communication between the external bony naris, the lateral diverticulum and the common median chamber (Evans, 2006): a tubular premaxillary passage extends caudodorsally from the bony naris to the lateral diverticulum, which is then connected to the common median chamber (Weishampel, 1981, Figs 4–6) (0); a tubular premaxillary passage directly connects the bony naris to the common median chamber (Weishampel, 1981, Figs 7, 8) (1).
176. Caudal extent of the nasal passage dorsal and/or caudal to the orbit (NPS8, http://www.morphbank.net/Show/?id=461407; modified from Evans, 2007b: character 9): absent, nasal passage restricted to the antorbital region of the skull (0); present, but not extending caudal to the occiput, with a nasal vestibule that flanks a common median chamber (1); present, nasal vestibule extending caudodorsal to the occipital region of the skull (2).
177. Composition of the caudal margin of the functional external naris (NPS9, http://www.morphbank.net/Show/?id=461408; modified from Horner *et al.*, 2004: character 29): formed by the nasal dorsally and the premaxilla ventrally (0); formed entirely by the nasal (1); formed entirely by the premaxilla (2).
178. Circumnarial fossa on the lateral surface of the facial region of the skull (CMN1, http://www.morphbank.net/Show/?id=461409; Wagner, 2001; Horner *et al.*, 2004: character 31): absent, circumnarial structure entirely enclosed (0); present (1).
179. Caudodorsal extension circumnarial fossa (homologous with the lateral diverticulum inside hollow supracranial crests) (CMN2, http://www.morphbank.net/Show/?id=461411 and http://www.morphbank.net/Show/?id=461412; Hopson, 1975; Wagner, 2001, 2004; modified from Horner *et al.*, 2004, characters 32): the fossa does not reach the caudal margin of the narial foramen and, thus, lacks a caudal margin (0); the fossa extends as far as to surround the caudal margin of the narial foramen, but does not reach the orbit (1); the fossa extends as far as the rostrodorsal region of the orbit (2); the fossa extends beyond the orbit, caudodorsal to its caudal margin (3).
180. Degree of excavation of the caudal region of the circumnarial fossa (CMN3, http://www.morphbank.net/Show/?id=461410; Horner *et al.*, 2004: character 32): lightly incised (0); deeply incised and invaginated (1).
181. Elevation of the skull roof dorsal to the ancestral lateral profile (i.e. presence of supracranial crest) (CRS1, http://www.morphbank.net/Show/?id=461413; Wagner, 2004): absent (0); present (1).

182. Composition of the supracranial crest (or the homologous region of the skull from which the crest forms) (excluding supporting elements) (CRS2, http://www.morphbank.net/Show/?id=461414; modified from Horner *et al.*, 2004: character 40): composed exclusively of the nasals (0); primarily composed of the nasals and frontals (1); primarily composed of the nasals and premaxillae (2).
183. Relative contribution of the nasal and premaxilla in the formation of hollow supracranial crests (CRS3, http://www.morphbank.net/Show/?id=461415; Wagner, 2001 and modified in part from Evans & Reisz, 2007: character 11): the nasals constitute half or a larger portion of the crest in the form of a caudal plate-like surface (0); the nasals form a smaller portion of the crest relative to the surrounding premaxillae (1).
184. General shape of the supracranial crest (CRS4, http://www.morphbank.net/Show/?id=461416, http://www.morphbank.net/Show/?id=461417, http://www.morphbank.net/Show/?id=461418, and http://www.morphbank.net/Show/?id=461419; modified from Horner *et al.*, 2004: character 36): dome-like broad and low protuberance (0); mediolaterally compressed arcuate protuberance, rostral or, in adults, dorsal to the level of the orbits (1); paddle-like and caudally (as well as slightly dorsally) directed solid blade of bone (2); mediolaterally narrow and paddle-like, extending caudal to the occiput (3); rostrally excavated and rostrally-facing protuberance, rostrodorsal to the orbit (4); nasal fold that rises dorsally or caudodorsally to form a laterally excavated promontory, with a caudal region that rests over the frontals (5); raised into a large vertical fan, formed by a solid plate-like extension of the premaxilla ('cockscomb') above the nasal passages in the rostral region of the crest (6); long and tubular, caudodorsally directed beyond the occiput and slightly arched (7).
185. Hollow crest–snout angle along the dorsal margin of the premaxilla in lateral view (in adults) (CRS5, http://www.morphbank.net/Show/?id=461420; Evans, 2007b: character 13): absent, the lateral profile of the snout is continuous with the lateral profile of the dorsal premaxillary margin of the crest (0); facial profile shallowly concave in lateral view, angle greater than 140° (1); angle between 110° and 140° (2); crest procumbent and rostrally inclined, angle less than 110° (3).
186. Caudal extension of the hook-like nasal process on the caudoventral region of helmet-shaped hollow supracranial crests (CRS6, http://www.morphbank.net/Show/?id=461421): rostral to or at the level of the caudal margin of the occiput (0); extended caudal to the level of the caudal margin of the occiput (1).
187. Palpebral (supraorbital) bone (PLP, http://www.morphbank.net/Show/?id=461422; Norman, 2002: character 13): absent (0); present (1).
188. Length/width proportions of the orbit (ORB, http://www.morphbank.net/Show/?id=461424; Wagner, 2001): nearly circular, approximately as wide as it is deep (0); elongated, dorsoventrally deeper than it is wide (1).
189. Presence of a gap (paraquadratic foramen) between the quadratojugal and the jugal (PQF, http://www.morphbank.net/Show/?id=461425): absent (0); present (1).
190. Size of the infratemporal fenestra relative to that of the orbit (ITF1, http://www.morphbank.net/Show/?id=461426; modified from Gates & Sampson, 2007): infratemporal fenestra both rostrocaudally wider and dorsoventrally deeper than the orbit (0); infratemporal fenestra rostrocaudally narrower than or approximately as wide as the orbit (1).
191. Shape and rostrocaudal width of the dorsal margin of the infratemporal fenestra relative to that of the dorsal orbital margin (ITF2, http://www.morphbank.net/Show/?id=461427 and http://www.morphbank.net/Show/?id=461428): subrectangular, with a dorsal infratemporal margin that is approximately as wide as the ventral margin (0); subtriangular, with a dorsal infratemporal margin that is narrower than the ventral margin (1). Within state (1), there is considerable variation in the width of the infratemporal fenestra within species of *Corythosaurus* and *Lambeosaurus*. The narrowest width among lambeosaurines was found in *Hypacrosaurus altispinus*, where the latter was approximately four times longer than wide.
192. Location of the dorsal margin of the infratemporal fenestra relative to the dorsal margin of the orbit (ITF3, http://www.morphbank.net/Show/?id=461564; modified from Gates & Sampson, 2007: character 86): the dorsal margin of the infratemporal fenestra lies approximately at the same level as the dorsal margin of the orbit, and the caudal region of the skull roof is subhorizontal or slightly sloping rostroventrally relative to the frontal plane (0); the dorsal margin of the infratemporal fenestra is substantially more dorsally located than the dorsal margin of the orbit, and the caudal region of the skull roof is rostroventrally inclined relative to the frontal plane (1); the dorsal margin of the infratemporal fenestra lies slightly or substantially below the level of the dorsal margin of the orbit, and the caudal region

of the skull roof is subhorizontal or slightly sloping caudoventrally relative to the frontal plane (2).

193. Morphology of the dorsal outline of the supratemporal fenestra (STF, http://www.morphbank.net/Show/?id=461565): subrectangular, with the long axis directed rostrally (0); oval, with the long axis directed rostrolaterally (1); oval and wider mediolaterally than rostrocaudally (2).
194. Length of the skull (measured from the caudal margin of the quadrate to the rostral end of the oral margin of the premaxilla) relative to its height (measured from the ventral surface of the quadrate to the dorsal border of the squamosal) (SK1, http://www.morphbank.net/Show/?id=461566; modified from You *et al.*, 2003: character 1): ratio up to 2 (sample mean ratio of 1.82) (0); relatively elongated skull, ratio greater than 2 (sample mean ratio of 2.18) (1).
195. Maximum transverse width of the cranium in dorsal view across the postorbitals relative to the width across the quadrate cotylus of the squamosals (SK2, http://www.morphbank.net/Show/?id=461699; modified from Horner *et al.*, 2004: character 67): the skull is more than 25% wider across the postorbitals (sample mean ratio of 0.35) (0); the skull is up to 25% wider across the postorbitals (sample mean ratio of 0.14) (1).
196. Shape of the occiput in caudal view (SK3, http://www.morphbank.net/Show/?id=461700; Horner *et al.*, 2004: character 68): rectangular (0); subtriangular, with the quadrates laterally splayed distally (1).

Vertebral characters (http://www.morphbank.net/myCollection/index.php?collectionID=461128)

197. Cervical vertebrae. Morphology of the dorsal flange of the axis (CRV1, http://www.morphbank.net/Show/?id=461701; modified from Campione, Evans & Cuthbertson, 2007): dorsally convex flange extending beyond or to the level of the cranialmost region of the postzygapophyses (0); presence of short cranial flange separated from the postzygapophyseal region by a prominent embayment (1).
198. Cervical vertebrae. Development of the postzygapophyseal proceses of cranial and middle cervical vertebrae (CRV2, http://www.morphbank.net/Show/?id=461702; modified from Horner *et al.*, 2004: character 74): relatively low and relatively short, less than three times the rostrocaudal breadth of the neural arch (0); relatively high and relatively long, three times or more longer than the breadth of the neural arch (1).
199. Number of cervical vertebrae (Horner *et al.*, 2004: character 72): 11 or less (0); 12 or more (1).
200. Height of the neural spine relative to that of the centrum of the tallest posterior dorsal or sacral vertebrae (in adults) (DRS1, http://www.morphbank.net/Show/?id=461703; modified from Norman, 2002: character 41): short neural spine, ratio up to 2.10 (mean ratio of 1.79) (0); ratio greater than 2.10 and up to 3.25 (mean ratio of 2.57) (1); very long neural spine, ratio greater than 3.25 (mean ratio of 3.97) (2).
201. Slightly elongated neural spines in the cranial dorsal vertebrae, forming a 'wither-like' region above the pectoral girdle (DRS2, http://www.morphbank.net/Show/?id=461704; Wagner, 2001): absent (0); present (1).
202. Minimum count of co-ossified vertebrae in the sacral region (including single dorsal and caudal contributions (Godefroit *et al.*, 2000: character 27): seven or fewer (0); eight or more (1). Brett-Surman (1989) suggested that the number of sacral vertebrae may increase with age. This is supported by the observation of the addition of two caudal vertebrae to the sacrum of a very large *Shantungosaurus*, giving a total of ten sacral vertebrae. However, some small hadrosaurid individuals, such as the *Saurolophus* juvenile ZPAL MgD-I 159, have as many as nine sacrals, compared with the eight sacrals observed in adult specimens such as MPC-D 100/706. The small exemplar of *Lambeosaurus*, AMNH 5340, showed the relatively large count of nine sacrals.
203. Chevron length relative to the length of the neural spines in the caudal vertebrae of the proximal half of the tail (CDL, http://www.morphbank.net/Show/?id=461705; Wagner, 2001): chevrons shorter or nearly as long as the neural spines (0); chevrons longer than the neural spines (1).

Pectoral and forelimb characters (http://www.morphbank.net/myCollection/index.php?collectionID=461121)

204. Sternal. Length of the 'handle-like' caudolateral process of the sternal relative to that of the craniomedial plate (excluding the caudoventral process) (ST, http://www.morphbank.net/Show/?id=461706; modified from Prieto-Márquez *et al.*, 2006a: character 100): caudolateral process slightly shorter or as long as the craniomedial plate (0); caudolateral process longer than the craniomedial plate (1).

205. Coracoid size relative to the length of the scapula (COR1, http://www.morphbank.net/Show/?id=461707; Horner *et al.*, 2004: character 77): relatively large coracoid, ratio between craniocaudal length of coracoid and length of scapula of approximately (0); coracoid reduced in size relative to the scapula (1).
206. Coracoid. Ratio between the length of the lateral margin of the facet for the scapular articulation and the length of the lateral margin of the glenoid (COR2, http://www.morphbank.net/Show/?id=461708): longer scapular facer, with a ratio greater than 1.30 (sample mean ratio of 1.48) (0); slightly longer scapular facet, with a ratio of greater than 1 and up to 1.30 (sample mean ratio of 1.14) (1); glenoid longer than the scapular facet, with a ratio of up to 1 (sample mean ratio of 0.75) (2).
207. Coracoid. Angle between the lateral margins of the facet for scapular articulation and the glenoid (COR3, http://www.morphbank.net/Show/?id=461709): angle greater than 115° (sample mean angle of 124°) (0); angle up to 115° (sample mean angle of 102°) (1).
208. Coracoid. Morphology of the craniomedial margin of the coracoid (COR4, http://www.morphbank.net/Show/?id=461710; Horner *et al.*, 2004: character 78): convex or straight, associated with a moderate development and slightly projected biceps tubercle (0); concave, associated with a relatively large and lateroventrally projected biceps tubercle (1).
209. Coracoid. Development of the 'hook-like' ventral process of the coracoid, measured as the ratio between the dorsoventral depth and the breadth of the process (COR5, http://www.morphbank.net/Show/?id=461711; modified from Godefroit *et al.*, 2000: character 25): relatively short, ratio less than 0.65 (sample mean ratio of 0.55) (0); ratio between 0.65 and 0.80 (sample mean ratio of 0.71) (1); long process, nearly as deep as it is wide, with a ratio of greater than 0.80 (sample mean ratio of 0.96) (2).
210. Coracoid. Curvature of the ventral 'hook-like' process of the coracoid (COR6, http://www.morphbank.net/Show/?id=461712; Godefroit *et al.*, 2000: character 25): ventrally directed (0); recurved, so that the process is caudoventrally directed (1).
211. Scapula. Lateral profile of the dorsal margin of the scapula (SCP1, http://www.morphbank.net/Show/?id=461713; modified from Sereno, 1986): craniocaudally straight from the cranial margin of the coracoid facet to the distal end of the blade (0); curved, dorsally convex, curvature originating at the level of the dorsal margin of the pseudoacromion process, and most pronounced over the dorsoventral constriction (1).
212. Scapular length, ratio between the craniocaudal length of the scapula (from the cranial end of the pseudoacromion process to the distal margin of the blade) and the dorsoventral depth of the cranial end (from the cranial end of the pseudoacromion process to the ventral apex of the glenoidal facet) (SCP2, http://www.morphbank.net/Show/?id=461714): relatively short scapula, ratio of up to 4 (sample mean ratio of 3.54) (0); relatively long scapula, ratio of greater than 4 (sample mean ratio of 4.64) (1).
213. Dorsoventral expansion of the distal region of the scapular blade (measured as a ratio between the depth of the distal end of the blade and the depth of the proximal region) (SCP4, http://www.morphbank.net/Show/?id=461716): ratio less than 1 (sample mean ratio of 0.80) (0); ratio of 1 or greater (sample mean ratio of 1.15) (1).
214. Scapula. Proximal constriction (scapular 'neck'), ratio between the dorsoventral width of the proximal constriction and the dorsoventral depth of the cranial end of the scapula (SCP5, http://www.morphbank.net/Show/?id=461717): narrow 'neck', ratio of up to 0.60 (sample mean ratio of 0.53) (0); relatively broad 'neck', ratio of greater than 0.60 (sample mean ratio of 0.68) (1).
215. Scapula. Morphology and orientation of the pseudoacromion process (SCP6-7, http://www.morphbank.net/Show/?id=461718; modified from Horner *et al.*, 2004: character 80): recurved, so that the cranial region is dorsally or craniodorsally directed (0); horizontal, occasionally with minor and subtle dorsal or ventral curvatures, so that the cranial region is cranially or mostly cranially directed (1).
216. Scapula. Degree of curvature of the dorsally oriented pseudoacromion process of the scapula (SCP6-7, http://www.morphbank.net/Show/?id=461718; modified from Horner *et al.*, 2004: character 80): strongly recurved, so that the cranial region of the process is dorsally oriented (0); slightly recurved, with concave lateral profile of the dorsal margin, so that the cranial region of the process is craniodorsally oriented (1).
217. Scapula. Cranial extension of the craniodorsal region of the scapula (bearing the coracoid facet), measured as a ratio between the distance from the coracoid joint and the cranial end of the pseudoacromion process, and the height between this and the ventral apex of the glenoidal facet (SCP8, http://www.morphbank.net/Show/?id=461719): short craniodorsal region, ratio less than 0.45 (sample mean ratio of 0.35)

(0); long craniodorsal region, ratio of 0.45 or greater (sample mean ratio of 0.53) (1).

218. Scapula. Development of the deltoid ridge (SCP9, http://www.morphbank.net/Show/?id=461720): dorsoventrally narrow convexity limited to the proximal region of the scapula, near the pseudoacromion process from which it develops, with a poorly demarcated ventral margin (0); dorsoventrally deep and craniocaudally long, with a well-demarcated ventral margin (1).
219. Humerus. Length of the deltopectoral crest of the humerus (measured as the ratio between the proximodistal length of the crest and the proximodistal length of the humerus (HM1, http://www.morphbank.net/Show/?id=461721; modified from Godefroit *et al.*, 2000: character 26): proximodistally short crest, ratio less than 0.48 (sample mean ratio of 0.44) (0); ratio between 0.48 and 0.55 (sample mean ratio of 0.52) (1); very long crest, ratio greater than 0.55 (sample mean ratio of 0.59) (2).
220. Humerus. Lateroventral expansion of the deltopectoral crest of the humerus (measured as the ratio between the width of the humerus across the distal fourth of the deltopectoral crest and the width of the distal shaft at the point of maximum curvature) (HM2, http://www.morphbank.net/Show/?id=461722; modified from Horner *et al.*, 2004): poorly expanded deltopectoral crest, ratio less than 1.65 (sample mean ratio of 1.53) (0); ratio between 1.65 and 1.90 (sample mean ratio of 1.76) (1); very expanded deltopectoral crest, ratio greater than 1.90 (sample mean ratio of 2) (2). No substantial increase in the lateroventral expansion of the deltopectoral crest was found through ontogeny. For example, juveniles of *Bactrosaurus johnsoni*, AMNH 6378 and AMNH 30239, showed a ratio of 1.66 and 1.76, respectively, which are within the range of the 1.74 value measured for a much larger specimen (SBDE/95E). The same applied to other taxa: *Hypacrosaurus altispinus* (juvenile TMP 82.10.1, with a ratio of 2.01, and adult CMN 8501, with a ratio of 2.06); *Prosaurolophus maximus* (juvenile TMP 86.34.3, with a ratio of 1.79, and adult TMP 84.1.1, with a ratio of 1.80); and *Corythosaurus* (juvenile ROM 1947, with a ratio of 1.98, and adult ROM 845, with a ratio of 2.03).
221. Humerus. Degree of angulation of the ventral margin of the deltopectoral crest (HM3, http://www.morphbank.net/Show/?id=471338; Weishampel *et al.*, 1993: character 37): well-rounded (0); extending abruptly from the humeral shaft to give a distinct angular profile (1).
222. Humerus. Overall proportions of the humerus (measured as a ratio between the total length and the width of the lateral surface of the proximal end of the humerus) (HM4, http://www.morphbank.net/Show/?id=461724; modified from Weishampel *et al.*, 1993: character 36): relatively short and stocky humerus, ratio less than 4.25 (mean ratio of 3.85) (0); ratio between 4.25 and 4.90 (sample mean ratio of 4.60) (1); relatively long and thin humerus, ratio greater than 4.90 (mean ratio of 5.4) (2).
223. Ulna. Length of the ulna relative to its dorsoventral thickness (measured at mid-shaft) (UL1, http://www.morphbank.net/Show/?id=461725): ratio length/width less than 10 (0); ratio length/width equal or larger than 10 (1).
224. Ulnar length relative to humeral length (UL2, http://www.morphbank.net/Show/?id=461726; Norman, 2002: character 47): ulna shorter than or as long as the humerus (0); longer ulna, up to 20% longer than the humerus (1); longer ulna, being more than 20% longer than the humerus (2).
225. Composition of the carpus (MN1, http://www.morphbank.net/Show/?id=461727; adapted from Horner *et al.*, 2004: character 86): presence of fused ulnare, radiale, intermedium, and distal carpals (0); number of carpal bones reduced to a maximum of two unfused elements (1).
226. Manual digit I (Norman, 2002: character 49) (MN2, http://www.morphbank.net/Show/?id=461728): presence of metacarpal I and one ungual phalanx (0); entire digit I absent (1).
227. Elongation of the manus exemplified by elongation of metacarpals II–IV, measured as the ratio between the length of metacarpal III and the width of its mid-shaft (MN3, http://www.morphbank.net/Show/?id=461729; modified from Horner *et al.*, 2004: character 84): relatively short and blocky, ratio of up to 5 (sample mean ratio of 4.25) (0); relatively long and slender, ratio of greater than 5 (sample mean ratio of 8.54) (1).
228. Elongation of metacarpal V, so that it is more than twice as long as it is proximally wide (MN4, http://www.morphbank.net/Show/?id=461730): absent (0); present (1).
229. Length/width proportions of manual phalanx III1 (MN6, http://www.morphbank.net/Show/?id=461732; modified from Prieto-Márquez *et al.*, 2006a: character 114): proximodistally compressed, mediolaterally wider than it is long (0); slightly longer proximodistally than it is wide mediolaterally (1); very elongated, proximodistal length that is at least twice its mediolateral width at the middle of its longitudinal axis (2).

230. Shape of manual ungual II (MN7, http://www.morphbank.net/Show/?id=461733; Norman, 2002: character 53, in part): claw-like (0); hoof-like (1).
231. Proximodistal length of manual palanx II1 relative to that of II2 (MN8, http://www.morphbank.net/Show/?id=461734; modified from You *et al.*, 2003: character 55): phalanx II1 less than three times longer than phalanx II2 (0); phalanx II1 three times or more longer than phalanx II2 (1). This character may appear similar to the elongation of the manus (character 237). However, the length of phalanx II2 is proportionally less than that of phalanx II1.

Pelvic characters (http://www.morphbank.net/myCollection/index.php?collectionId=461092)

232. Ilium. Angle of ventral deflection of the preacetabular process of the ilium (IL1, http://www.morphbank.net/Show/?id=461735; modified from Suzuki *et al.*, 2004: character 69): angle greater than 150° (sample mean angle of 162°) (0); angle of 150° or less (sample mean angle of 143°) (1).
233. Ilium. Dorsoventral depth of the proximal region of the preacetabular process (measured as a ratio between this and the dorsoventral distance between the pubic peduncle and the dorsal margin of the ilium) (IL3, http://www.morphbank.net/Show/?id=461737): shallow, less than half the depth of the cranial central plate, ratio less than 0.50 (sample mean ratio of 0.42) (0); approximately as deep as the cranial central plate depth, ratio between 0.50 and 0.55 (sample mean ratio of 0.51) (1); deeper than half the depth of the cranial central plate, ratio greater than 0.55 (sample mean ratio of 0.62) (2).
234. Ilium. Dorsoventral depth of the central plate of the ilium (expressed as a ratio between this and the distance between the pubic peduncle and the caudodorsal prominence of the ischial peduncle) (IL4, http://www.morphbank.net/Show/?id=461738): ratio of 0.80 or greater (sample mean ratio of 0.90) (0); ratio less than 0.80 (sample mean ratio of 0.71) (1).
235. Ilium. Position of the ventralmost margin of the supra-acetabular process relative to the caudoventral margin of the lateral ridge of the caudal protuberance of the ischial peduncle of the ilium (IL5, http://www.morphbank.net/Show/?id=461739; Brett-Surman & Wagner, 2007): apex located caudodorsally (0); apex located craniodorsally (1).
236. Ilium. Development of the lateroventral projection of the supra-acetabular process of the ilium (IL6, http://www.morphbank.net/Show/?id=461740; modified from Horner *et al.*, 2004: character 91): forms a longitudinal and continuous 'swelling' or reflected border along the dorsal margin of the central plate and the proximal region of the postacetabular process, with a depth of up to 25% the depth of the ilium (0); projected lateroventrally at least 25% (but less than half) the depth of the ilium (1); projects lateroventrally between half and three quarters of the dorsoventral depth of the ilium (2); projects lateroventrally to overlap totally or at least half of the lateral ridge of the caudal prominence of the ischial peduncle (3).
237. Ilium. Craniocaudal breadth of the supra-acetabular process, measured as the ratio between the breadth of the process across its dorsal region and the craniocaudal length of the central iliac blade from the caudal ischial peduncle to the pubic one (IL7, http://www.morphbank.net/Show/?id=461741): craniocaudally wider than the central plate of the ilium, ratio greater than 0.85 (sample mean ratio of 1.16) (0); craniocaudally broad, ratio between 0.70 and 0.85 (sample mean of 0.73) (1); slightly broader than half the length of the central iliac blade, ratio between 0.55 and 0.69 (sample mean ratio of 0.62) (2); short, ratio less than 0.55 (sample mean ratio of 0.48) (3).
238. Ilium. Symmetry of the lateral profile of the supra-acetabular process (IL8, http://www.morphbank.net/Show/?id=461742): asymmetrical, with a caudally skewed lateral profile (0); symmetrical or with a slightly caudally skewed profile (1).
239. Ilium. Morphology of the lateroventral margin of the supra-acetabular process (IL9, http://www.morphbank.net/Show/?id=461743): craniocaudally sinuous (0); widely arched (1); U- or V-shaped (2); subrectangular, with a shallow notch that divides the ventral margin in two poorly demarcated lobes (3).
240. Ilium. Demarcation of the caudodorsal margin of the lateroventral rim of the supra-acetabular process: the caudodorsal margin is a well-defined ridge that is continuous with the dorsal margin of the proximal region of the postacetabular process (IL10, http://www.morphbank.net/Show/?id=461799) (0); the caudodorsal margin is poorly defined and appears discontinuous with the dorsal margin of the proximal region of the postacetabular process because of the lack of a well-demarcated caudodorsal ridge (http://www.morphbank.net/Show/?id=461744) (1).
241. Ilium. Morphology of the pubic peduncle of the ilium (IL11, http://www.morphbank.net/Show/

?id=461745 and http://www.morphbank.net/Show/?id=461746; modified from Sereno, 1986; Horner *et al.*, 2004; character 92): relatively large and dorsoventrally deep (longer than wide), subconical, with a proximal region that is only slightly craniocaudally wider than the distal end of the process (0); relatively shorter (wider or as wide as long) and triangular, with a proximal region that is much craniocaudally wider than the distal end (1).

242. Ilium. Morphology of the ischial peduncle of the ilium (IL12, http://www.morphbank.net/Show/?id=461747 and http://www.morphbank.net/Show/?id=461748; modified from Godefroit *et al.*, 2001: character 30): formed by a single and large, oval ventral protrusion (0); composed of a large and oval ventral protrusion, and by a smaller, caudodorsally located prominence emerging from the caudodorsal ridge (1); formed by two protrusions of similar size, the caudalmost one located slightly caudodorsally (2).
243. Ilium. Ratio between the craniocaudal length of the postacetabular process and the craniocaudal length of the central plate of the ilium (IL13, http://www.morphbank.net/Show/?id=461749): short postacetabular process, ratio up to 0.80 (sample mean ratio of 0.70) (0); postacetabular process nearly as long as the central plate, ratio greater than 0.80 but less than 1.1 (sample mean ratio of 0.90) (1); postacetabular process substantially longer than the central plate, ratio of 1.1 or greater (sample mean ratio of 1.23) (2).
244. Ilium. Brevis shelf at the base of the postacetabular process of the ilium (IL14, http://www.morphbank.net/Show/?id=461750; modified in part from Horner *et al.*, 2004: character 93): absent (0); present (1). A number of hadrosaurid taxa showed a structure that could only be compared with the brevis shelf of non-hadrosaurid iguanodontoideans. The structure present in the hadrosaurids *Secernosaurus koerneri*, the Salitral Moreno OTU, *Hypacrosaurus altispinus* (AMNH 5204), and *Velafrons coahuilensis* differed from that in non-hadrosaurid taxa in that it appeared to have originated from dorsomedial rotation of the postacetabular process, rather than being the ventral surface of a mediolaterally thickened process. However, no such distinction was included in the definition and coding of this structure, in order to let the phylogenetic analysis infer whether those two types of shelves were homologous or not. The results of the phylogenetic analysis indicated that the brevis shelf in hadrosaurids evolved independently form that in outgroup iguanodontoideans.
245. Ilium. Medioventral ridge on the medial side of the postacetabular process, crossing the bone surface from the proximoventral to the caudodorsal margins, and orientation of the brevis shelf (IL15, http://www.morphbank.net/Show/?id=468875): absent or presence of a faint ridge (0); well-defined ridge bounding the medial margin of the brevis shelf, the latter faces medioventrally, and in medial view appears restricted to the caudal region of the postacetabular process (1); well-defined ridge forming the medial margin of a medioventrally-facing shelf, with a postacetabular process that is progressively expanded mediolaterally towards the caudal end (2); well-developed, oblique, and expanded flange forming the medial margin of an extensive brevis shelf that faces more ventrally than medially (3).
246. Ilium. Craniocaudally oriented median ridge on the laterodorsal surface of the postacetabular process (IL16, http://www.morphbank.net/Show/?id=461752): absent (0); present (1).
247. Ilium. Geometry of the lateral profile of the postacetabular process of the ilium (IL17, http://www.morphbank.net/Show/?id=461753 and http://www.morphbank.net/Show/?id=461754; modified from Horner *et al.*, 2004: character 93): the ventral margin converges caudodorsally to meet the horizontal dorsal margin, forming a tapering caudal end, and producing a triangular lateral profile of the process (0); dorsal and ventral margins parallel or slightly convergent, forming a distinct (rectangular or subcircular) caudal margin (1).
248. Ilium. Orientation of the dorsal margin of the postacetabular process relative to the acetabular margin (IL18, http://www.morphbank.net/Show/?id=461755): horizontal dorsal margin parallel or nearly parallel with the acetabular margin (0); caudodorsally oriented dorsal margin, rising dorsally relative to the acetabular margin (1).
249. Ilium. Position of the medial sacral ridge within the medial surface of the central plate of the ilium (IL19, http://www.morphbank.net/Show/?id=461756): ridge well separated ventrally from the dorsal margin of the ilium, set between 50 and 30% of the dorsoventral depth of the central plate (0); ridge located more dorsally, closer to the dorsal margin, within the dorsal third (less than 30% of the depth) of the central plate (1).
250. Ilium. Orientation of the medial sacral ridge of the ilium (IL20, http://www.morphbank.net/Show/?id=461757): craniocaudally directed, parallel with the dorsal margin of the ilium, and ending caudal to the level of the ischial peduncle, well into the proximal region of the postacetabular process (0); diagonal, cranioventrally

to caudodorsally oriented, concave ventrally and converging with the dorsal margin at the level of the ischial peduncle (1).

251. Ilium. Lateral profile of the dorsal or laterodorsal margin of the ilium (IL21, http://www.morphbank.net/Show/?id=461758; modified from Horner *et al.*, 2004: character 100): straight or slightly convex (0); distinctly depressed over the supra-acetabular process, and dorsally bowed over the proximal region of the preacetabular process (1).
252. Pubis. Orientation of the dorsoventral expansion of the prepubic process (PB1, http://www.morphbank.net/Show/?id=461759): the dorsal region of the expansion is more expanded than the ventral region, so that distally the process is dorsally directed (0); the ventral region is more expanded than the dorsal region, so that the distal expansion is ventrally directed (1).
253. Pubis. Geometry of the dorsoventral expansion of the prepubic process of the pubis (in lateral or medial views) (PB2, http://www.morphbank.net/Show/?id=461760, http://www.morphbank.net/Show/?id=461761, and http://www.morphbank.net/Show/?id=461762; modified in part from Wagner, 2001): circular to oval expansion, extensive and convex ventral margin (0); subsquared distal dorsal margin, expansion dorsoventrally taller than cranioventrally long, very pronounced proximal dorsal concavity and nearly straight distal ventral margin (1); ellipsoidal, expansion craniocaudally longer than dorsoventrally tall, well-pronounced concavities of the dorsal and ventral proximal margins (2); oval expansion, dorsoventrally taller than craniocaudally long, well-pronounced concave profiles of dorsal and ventral proximal margins (3); rectangular, craniocaudally longer than dorsoventrally tall, nearly straight profiles of the dorsal and ventral proximal margins (4). The shape of the prepubic process of the pubis remained constant throughout ontogeny in the few ontogenetic series recorded (e.g. lambeosaurine taxon, cf. *Hypacrosaurus stebingeri*, juveniles MOR 548 and adult MOR 549; *Maiasaura peeblesorum*, subadults MOR 547 and adult ROM 44770; *Edmontosaurus* spp., subadults LACM 7241, LACM 23504, and adults CMN 8399, DMNH 1943, SM 3046, CMN 2289, etc., to name just a few examples). It was also observed that, within the characteristic 'fist-like' shape of the lambeosurine pubis, *Corythosaurus* (e.g. AMNH 5240 and possibly AMNH 3971) and *Lambeosaurus* (e.g. TMP 66.4.1) showed a more elongated prepubic constriction relative to that of other forms such as *Hypacrosaurus altuspinus* (e.g. CMN 8501), *Hypacrosaurus stebingeri* (MOR 549), and *Lambeosaurus laticaudus* (e.g. LACM 26874).
254. Pubis. Depth of the dorsoventral expansion of the distal region of the prepubic process relative to the width of the acetabular margin of the pubis (PB3, http://www.morphbank.net/Show/?id=461763): distal expansion as wide as or shallower than the width of the acetabular margin (0); dorsoventral expansion deeper than the acetabular margin (1).
255. Pubis. Craniocaudal length of the proximal constriction of the prepubic process of the pubis relative to the length of the dorsoventral expansion (PB4, http://www.morphbank.net/Show/?id=461764; modified from Horner *et al.*, 2004: character 96): constriction longer than the dorsoventral expansion, i.e. restricted to the distal region of the process (0); constriction and distal expansion have approximately the same length (1); constriction slightly shorter than the dorsoventral expansion that begins at the proximal region of the process (2).
256. Pubis. Relative position of maximum concavity of the dorsal and ventral margins of the prepubic process of the pubis (PB5, http://www.morphbank.net/Show/?id=461765): maximum ventral concavity achieved adjacent to the proximal region of the postpubic process, maximum dorsal concavity located further distally (0); maximum ventral concavity located ventral to or slightly caudal to the maximum dorsal concavity (1).
257. Pubis. Morphology of the acetabular margin, ventral to the lateral edge of the iliac peduncle (PB6, http://www.morphbank.net/Show/?id=461766): the lateral margin of the iliac peduncle extends ventrally forming a prominent ridge that merges with the proximal region of the ischial peduncle (0); the lateral margin of the iliac peduncle progressively disappears ventrally into the lateral surface of the region adjacent to the acetabular margin (1).
258. Pubis, obturator foramen (PB7, http://www.morphbank.net/Show/?id=461767; modified from Horner *et al.*, 2004: character 97): present, proximal postpubic ramus has a caudodorsally oriented short process that contacts totally or partially with the ischial peduncle to form the obturator foramen (0); absent, proximal postpubic ramus lacks a dorsocaudally oriented process (1).
259. Pubis. Length/width ratio of the ischial peduncle of the pubis (PB8, http://www.morphbank.net/Show/?id=461768): very short ischial peduncle, ratio less than 1.85 (sample mean ratio of 1.5) (0); ratio ranging from 1.85 to less than 3 (sample

mean ratio of 2.4) (1); very long, ratio of 3 or more (with a sample mean ratio of 4) (2).

260. Pubis. Lateroventral protuberance on the proximal region of the ischial peduncle of the pubis (PB9, http://www.morphbank.net/Show/?id=461769): absent or very faintly developed (0); present (1).
261. Pubis. Depth/width proportions of the iliac peduncle of the pubis (PB10, http://www.morphbank.net/Show/?id=461770): craniocaudally broader than dorsoventrally tall (0); taller dorsoventrally than broad craniocaudally (1).
262. Pubis. Total length of the pubis, as the ratio between the craniocaudal distance from the acetabular margin to the distal margin of the prepubic process, and the distance from the dorsal margin of the iliac peduncle and the ventral margin of the proximal postpubic shaft (PB11, http://www.morphbank.net/Show/?id=471324): short, ratio less than 2.70 (sample mean raio of 2.30) (0); long, ratio between 2.70 and 3 (sample mean ratio of 2.84) (1); very long, ratio greater than 3 (sample mean ratio of 3.53) (2).
263. Ischium. Development of a caudal curvature of the distal margin of the iliac peduncle of the ischium (IS1, http://www.morphbank.net/Show/?id=461772 and http://www.morphbank.net/Show/?id=461773; Brett-Surman & Wagner, 2007): curvature absent, distal margin slightly rounded, and, in some exemplars, slightly curved cranially (0); presence of a very short and slight curvature in the caudodorsal corner (1); presence of a well-developed curvature in the caudodorsal corner, so that the peduncle appears 'thumb-like' in lateral and medial profiles (2).
264. Ischium. Orientation of the distal articular surface of the iliac peduncle, measured as the angle that it forms with the acentabular margin of the peduncle (IS2, http://www.morphbank.net/Show/?id=461774): angle up to 115° (sample mean angle of 95°), angular craniodistal edge of the iliac peduncle (0); angle greater than 115° (sample mean angle of 125°), the distal surface of the peduncle is further cranially oriented (1).
265. Ischium. Elongation of the iliac peduncle of the ishium (ratio between the proximodistal length and the craniocaudal width of the distal margin) (IS3, http://www.morphbank.net/Show/?id=461775): relatively short peduncle, ratio less than 1.5 (sample mean ratio of 1.27) (0); ratio between 1.5 and 2 (sample mean ratio of 1.78) (1); relatively long peduncle, ratio greater than 2 (sample mean ratio of 2.30) (2).
266. Ischium. Relative orientation of the acetabular and caudodorsal margins of the iliac peduncle of the ischium (IS4, http://www.morphbank.net/Show/?id=461776): margins are either parallel or slightly convergent with each other (correlated with a greater expansion of the craniodorsal corner of the peduncle) (0); margins become slightly to greatly divergent near the proximal region of the peduncle (1).
267. Ischium. Orientation of the craniocaudal axis of the pubic peduncle (perpendicular to its articular margin) relative to the ischial shaft (IS5, http://www.morphbank.net/Show/?id=461777): ventrally inclined, angle up to 130° (sample mean angle of 118°) (0); slightly inclined ventrally, angle greater than 130 and up to 170° (sample mean angle of 157°) (1); pubic peduncle parallel with the ischial shaft (2).
268. Ischium. Length/width proportions of the pubic peduncle of the ishium (IS6, http://www.morphbank.net/Show/?id=461778): proximodistally longer than the distal articular surface is wide (0); approximately as long proximodistally as the distal articular surface is dorsoventrally wide (1); proximodistally shorter than the dorsoventral width of the distal articular surface (2).
269. Ischium. Relative position of the dorsal acetabular margin of the pubic peduncle (IS7, http://www.morphbank.net/Show/?id=461779): ventral to or at the same level as the dorsal margin of the ischial shaft (0); peduncular margin set dorsal to the dorsal margin of the ischial shaft (1).
270. Ischium. Dorsoventral thickness of the mid-shaft of the ischium (measured as a ratio between this and the length of the entire shaft) (IS8, http://www.morphbank.net/Show/?id=461780; modified from Wagner, 2001): very thin shaft, up to 5% the length of the ischial shaft (sample mean of 4.6%) (0); thickness ranging from more than 5% and up to 7.5% the length of the ischial shaft (sample mean of 6.7%) (1); very thick shaft, thickness greater than 7.5% the length of the ischial shaft (sample mean of 8.4%) (2).
271. Ischium. Morphology of the distal region of the ischial shaft (IS9, http://www.morphbank.net/Show/?id=461781 and http://www.morphbank.net/Show/?id=462510; modified from Godefroit *et al.*, 2001: character 31): slightly expanded into a blunt end (0); ventrally expanded forming a large 'foot' or 'boot-like' process (1).
272. Ischium. Degree of ventral projection of the distal expansion of the ischium (expressed as the ratio between the length of the ischial shaft and the length of the distal ventral expansion) (IS10, http://www.morphbank.net/Show/?id=461783; Evans & Reisz, 2007: character 90): ratio less than 0.25 (sample mean ratio of 0.18) (0); ratio of 0.25 or greater (sample mean ratio of 0.28) (1).

273. Ischium. Morphology of the cranial margin of the ventral expansion of the distal ischial shaft (IS11, http://www.morphbank.net/Show/?id=461784): slightly concave and directed caudoventrally to meet the caudal margin to nearly a point (0); strongly concave, recurved cranial margin (1).
274. Ischium. Orientation of the long axis of the distal 'foot' relative to the ischial shaft (IS12, http://www.morphbank.net/Show/?id=461785): straight, ventrally directed (0); cranioventrally directed, the inclination starting at the dorsal margin of the 'foot' (1).

Hindlimb characters (http://www.morphbank.net/myCollection/index.php?collectionID=461037)

275. Femur. Degree of curvature of the distal half of the femoral shaft (FM1 (http://www.morphbank.net/Show/?id=461786; Norman, 2002: character 62): slightly curved caudomedially (0); absence of curvature, straight distal shaft (1).
276. Femur. Lateral profile of the caudoventral margin of the fourth trochanter of the femur (FM2, http://www.morphbank.net/Show/?id=461787; modified from Wagner, 2001): triangular and ending in a caudally, and slightly ventrally, directed point (0); smooth and arcuate (1).
277. Tibia. Extension of the cnemial crest of the tibia (TB, http://www.morphbank.net/Show/?id=461788; Godefroit *et al.*, 2000: character 31): the cnemial crest is restricted to the proximal end of the tibia (0); cnemial crest further extended along the cranial surface of the proximal half of the diaphysis (1).
278. Fibula. Shape of the cranially expanded distal end of the fibula (FB, http://www.morphbank.net/Show/?id=461789; modified from Godefroit *et al.*, 2000: character 32): subtriangular, with a straight or slightly concave cranial margin (0); club-shaped, with a concave cranial margin and prominent cranial expansion (1). Godefroit *et al.* (2000) regarded state 1 of this character as synapomorphic for *Parasaurolophus cyrtocristatus* and *Charonosaurus jiayinensis*. However, a club-like distal end of the fibula is also present in other taxa, such as *Corythosaurus intermedius* (e.g. ROM 845) and even in a juvenile cf. *Hypacrosaurus stebingeri* (MOR 548).
279. Astragalus. Development of the medial platform of the astragalus (AS, http://www.morphbank.net/Show/?id=461790): it extends medially to completely underlie the medial malleolus of the tibia (0); short, wedges laterally, underlying only part of the medial malleolus of the tibia (1).
280. Distal tarsals II and III (Horner *et al.*, 2004: character 102): present (0); absent (1).
281. Metatarsal I (modified from Norman, 2002: character 66): absent (0); slender and splint-like element (1).
282. Length/width proportions of metatarsal III (measured as the ratio between its proximodistal length and its mediolateral breadth at midshaft; PES2, http://www.morphbank.net/Show/?id=461791): ratio less than 4.50 (mean ratio of 4.02) (0); elongated, ratio of 4.50 or greater (mean ratio of 5.12) (1).
283. Length/width proportions of pedal phalanx II2 (PES3, http://www.morphbank.net/Show/?id=461792): proximodistally shortened, being twice as wide mediolaterally as it is proximodistally long (0); subsquared, only slightly shorter proximodistally than it is wide mediolaterally (1).
284. Length/width proportions of the disc-shaped pedal phalanges III2 and III3 (PES4, http://www.morphbank.net/Show/?id=461793; modified from Horner *et al.*, 2004: character 104): up to three times (or less) wider than they are proximodistally long (0); more than three times wider than they are proximodistally long (1).
285. Morphology of the pedal unguals (PES6, http://www.morphbank.net/Show/?id=461795; Norman, 2002: character 67): proximodistally elongated and arrow-shaped, with a bluntly truncated tip and prominent claw grooves (0); mediolaterally broad and proximodistally shortened, rounded shield or hoof-like shaped, with reduced or absent claw grooves (1).
286. Ridge on the plantar surface of pedal unguals (PES7, http://www.morphbank.net/Show/?id=461796; Prieto-Márquez, 2005: character 47): absent (0); present (1).

Additional autapomorphic characters for inclusion in the Bayesian analysis

287. *Iguanodon bernissartensis*. Very large posterodorsal buttress of the quadrate (Paul, 2008).
288. *Iguanodon bernissartensis*. Massive manus (Paul, 2008).
289. *Iguanodon bernissartensis*. Forelimb about 70% the length of the hindlimb (Paul, 2008).
290. *Mantellisaurus atherfieldensis*. Distal pedal phalanges not strongly abbreviated (Paul, 2008).
291. *Mantellisaurus atherfieldensis*. Relatively large pelvis (Paul, 2008).
292. *Equijubus normani*. Finger-like process extending dorsally from the rostral process of the jugal to the lacrimal (Hai-lu You *et al.*, 2003).
293. *Equijubus normani*. Dentary teeth lacking a median primary ridge (Hai-lu You *et al.*, 2003).

294. *Equijubus normani*. Anterior process of the lacrimal wedging between premaxilla and maxilla (Paul, 2008).
295. *Equijubus normani*. Ventral margin of the lacrimal lying at the level of the dorsal edge of the maxilla (Paul, 2008).
296. *Protohadros byrdi*. Ventrally deflected muzzle, including a massive predentary and a robust, rostrally expanded, and deflected dentary (Head, 1998).
297. *Protohadros byrdi*. Strongly bilobate jugal–maxillary articulation (Head, 1998).
298. *Bactrosaurus johnsoni*. Rather narrow caudal process of jugal (Godefroit *et al.*, 1998).
299. *Bactrosaurus johnsoni*. Postcotyloid process of the quadrate markeldly curved posteriorly (Godefroit *et al.*, 1998).
300. *Telmatosaurus transsylvanicus*. Large caudal ectopterygoid shelf (Weishampel *et al.*, 1993).
301. *Telmatosaurus transsylvanicus*. Relatively long post-metotic braincase (Weishampel *et al.*, 1993).
302. *Telmatosaurus transsylvanicus*. Relatively large basipterygoid processes of the basisphenoid (Weishampel *et al.*, 1993).
303. *Telmatosaurus transsylvanicus*. Relatively large scar for m. protractor pterygoideus on the lateral side of the basisphenoid (Weishampel *et al.*, 1993).
304. *Telmatosaurus transsylvanicus*. Well-developed channel for the palatine branch of the facial nerve that also accommodated the median cerebral vein (Weishampel *et al.*, 1993).
305. *Wulagasaurus dongi*. Very slender dentary, with a dental battery length/maximum height of the dentary ramus at middle of dental battery ratio greater than 4.5 (Godefroit *et al.*, 2008).
306. *Wulagasaurus dongi*. Lateral side of the dentary not pierced by foramina (Godefroit *et al.*, 2008).
307. *Wulagasaurus dongi*. Humeral articular head extending distally as a very long and prominent ridge (Godefroit *et al.*, 2008).
308. *Sahaliyania elunchunorum*. Long and very slender paroccipital process, with slightly convex dorsal border and slightly concave ventral margin (Godefroit *et al.*, 2008).
309. *Sahaliyania elunchunorum*. Lateral depressions on the dorsal surface of the frontal better developed than in other lambeosaurines, without being associated with the median doming of the element (Godefroit *et al.*, 2008).
310. *Sahaliyania elunchunorum*. Ventrally displaced quadratojugal notch (Godefroit *et al.*, 2008).
311. *Amurosaurus riabinini*. Sagittal crest particularly elevated on the caudal part of the parietal, forming a high, triangular, and deeply excavated triangular process on the occipital region (Godefroit *et al.*, 2004a).
312. *Amurosaurus riabinini*. Caudal process of the postorbital particularly elongated, narrow, and regularly convex upwardly (Godefroit *et al.*, 2004a).
313. *Amurosaurus riabinini*. Prefrontal forming at least half of the width of the floor for the supracranial crest (Godefroit *et al.*, 2004a).
314. *Aralosaurus tuberiferus*. Paired nasals rising dorsally far in front of the orbits, forming or participating in a hollow crest-like structure (Godefroit *et al.*, 2004b).
315. *Aralosaurus tuberiferus*. Well-developed curved crest bordering laterally the posterior region of the premaxillary shelf, producing a trapezoidal lateral profile in the maxilla (Godefroit *et al.*, 2004b).
316. *Brachylophosaurus canadensis*. Prefrontal projected posteriorly, resting dorsomedially over anterior process of postorbital and, more posteriorly, extending ventromedially to underlie the nasal (Prieto-Márquez, 2005).
317. *Maiasaura peeblesorum*. Elongate rostrum bearing a dorsal surface that is distinctly angular in lateral aspect (Trexler, 1995).
318. *Maiasaura peeblesorum*. Dorsal surfaces of the rostrum caudal and rostral to the mid-nares, being straight but at an angle to each other because of a curvature of small radius located above the middle of the narial opening (Trexler, 1995).
319. *Charonosaurus jiayinensis*. Lateral side of squamosal nearly completely covered by caudal ramus of postorbital (Godefroit *et al.*, 2001).
320. *Charonosaurus jiayinensis*. Paroccipital and postcotyloid processes very low, extending only to mid-height of foramen magnum (Godefroit *et al.*, 2001).
321. *Corythosaurus casuarius*. Caudal margin of the crest smoothly convex in lateral view (Evans, 2007b).
322. *Corythosaurus casuarius*. Crest larger than in *Corythosaurus intermedius*, with a rostral margin of the dorsal process that forms a steeper angle with the snout than in the latter species (Evans, 2007b).
323. *Corythosaurus intermedius*. Caudal margin of the crest that is shallowly concave in lateral view and has a caudoventral nasal process (Evans, 2007b).
324. *Corythosaurus intermedius*. Crest smaller than in *Corythosaurus casuarius*, with a rostral margin of the dorsal process forming a shallower angle with the rostrum (Evans, 2007b).

325. *Hypacrosaurus altispinus*. Constricted external naris bounded caudally by the premaxillary dorsal process (Evans, 2007b).
326. *Hypacrosaurus altispinus*. Postorbital with unbranched posterior ramus (Evans, 2007b).
327. *Hypacrosaurus altispinus*. Jugal with angular ventral flange and straight caudoventral margin between the ventral and the quadratojugal flanges (modified from Evans, 2007b).
328. *Lambeosaurus magnicristatus*. Supracranial crest strongly inclined rostrally such that the angle between the dorsal premaxillary process and the rostrum is less than 85° (Evans, 2007b).
329. *Lambeosaurus magnicristatus*. Crest strongly overhanging the rostrum (Evans, 2007b).
330. *Lambeosaurus magnicristatus*. Caudoventral premaxillary process enlarged rostrodorsally to a greater degree than in any other lambeosaurine with a broadly rounded profile (Evans, 2007b).
331. *Kerberosaurus mankini*. Basisphenoid process of prootic deeply excavated by a pocket-like depression (Bolotsky & Godefroit, 2004).
332. *Kerberosaurus mankini*. Groove for ramus ophtalmicus of trigeminal foramen particularly widened on lateral side of laterosphenoid (Bolotsky & Godefroit, 2004).
333. *Kerberosaurus mankini*. Postotic foramina not limited rostrally by a prominent ridge (Bolotsky & Godefroit, 2004).
334. *Kerberosaurus mankini*. Circumnarial depression limited dorsocaudally by a strong, wide, and flattened crest on the lateral side of the nasal around the external nares (Bolotsky & Godefroit, 2004).
335. *Kerberosaurus mankini*. Very prominent hook-like palatine process on maxilla (Bolotsky & Godefroit, 2004).
336. *Nipponosaurus sachalinensis*. Robust coronoid process of the surangular (Suzuki *et al.*, 2004).
337. *Nipponosaurus sachalinensis*. Poorly developed neural spine of the axis (Suzuki *et al.*, 2004).
338. *Velafrons coahuilensis*. Quadrate with narrow qudratojugal notch (Gates *et al.*, 2007).
339. *Velafrons coahuilensis*. Postorbital with dorsally positioned, high-arching squamosal process (Gates *et al.*, 2007).
340. *Kritosaurus navajovius*. Nasal arch extending above the orbits and posteriorly (in adult specimens) to between the orbits (Williamson, 2000).
341. *Kritosaurus navajovius*. Circumnarial depression that, at its posterior region, extends from near the dorsal margin of the nasal laterally onto the prefrontal and lacrimal (Williamson, 2000).
342. *Gryposaurus latidens*. Excavations on the ventral surface of the premaxilla for the union of the rostroventral process of the maxilla (Horner, 1992).
343. *Gryposaurus notabilis*. Extreme rostrocaudal thickening of the proximodorsal ridge of the paroccipital process.
344. *Gryposaurus monumentensis*. Predentary and premaxillary oral margins with pronged denticles (Gates & Sampson, 2007).
345. *Gryposaurus monumentensis*. Surangular with distinct dorsal process on the medial ridge (Gates & Sampson, 2007).
346. *Olorotitan ararhensis*. Helmet-like hollow crest and lateral premaxillary process developed caudally far beyond the level of the occiput; caudolateral part of the dorsal premaxillary process depressed along the midline (Godefroit *et al.*, 2003).
347. *Olorotitan ararhensis*. Very high postorbital process of the jugal (ratio height of postorbital process/length of jugal = 0.9) (Godefroit *et al.*, 2003).
348. *Olorotitan ararhensis*. Rostral portion of the jugal shorter than in other lambeosaurines, with a perfectly straight rostral margin (Godefroit *et al.*, 2003).
349. *Olorotitan ararhensis*. Very asymmetrical maxilla in lateral view, with ventral margin distinctly downturned (Godefroit *et al.*, 2003).
350. *Olorotitan ararhensis*. Neck and sacrum very elongated, with, respectively, 18 cervical and 15 or 16 sacral vertebrae (Godefroit *et al.*, 2003).
351. *Parasaurolophus walkeri*. Narial crest consisting of two dorsal tubes that extend posteriorly, U-bend at the apex of the crest, and return along the ventral margin where they coalesce internally with the lateral diverticulae (Sullivan & Williamson, 1999).
352. *Parasaurolophus walkeri*. Dorsal and ventral tracts separated by a lateral groove on each side of the narial crest (Sullivan & Williamson, 1999).
353. *Parasaurolophus cyrtocristatus*. Short tubular narial crest that curves sharply posteroventrally (Sullivan & Williamson, 1999).
354. *Parasaurolophus cyrtocristatus*. Internal network of simple, paired tubes that extend from the external nares posteriorly to the apex of the narial crest, where they make a U-bend and continue anteriorly descending into the choana (Sullivan & Williamson, 1999).
355. *Parasaurolophus cyrtocristatus*. Lateral diverticulae situated medially between the dorsal ascending and ventral ascending tracts, and divided dorsally by internal sagittal septum

descending from the floor of the paired dorsal ascending tracts (Sullivan & Williamson, 1999).

356. *Parasaurolophus tubicen*. More complex narial crest consisting of a pair of forsal tubes that extend from behind the external narial openings (and presumably are contiguous with them), forming a U-bend posteriorly where they coalesce into a single pair of ventral tubes and return anteriorly, forming the ventral margin of the narial crest where they rise slightly above the nasal and frontal region, and fuse with the ventral tubes of the lateral diverticulae above, before entering the choana (Sullivan & Williamson, 1999).
357. *Parasaurolophus tubicen*. Paired lateral diverticulae that arise anteriorly (presumably communicate with external nares), extend posteriorly, forming a tight U-bend, and return ventrally above the ventral tubes, and coalesce with the ventral tubes anteriorly before entering the choana (Sullivan & Williamson, 1999).
358. *Parasaurolophus tubicen*. Dorsal and dorsolateral exterior surface of the narial crest bearing anastomosing furrows (Sullivan & Williamson, 1999).
359. *Prosaurolophus maximus*. Laterally excavated nasal crest located above the anterior margin of the orbit, with the posterior wall of the nasal excavation extending lateroventrally onto the prefrontal (Horner, 1992).
360. *Prosaurolophus maximus*. Only four predentary denticles located laterally to the median one.
361. *Secernosaurus koerneri*. V-shaped nasofrontal suture where the anterior margin of each frontal forms a median triangular process that is laterally deep, anteriorly excavated, and has an anteriorly offset ventral margin (A. Prieto-Márquez and G. Salinas, unpubl.data).
362. *Pararhabdodon isonensis*. Broad, nearly subrectangular anterodorsal region of the maxilla, accompanied by elevation of jugal facet of maxilla such that ventralmost extent is well above level of lateral margin of ectopterygoid shelf, maxilla forms acute embayment extending ventral to jugal process between jugal facet and ectopterygoid shelf (A. Prieto-Márquez and J.R. Wagner, unpubl. data).
363. *Tsintaosaurus spinorhinus*. Nasals forming a 'tube-like' process projecting dorsally and anteriorly, with the distal region broadening and separated (Young, 1958).
364. *Tsintaosaurus spinorhinus*. Supratemporal opening that is broader mediolaterally than anteroposteriorly (Young, 1958).
365. *Tsintaosaurus spinorhinus*. Oral margin of the premaxilla increasing in thickness posterolaterally, where it becomes extremely broad and lacks a distinct anterolateral corner.
366. *Tsintaosaurus spinorhinus*. External nares on premaxilla crossed obliquely by two long ridges that are anterolaterally directed and divide the former into three separate fossae.
367. *Tsintaosaurus spinorhinus*. Prefrontal bearing a large anteromedial flange and a curved, dorsally ascending anterior process.
368. *Tanius sinensis*. Postorbital process of the laterosphenoid that is longer than the mediodorsal flange of this element.
369. *Lophorhothon atopus*. Nasal with extensive but shallow rostrodorsal excavation and wedge-shaped posterior process that projects posterodorsally.
370. *Lophorhothon atopus*. Pefrontal with an extensive and laterally-facing anterior wing.